Conception de nanomatériaux de TiO2 pour le stockage d'énergie : batteries à ion lithium

Wenpo Luo

Wenpo Luo. Conception de nanomatériaux de TiO2 pour le stockage d'énergie : batteries à ion lithium. Chimie analytique. Université Paris sciences et lettres, 2021. Français. NNT : 2021UPSLC023 . tel-03956293

HAL Id: tel-03956293
https://pastel.hal.science/tel-03956293v1
Submitted on 25 Jan 2023

PSL UNIVERSITÉ PARIS

THÈSE DE DOCTORAT DE L'UNIVERSITÉ PSL

Préparée à Chimie ParisTech

Design of TiO_2 nanomaterials for energy storage: Lithium-ion batteries

Soutenue par

Wenpo LUO

Le 30 Juin 2021

Ecole doctorale n° 388

Chimie physique et chimie analytique de Paris centre

Spécialité

Chimie Analytique

Composition du jury :

Jolanta, SWIATOWSKA
Dr, Chimie Paristech
Présidente

Mustapha, JOUIAD
Prof, Université Picardie Jules Verne
Rapporteur

Ismaël, SAADOUNE
Prof, Université Cadi Ayyad Marrakech Maroc
Rapporteur

Arnaud, DEMORTIERE
Dr, Université Picardie Jules Verne
Examinateur

Abdelhafed, TALEB
Dr, Sorbonne Université
Directeur de thèse

Chimie Paris ParisTech | PSL

Summary

ACKNOWLEDGEMENTS

"One more spirits I propose, no old friends can be found in the west of Yangguan (劝君更进一 杯酒，西出阳关无故人) ". This is the famous poem and song written by Wang Wei (701-761, Tang Dynasty) when he sent his friend Yuan Er to AnXi (Kuche, Xinjiang, China) for taking his official post. This always reminds me the day when I left China to France. I was excited yet quite worried about the coming days. I was a little bit anxious about the language, eating habit, way of working/living and so on. I would be a foreigner to French whom I had always taken to be "foreigner". Now reflecting on the past three years, I have never felt so gratitude to my insightful PhD supervisors, precious friends, supportive parents. Thank you all for giving me the memorable time in Paris.

Firstly, I would like to acknowledge my doctoral supervisor: Dr. Abdelhafed Taleb, thank you for being with me all the time throughout the three years from grammar corrections to the setting of research plans. The daily email exchange and constant discussion/debate with you lay the foundation for my achievement.

Secondly, I thank the all the jury member for accepting my Ph.D defence. Thank you, Pr. Mustapha Jouiad and Pr. Ismaël Saardoune, for reviewing my Ph.D manuscript. Thanks Dr. Jolanta Swastoska and Dr. Arnaud Demortière for being my examiner.

Thirdly, I am deeply grateful to all my colleagues and friends for their help, their support, for all the great times we shared, and many scientific discussions. I would like to thank in particular Saida Mehraz, Sana Falah, Habiba Mamori, Anna Pyanko, Tao Zhu, Daming Zheng and many others. Those memories with you remind me happy time of ENSCP and Paris.

Finally, I indebt everything to my family. The love from my parents and my sister is the pillar that supports my PhD study in Paris. When the cloud comes, I know the sun is somewhere behind. When the wind come, I know where the harbor is.

Thanks all of you

Introduction

In the current context where the protection of the environment has taken on major importance, and where global warming has become a worldwide concern, renewable energies are identified by energy experts as mature technologies to ensure a sustainable alternative to fossil fuels (coal, oil, gas). The latter are the main sources of environmental pollution and global warming. As part of its energy policy for its member countries, the European Union has set ambitious objectives in terms of developing renewable energy. In addition to improving energy efficiency, the European Union wants to increase the share of renewable energy to at least 30% of the energy mix by 2030 [1]. Like Paris, some cities have gone even further, setting a target of 50% and then 100% by 2050.

Renewable energies, such as photovoltaic, wind, hydro, biomass or geothermal, offer the advantage of being non-polluting and sustainable green energies, but their dependence on climatic conditions makes them intermittent and not available on demand. This obstacle hinders their continuous use, which has necessitated the development of suitable storage systems to ensure a continuous supply at any time of the year. Energy storage systems will also help to increase the share of renewable energy in the energy mix, and meet the ambitious targets set by the EU for its member countries. It is estimated that the battery market could be worth 250 billion euros by 2025[2].

In order to optimize the use of renewable energies and to overcome the problem of intermittence, various storage systems have been developed to conserve energy and ensure its restitution on demand. Historically, lead batteries were the first to meet the need for energy storage. They have the advantage of being economical and easily recyclable, but nevertheless have the disadvantage of being environmentally polluting in the longer term. Indeed, the presence of lead in one of its components, which is a heavy metal dangerous for human health and the environment, may be released into the environment at the end of the battery's life. Today, lithium-ion batteries represent the most mature storage technology in the short term and the most popular, for domestic use (electric vehicles, portable devices, bicycles, scooters, electric scooters, industrial robots, tools, electricity storage on networks etc.), telecommunication (cell phones) or space (spacecraft). Lithium-ion batteries have the advantage of being able to restore energy quickly and reliably for a long period (more than 10 years). Moreover, they have the advantage of having a high density of energy storage, and of operating in extreme conditions of important temperature variations, shocks, vibrations and long duration. Other innovative battery technologies that are less polluting and more powerful have been developed to meet the growing need for sustainable energy storage. These technologies include: sodium-ion batteries, solid-state batteries.

Current lithium-ion batteries consist of two electrodes, an anode and a cathode, immersed in an electrolyte. They work by cycles of charge and discharge during which the lithium ions move from one electrode to the other through an electrolyte. For the different uses of lithium-ion batteries, it is essential to provide energy with the same performance for more than ten years. The possible ageing of one of the battery's components can hinder its optimal functioning and lead to a decrease in its performance. The aging phenomena affect the different components of the battery, and is manifested by a change in their properties. The quality of the different components of the battery has a considerable influence on its performance in terms of life expectancy, cyclability and power. The growth of a passivation layer at the electrode-electrolyte interface (Solid Electrolyte Interphase (SEI)), favors a better reversibility of lithium ion insertion without solvent intercalation, while maintaining a good charge transfer. Furthermore, the structure, architecture and composition of the electrode materials also play an important role in the optimization of battery performance. However, their evolution during the battery cycling is still poorly understood and is a hot topic in the battery field. Several results in the literature have highlighted the importance of the porosity and the specific surface of the powders used as electrode materials in the determination of the performance of batteries.

In order to understand the different parameters influencing the performance of lithium-ion batteries, the research work in this thesis will be oriented towards the study of the different mechanisms at the origin of a control of the morphology of titanium dioxide nanoparticles, during a hydrothermal synthesis. Moreover, the interest of a control of the morphology of titanium dioxide nanoparticles, in order to use them as anode materials for lithium-ion batteries will be explored. The importance of the porosity and the specific surface of titanium dioxide powders in the determination of the performances of lithium-ion batteries will be studied.

Chapter I is a bibliographical study of the state of the art, on titanium dioxide nanoparticles and lithium-ion batteries. The first part will be dedicated mainly to the synthesis methods of titanium dioxide nanoparticles, with a particular attention to the hydrothermal method. We will present in this part, the different parameters characterizing TiO_2 nanoparticles. The applications of

TiO2 nanoparticles will also be discussed. The second part of this chapter will be dedicated to lithium-ion batteries and the interest to use TiO_2 nanostructures as anode materials. Particular attention will be paid to the positioning of the work in relation to the literature in the field. We will also present the potential challenges of lithium-ion batteries.

Thereafter, the manuscript is structured in articles exposing the obtained results, and each article is preceded by an abstract, describing in a succinct way the results reported in this article. The different results reported, discuss the mechanism at the origin of the control of the morphology, in the case of the hydrothermal synthesis of TiO_2 nanoparticles. The roles of the specific surface and the porosity of the anode materials, in the determination of the performances of the lithium-ion batteries will be illustrated.

The last chapter will be devoted to the general conclusion, which summarizes the main results of the thesis, and highlights the contribution of the work done to the identification of key parameters for the preparation of lithium-ion batteries with better performances. In addition, following the conclusion, ways to improve the performance of lithium-ion batteries will be discussed, and may be the subject of perspectives for the continuation of this thesis work.

References

[1] https://www.ecologique-solidaire.gouv.fr/cadre-europeen-energie-climat#e4

[2] https://www.lemonde.fr/economie/article/2019/06/23/batteries-electriques-l-europe-sonne-la-charge_5480387_3234.html

Chapter I: Bibliographic state of the art

In recent years, a new class of materials has emerged, with the development of new synthesis methods and characterization tools, such as the scanning tunneling microscope and the atomic force microscope. This class of material at the nanometer scale, offers a new configuration where the atoms in volume are in negligible proportion compared to those of the surface. Moreover, their dimension becomes of the same order of magnitude as a certain number of physical quantities, such as the Bloch walls [1-2] or the mean free path [1-2]. These materials, commonly called nanomaterials, offer new properties, which differ from those of the solid material of the same chemical composition. Nanomaterials have the specificity to offer new parameters, for the control of their properties, which are: their size, their morphology and their assembly [3-4].

Currently, nanomaterials are identified as a driver of development in the field of innovative materials, and at the origin of many disruptions and technological revolution in several areas. Nanomaterials are at the heart of many revolution in the field of renewable energies and energy storage systems. They offer scientists and industrialists the possibility to elaborate new materials from nanomaterials as elementary building blocks, to obtain the properties necessary to optimize the targeted application.

In the field of batteries, electrode materials have the difficult task of meeting several challenges to improve the performance of batteries in terms of energy storage, charging time and life span (cyclability). Electrodes based on nanomaterials offer to the batteries the possibility to have a significantly higher storage capacity, as well as an increased charging speed. The nanoscale of nanomaterials offers a large specific surface and porosity, which facilitates the diffusion of ions and allows them to easily access the surface of the electrodes. This, in turn, allows for a significant reduction in recharge time and an increase in storage capacity. The miniaturization of batteries is also made possible by the use of nanomaterials.

In the case of lithium-ion batteries, the anode, which is the negative electrode, is usually made of graphite. Titanium oxide is another alternative to graphite as an anode material, and it has the advantage of being non-toxic, inexpensive, and fairly available. In addition, titanium oxide anodes improve the performance of lithium-ion batteries, especially the safety.

Methods of synthesis and properties of titanium dioxide nanomaterials

Titanium dioxide is a material, which is found in natural minerals with contents ranging from 45% (ilmenites) to 95% (rutiles). Titanium dioxide crystallizes in different polymorphs, of which the best known are: anatase, rutile, brookite and TiO_2-B. TiO_2 polymorphs differ in their crystal structures, as well as in their physicochemical properties. The remarkable properties of TiO_2 make it a raw material of choice for various applications. TiO_2 nanomaterials are frequently used in many industrial sectors, such as automotive, food, cosmetics etc. The European consumption of TiO_2 for industrial applications reached 7 million tons in 2016 [5]. The strong and growing demand for this raw material has led to the development of industrial processes for large-scale production, but also to the development of synthesis methods on a laboratory scale. The growing interest in TiO_2 is largely due to its interesting photocatalytic properties, exploited in photo-pollution and renewable energies, such as photovoltaics. Moreover, its harmlessness and its low production cost make it an interesting material from an industrial point of view, TiO_2 being the most photoactive compound under ultraviolet (UV) light.

The properties of nanomaterials depend strongly on their size, morphology, composition, crystallinity and assembly. Those of TiO_2 at the nanometric scale also obey this rule. However, the properties-structure relationship in the case of TiO_2 nanomaterials has been the subject of several reviews in the literature [6-7]. Until now, the relationship between the properties of TiO_2 nanomaterials, in particular the architecture of their assembly, and the performance of the devices integrating them is not yet fully understood and is the subject of contradictory reports in the literature. The observed disagreements are related to the different parameters of the synthesis method, leading to the formation of TiO_2 nanomaterials, with different physicochemical characteristics. Depending on the parameters of the synthesis method, different morphologies were obtained, with better control of size and composition. If the nanosphere [6-7] is the most abundantly prepared morphology for TiO_2 nanomaterials, a whole zoology of morphologies has been reported in the literature, such as, nanotubes, nanowires, nanoribbons, nanourchins etc. Even if the protocols allowing the synthesis of these morphologies are well established, the phenomena of their formation are still poorly understood. In the rest of this chapter, we will focus on the synthesis methods of TiO_2 nanomaterials, and we will focus on the hydrothermal synthesis and on the phenomena that control the morphology.

1.1. Synthesis methods of TiO_2

Different synthesis techniques have been used for the elaboration of TiO_2 nanomaterials, which can be classified in 3 categories: chemical or physical methods in liquid or gas phase, and mechanical methods. In the remainder of this chapter, we will expose the most commonly used synthesis methods. Then, we will focus on the hydrothermal synthesis method, because of its numerous advantages, including its low cost, the possibility of a large-scale production and a better control of the shape and size of TiO_2.

1.1.1. Mechanical synthesis method.

Mechano-synthesis or ball milling is a method that consists of grinding a micrometric powder of TiO_2, by means of a mill using tungsten carbide or agate balls. At a high grinding speed of about 710 rpm, it is possible to obtain a nanosized TiO_2 powder [8]. During the milling process, the transformation of the anatase phase into rutile can take place [9], which is one of the advantages of this method since this phase transition usually requires high temperatures. On the other hand, this method also has the advantage of being inexpensive and easy to implement, but it has the disadvantage of not offering better control over the shape and size of the TiO_2 nanomaterials.

1.1.2. Synthesis methods in gas phase.

In this section, we will give some examples of gas phase synthesis techniques.

1.1.2.1 Synthesis by physical deposition in gas phase.

The processes of physical deposition in gas phase (PVD), designate the family of techniques allowing the elaboration of thin layers. They do not involve the chemical reaction of a precursor, but rather the evaporation of the bulk material to be deposited. The material is first placed in a crucible, which is heated by an electron beam (EB-PVD) or a laser (PLD: Pulsed Laser Deposition). The atoms of the evaporated material are deposited on a substrate, where the nucleation/growth processes of particles or films take place [10-11]. Among the methods that belong to this family of synthesis methods, we find the sputtering technique [12], the radio frequency (RF) technique [13], the ion sputtering and the molecular jet epitaxy [14-15]. These techniques offer a good control of the particles growth but suffer from a low production and a rather high cost.

1.1.2.2 Synthesis by chemical gas phase deposition.

Chemical vapor deposition (CVD), unlike PVD, involves a chemical reaction during the deposition process. The precursor is evaporated in an oven, and then transported by a carrier gas to a substrate, where it is condensed to form solid nanomaterials. This synthesis technique is widely used for the elaboration of thin films. By controlling the synthesis parameters, such as carrier gas flow rate, pressure, temperature and geometry of the deposition reactor, various geometries of nanomaterials have been obtained [16-19].

1.1.3. Synthesis method in liquid phase.

1.1.3.1 Sol-gel synthesis method

The sol-gel technique is a process of materials elaboration (ceramic, organic-inorganic hybrid, thin layers), in solution and at room temperature. This process takes place in two steps, first the hydrolysis of a titanium precursor, generally an alkoxide ($Ti(OR)_4$, where R is an alkyl radical of the methyl, ethyl, isopropyl or tetra-butyl type, leading to the bonding of a hydroxide group with the metal atom. Subsequently, the condensation of the hydrolyzed product leads to the initiation of the nucleation/growth process, which leads in a subsequent step to the formation of a colloidal solution. The latter is transformed into a solid gel after evaporation of the solvent. During these reactions, an acid or basic catalyst is added, such as HCL, NaOH, NH_4OH etc. By varying the synthesis parameters, such as pH, precursor, catalyst etc. it is possible to control the properties of the synthesized materials, in terms of size, morphology and phase. Different morphologies have been obtained, using the sol gel synthesis process, such as nanowires, nanoparticles, nanoribbons etc. [20-23]. The family of sol gel synthesis techniques also includes the methods of synthesis by precipitation, which consists in mixing two solutions of reagents, to obtain a solid product after precipitation.

These sol-gel synthesis techniques have the advantage of being easy to implement, flexible, and allow to obtain pure materials and homogeneous deposits on large surfaces.

1.1.3.2 Methods of electrochemical synthesis.

Electrochemical methods, in particular electrodeposition, are frequently used for the elaboration of nanomaterials and thin films of TiO_2. To implement the electroplating process, two electrodes are needed, one acting as anode and the other as cathode. The two electrodes are immersed in an electrolyte, ensuring ionic conduction between the two electrodes, and containing the salt of the material to be deposited on the cathode. The most commonly used titanium precursors are: $TiO(SO_4)$, $(NH_4)TiO(C_2O_4)_2$, $TiCl_3$.

For the control of the morphology of electrodeposited nanomaterials, different approaches have been used. Alumina molds as anode, is one of the approaches for the preparation of TiO_2 nanotubes. On the other hand, by using the parameters of the technique, such as potential, precursor concentration, electrodeposition time, current density, temperature, or PH, it is possible to control the morphology and crystal structure of TiO_2 [24-25].

1.1.3.3 Hydrothermal and solvothermal synthesis methods.

These methods include different synthesis techniques, taking place in a solvent at high temperature and high pressure. When the solvent is an aqueous solution, it is called hydrothermal method, and when it is an organic solution, it is called solvothermal method. The synthesis is carried out in a sealed steel vessel called an autoclave (Figure 1). In the case of hydrothermal synthesis of TiO_2, the chemical reaction between a titanium precursor and an aqueous solvent is carried out in an autoclave at a temperature higher than 100°C and at a pressure higher than 221.2 bars. Under these conditions, the densities of the water gas and liquid are close, and the chemistry of the cations in solution is significantly modified.

Figure 1 : Photograph of a Parr company reactor used for hydrothermal synthesis.

The most used Ti precursors are titanium alkoxide Ti(OR) in the presence of acids, such as $TiOSO_4$, $H_2TiO(C_2O_4)_2$, $TiO(NO_3)_2$, amorphous gels of TiO_2, nH_2O or $TiCl_3$, $TiCl_4$, $TiOCl_2$, [26-30]. The first works on the synthesis of TiO_2 by the hydrothermal method were performed by Kasuga et al [31], later this technique was taken up by Armstrong et al for the preparation of TiO_2 nanowires [32].

These methods offer the advantage of preparing powders and nanomaterials on a large scale with perfectly controlled physicochemical characteristics, such as size distribution, morphology, purity, homogeneity, composition, structure, etc. They also have the advantage of creating unstable crystalline phases under standard conditions. Thus, it is possible to form only the anatase phase or the rutile phase or a mixture of both. This control of properties is made possible by adjusting the synthesis parameters: reaction time, precursor concentration [33-35], temperature [36-38], pH [39-43], addition of additives and pressure [44].

By using oxidants, such as H_2O_2, it is possible to prepare TiO_2 crystallites by a dissolution-precipitation mechanism. The addition of additives, such as NaX where X can be F^-, Cl^-, SO_4^{2-} or OH^-, allows the synthesis of different morphologies, such as nanowires, nanoribbons, nanosticks, nanotubes, and nanourchins. Moreover, the nature of the ion considerably influences the structure of the phase of prepared TiO_2 powders, thus the use of F^- and SO_4^{2-} ions allows the formation of the anatase phase, while Cl^- is rather the rutile or brookite phase [45-50].

This process is used in industry, and allows the controlled preparation of various powders, such as quartz (SiO_2), Berlinite ($AlPO_4$), as well as metastable phases, such as zeolites.

In this thesis, we used hydrothermal synthesis for the preparation of TiO_2 powders. For the synthesis, the chemical reactor we used is an autoclave manufactured by the Parr company, with a volume of 23ml (Figure. 1). The pressure in the reactor is autogenous and depends on both the synthesis temperature and the volume of the solution used. The synthesis temperatures are between 180 °C and 220 °C, which allows to reach pressures ranging from 10 to 23 bars. Under these conditions, the critical state of water is not reached (Tc H_2O=374 °C and pc H_2O=221) but allow to decrease sufficiently the dielectric constant of water and to influence considerably the reaction equilibria.

1.1.4. Structural and crystallographic properties of TiO_2

TiO_2 crystallizes under different polymorphs, the most known of which are: anatase, rutile, brookite. These three polymorphs are formed by assembling an octahedral structural unit to form different crystallographic structures of TiO_2. This structural unit is formed by a Ti^{4+} ion which is surrounded by six O^{2-} ions (Figure 2). Other polymorphs, eight in number, have been listed and prepared from rutile structure: Bronze (TiO_2-B), Columbite or srilankite (TiO_2 -II) of the same structure as PbO_2, Hollandite (TiO_2-H), Ramsdellite (TiO_2-R) Banddeleyite (TiO_2-III) [51]. These polymorphs were observed at particular pressures and temperatures, for example, the baddeleyite phase was observed at pressures of about 10 Gpa [52].

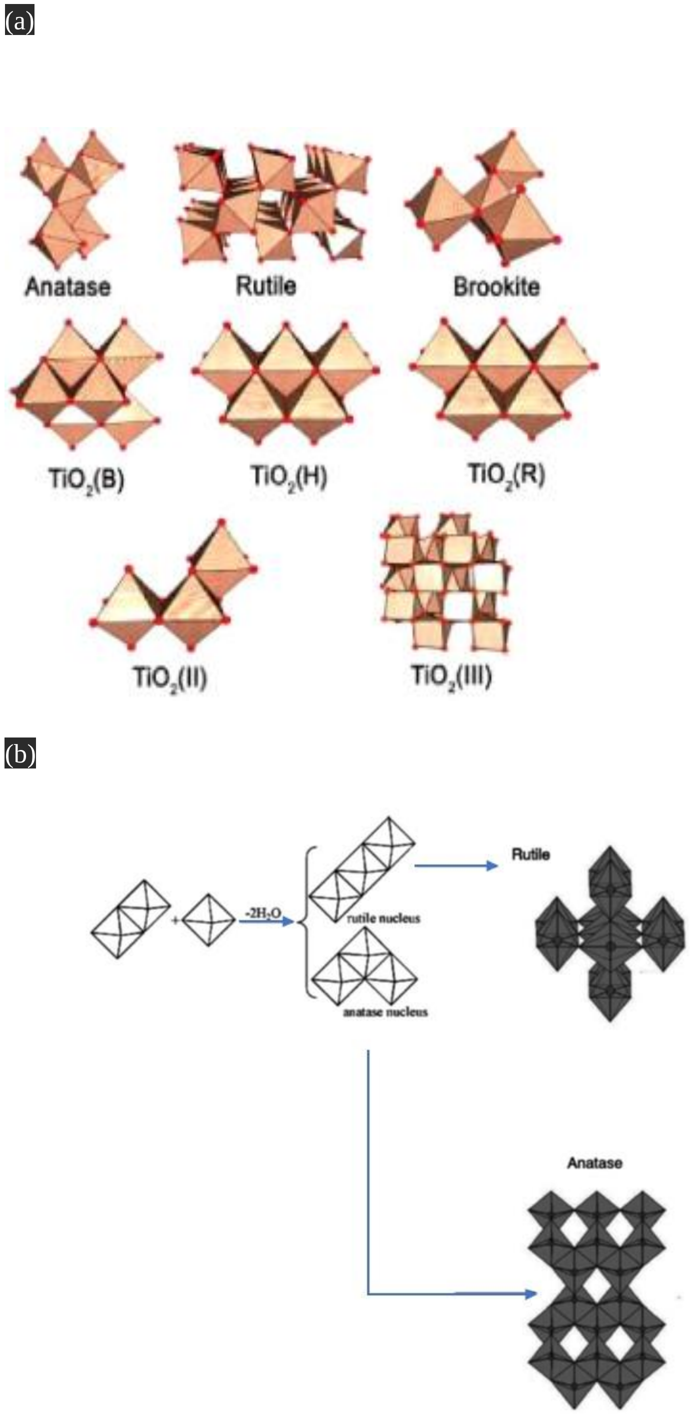

Figure 2 : (a) The different polymorphs of TiO_2 (b) Suggested mechanism of arrangement of the third TiO_6 octahedron for the formation of the rutile and anatase phases [53].

As schematized in Figure 2, the arrangement of the TiO_6 octahedra will define the crystal structure being formed. If the first stage of growth corresponds to the formation of a dimer in which the two octahedrons of TiO_6 share an edge, according to the configuration formed by the addition of the third octahedron, the rutile phase or mesh anatase is formed (Figure 2). The structure of the rutile phase is formed by TiO_6 octahedra, which share their two opposite edges with adjacent octahedra, thus forming a chain (Figure 2(b)). For the anatase phase, the TiO_6 octahedra are connected by edges to form a zigzag chain (Figure 2(b)). In the case of TiO_2(B), the TiO_6 octahedra are connected to each other by edges, to grow in a chain along one axis and in a zigzag along another axis (Figure 2(a)). The association of the chains by pooling their vertices is shown in Figures 2(a) and 2(b). The rutile phase is thermodynamically stable at high temperature, while the anatase phase is more stable at low temperature. On the other hand, the anatase crystallizes in the form of small particles, under the conditions of low temperature and in solution of low acidity unfavorable to the dissolution of the solid phase formed. In solutions with higher acidity, it is rather the rutile phase, which is more favorable, with the formation of particles of larger size. Moreover, it is clearly established that the equilibrium of dissolution-precipitation favors the formation of rutile phase to the detriment of the anatase phase [54].

Other experimental conditions can have a considerable influence on the formed phase or phases, thus the hydrolysis of the $TiCl_4$ precursor in vapor phase leads to the formation of the only rutile phase.

Furthermore, ions in solution can also have a control on the formed phase or phases, as already mentioned in the hydrothermal synthesis section. The stability of the anatase and rutile phases also strongly depends on the size of the TiO_2 nanomaterials and their surface state. It has been reported by theoretical studies, that the critical size for the anatase-rutile phase transition depends on the surface state of TiO_2 nanomaterials. For example, the adsorption of water on the surface of TiO_2 nanomaterials stabilizes the anatase phase and increases the critical size for the anatase-rutile transition to 15 nm [55].

1.1.4.1 Control of TiO_2 morphology.

Different morphologies of TiO_2 have been prepared by the hydrothermal method. The synthesis of TiO_2 nanotubes was first reported in the literature by the group of Kasuga et al [56]. Almost all the works on the synthesis of TiO_2, with different morphologies, share the fact of using the mixture of a TiO_2 precursor and a concentrated solution of NaOH. This step is followed by a heat treatment and a rinse with water or acid. Several parameters were varied, for the control of the TiO_2 morphology, such as the nature of the solid precursor (TiO, Ti_2O_3, TiO_2 anatase, TiO_2 rutile, etc), the concentration of the alkaline solution (5 - 15 mol. L^{-1}) and that of the titanium (0.01 - 0.62 mol. L^{-1}). Other parameters such as the synthesis and heat treatment temperature and time play an important role. The size of the solid titanium precursor, the nature of the rinsing solvent (water and/or acid) and the volume introduced in the autoclave contribute to control the morphology of TiO_2.

By controlling the synthesis parameters, different morphologies have been prepared, such as nanosheet, nanotube, nanowire, nanobaguette, nanofiber, nanocore or nanoribbon. These morphologies are classified in 4 families according to Bavykin et al [57] (figure 3).

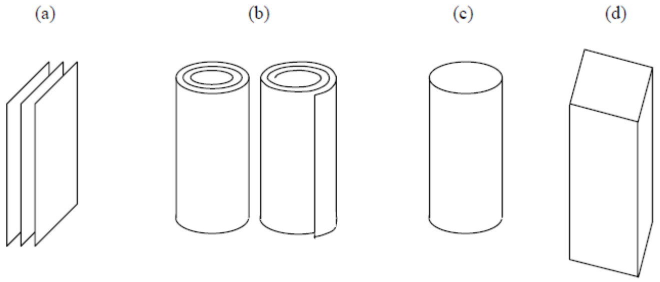

Figure 3 : The different nanotitanate morphologies reported in the literature following alkaline treatment (hydrothermal or thermohydrolysis) of precursor TiO_2. (a) Nanosheet (b) nanotube, (c) nanowire, (d) nanofiber, nanoribbon or nanobelt.

The transition from one morphology to another was studied by the group of Morgan et al, in a diagram based on the temperature of the heat treatment and the concentration of the NaOH solution (figure 4) [58].

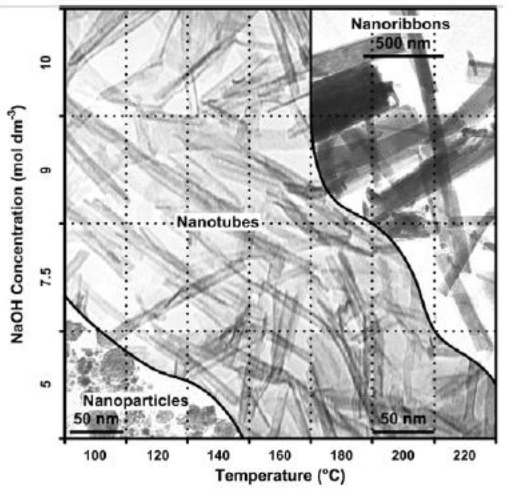

Figure 4 : Morphological phase diagram of TiO_2 particles (Degussa P25) after 20 h of alkaline treatment. The phase boundaries are estimated from the relative concentrations of the nanostructures obtained by X-ray diffraction and Raman spectroscopy [58].

In the phase diagram, we distinguish three domains corresponding to those of nanoparticles, nanotubes and nanorubans. It can be noticed that nanotubes and nanorubans are obtained and favored by high temperatures and concentrations, and that the nanotube/nanoruban transition happens at higher temperature and concentration of solution. On the other hand, the formation of nanosheets takes place at low temperature, and can be favored by short processing times. The nanoparticle/nanotube transition zone is formed by a mixture of nanosheets and nanotubes, which may suggest that it is probably the nanosheets that evolve into nanotubes, through coiling mechanisms (Figure 5). The details of these mechanisms remain very controversial in the literature and it is an open question.

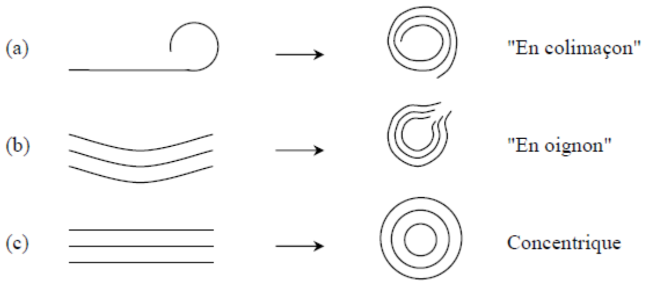

Figure 5 : Illustrative diagram of the possible mechanisms of nanotube formation from nanosheets: (a) spiral winding of a nanosheet, (b) bending of a few nanosheets and (c) direct production of concentric multiwall nanotubes.

Three configurations of nanosheet winding have been reported in the literature [59]. As shown in Figure 5, there can be spiral winding of a nanosheet, bending of a set of nanosheets, to form an onion structure or concentric assembly of nanosheets. Among these configurations, the spiral winding of nanosheets is the most observed [60-62]. However, onion-type nanotubes [63] remain very rare and concentric-type nanotubes very unlikely.

Given the different controversial results in the literature, it is very difficult to lean towards one mechanism and not another. The mechanism of formation of nanoribbons, remains unknown and subject to debate in the literature [64].

1.1.5. Relationships Properties and applications in the case of TiO_2 nanomaterials

1.1.5.1 Electronic and optical properties of TiO_2.

The properties of TiO_2, are mainly related to its electronic band structure, which is different for each of its phases. TiO_2 is a semiconductor, which has a large band gap, located between the valence band maximum and the conduction band minimum. Moreover, the valence band is formed by the p-orbitals of oxygen, while the conduction band is formed by the d-orbitals of titanium. For the best-known polymorphs of TiO_2, the energy of the band gap is 3.26 eV, 3.05 eV and 3.14 eV for the anatase, rutile and brookite phases respectively.

When TiO_2 polymorphs are irradiated by a UV photon flux, with an energy equal to or higher than their band gap, the electrons of the valence band are excited by absorption of a UV photon and pass into the conduction band. Following this absorption phenomenon, a hole is formed in the valence band at the femtosecond scale and an electron-hole pair is created. The latter diffuse in the material, to be trapped either in volume, or in surface at time scales respectively of the order of 10 ns and 100 ns, before recombining at time scales between 10 and 100 ns.

In addition, TiO_2 has very interesting optical properties, including a very high refractive index required for transparent components with antireflective properties. Among the three most known phases of TiO_2, the rutile phase has the highest refractive index and is able to reflect 96% of the light in the visible range. This property gives micrometric TiO_2 powders a white color, which makes them the pigments of choice in industry (paints, coatings, plastics, inks, medicines and toothpastes, food coloring...).

1.1.5.2 Applications of TiO_2 nanomaterials.

Titanium dioxide has remarkable properties, which make it a material of choice for many industries, such as automotive, food, cosmetics etc. The first commercialization of TiO_2 was in 1921, as a pigment in paints. Moreover, the degradation of these pigments under the effect of sunlight, highlighted the photoactivity of TiO_2 around 1929, and the results on the discoloration of pollutants were published in 1938 [65]. Mashio et al was the first to use the terminology "photocatalysis" in 1956, to designate the oxidation of alcohol under irradiation. The dissociation of water under light exposure, also called photolysis, to produce hydrogen and oxygen using TiO_2 was achieved in 1972 [66]. The low potential of the valence band of TiO_2, makes it very oxidizing, when exposed to high energy radiation such as UV rays.

TiO_2 has also been used in the food industry as a colorant under the reference E-171. In addition, TiO_2 is used in the cosmetics industry, in particular in sunscreens with high protective power, for the elimination of UV radiation harmful to health. The antibacterial properties of TiO_2 have been widely used for sterilization and thus elimination of bacterial germs [67-72]. The team of Fujishima et al. highlighted another property of TiO_2, which is the photoinduced super hydrophobicity upon exposure to UV radiation. Based on this property, the anti-fogging application was developed [73]. On the other hand, by combining the two properties of TiO_2 superhydrophilicity and photocatalysis, another application as a self-cleaning coating has been developed [74]. Indeed, the photocatalytic property ensures the degradation of pollutants on the surface by oxidation, and the superhydrophilic property takes care of their removal thanks to the water film on the surface [75]. Saint-Gobain has used these properties of TiO_2 to develop self-cleaning glasses. Gas detection is another application of TiO_2, using the variation of its electrical conductivity when interacting with a gas [76].

In addition, TiO_2 has been widely used in the energy field for various solar energy conversion and storage applications. In 1991 Grätzel and O'Regan [78] developed dye-sensitized solar cells, based on TiO_2 sensitized by a dye to be able to absorb in the visible and infrared spectral regions. TiO_2 has also been used as an anode material for lithium-ion batteries [79].

State of the art on Lithium-ion batteries

The exploitation of renewable energies has raised the issue of intermittency, and to remedy this and ensure the restitution of energy on demand, various storage systems have been developed. These are classified into several families, firstly batteries which are primary non-rechargeable systems, and accumulators which are secondary reversibly rechargeable systems allowing to convert chemical energy into electricity. Finally, the term "battery" refers to a set of several accumulators, connected in parallel or in series.

Historically, lead-acid batteries were the first to meet the need for energy storage, for 150 years and still exist. These batteries are mainly used in the automotive industry and have the advantage of being economical and easily recyclable, but nevertheless have the disadvantage of having a relatively low energy density (Figure 6). Moreover, because of their weight, they are not adapted to portable technologies (figure 6). The presence of lead in these batteries makes them very dangerous pollutants for the environment and health. In 1950, nickel cadmium batteries were developed, and for years they were the consumer technology. Because of the toxicity of cadmium, the marketing of these batteries was imposed the respect of certain rules for the protection of the environment. Ni-MH (Nickel Metal Hybrid) batteries were developed in the 1990s. This family of batteries offers the advantage of having a moderate memory effect, but a low storage density (figure 6), and poor performance at low temperatures. Another handicap of these batteries is their high self-discharge rate of about 30% per months.

Currently, among the family of secondary batteries, lithium-ion batteries are the most suitable for portable technologies. They offer both a high theoretical energy density of 3860mAh/g (Figure 6) and a high voltage, as well as a low self-discharge of about 10% per year.

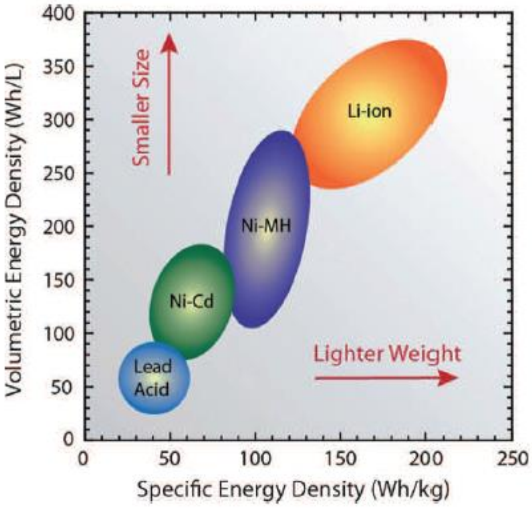

Figure 6 : Comparison of gravimetric and volumetric energy density for different secondary batteries [80].

2.1. Chemical constituents of batteries

In general, a battery consists of a cathode and an anode, which represent the positive and negative poles, respectively. The two electrodes are separated by an electrolyte and connected to the external electrical circuit by means of a current collector.

2.1.1 electrolyte

For Lithium-ion batteries, different electrolytes have been used in liquid, gel, or polymer form. The electrolyte used must have a good ionic conductivity, but its electronic conductivity must be low to avoid short-circuiting the battery. The electrolyte used in lithium-ion batteries often consists of a lithium salt dissolved in a dipolar aprotic solvent. During operation of the lithium-ion battery, oxidation or reduction of the electrolyte can occur, as none of the components of the currently used electrolytes can remain electrochemically inert between 0 V and 4.5 V with respect to Li^+ /Li.

Alkyl carbonates have been used extensively as solvents in lithium-ion batteries. Cyclic esters, such as propylene carbonate (PC) and ethylene carbonate (EC), are added to the electrolyte to improve its ionic conductivity. These solvents have the advantage of having a high dielectric constant, a consequence of their high dipole moment, and their strong intermolecular bonds give them a high viscosity. Other solvents, such as diethyl carbonate (DEC) or dimethyl carbonate (DMC) are added to the electrolyte to reduce the viscosity of the mixture. In order to improve the performance of the electrolyte, other solvents have been developed and tested, such as butylene trans-carbonate [81] and chlorinated [82] and fluorinated alkyl carbonates [83].

2.1.2 The positive electrodes: Cathode

As cathode materials, lithiated transition metal oxides, such as $LiCoO_2$ and $LiNiO_2$ have been used extensively, due to their better electronic conductivity and reversibility of lithium-ion intercalation at high potentials (Figure 7). Other materials, such as $LiMn_2O_4$ or $LiFePO_4$ have been used because of their low cost and low toxicity.

Among the developed materials, $LiCoO_2$ remains the material of choice frequently used in commercialized lithium-ion batteries. Its lamellar and hexagonal structure gives it a theoretical capacity of about 274 mAh/g corresponding to the intercalation of a lithium ion at a potential of 4V compared to Li^+/Li. Even if $LiCoO_2$ presents several advantages, it suffers from a handicap related to the irreversibility of the intercalation of lithium ions. This is due to phase transitions in the material, during intercalation at potentials higher than 4.2V. Furthermore, the dissolution of Co and the irreversibility of lithium intercalation lead to a decrease of the battery capacity to about 150 mAh/g, which corresponds to the intercalation of 0.5 moles of lithium per mole of cobalt. To remedy this problem, solutions have been reported in the literature, such as the deposition of coatings based on ZrO_2 [84], MgO [85], Al_2O_3 [86] or AlF_3 [87-89], to protect the cathode.

Until today, the $LiCoO_2$/graphite couple remains the most abundantly used, for lithium-ion batteries, because of its better performances, operating potential, and mass capacity.

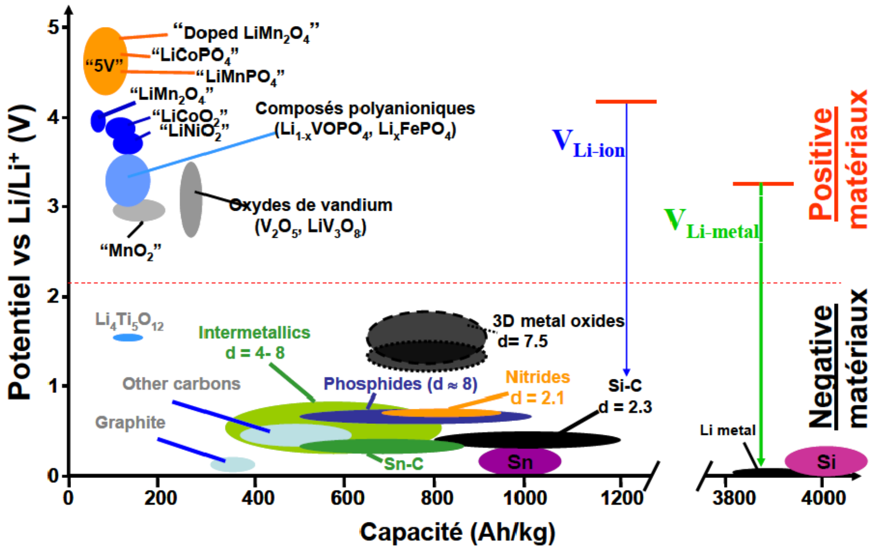

Figure 7 : The most used electrode materials according to their capacity and potential [90].

2.1.3 The negative electrodes: Anode

Different materials have been used as anode materials for lithium-ion batteries (Figure 7). Spinel type materials such as $Li_4Ti_5O_{12}$ have been used, but due to their very limited performances, such as, their low capacity of 175 mAh.g^{-1} and their voltage of 1.5 V compared to Li^+ /Li, have been the reason of their perennial use. On the other hand, tin-based materials, such as Li_2CuSn [91] and Cu_6Sn_5 [92] have also been used. Other materials have been investigated, such as those based on aluminum, silicon and antimony [93].

Among these materials, carbonaceous materials have been used in abundance (in particular graphite), because of their better cyclability, their low cost, their electrochemical potential close to that of lithium and finally their lightness which favors their use in portable technology. It has been shown that the theoretical capacity of graphite is 372 mAh/g, which corresponds to a maximum insertion of one lithium atom for 6 carbon atoms (LiC_6).

One of the problems encountered with this type of anode is the presence of an irreversible capacity, during the first cycles of the battery. This is due to the formation of a passivation layer on the surface of the electrode, and the consumption of part of the cathode and lithium in the electrolyte. In spite of this drawback, carbon graphite offers a significant advantage, which is its low volume variation (<10%), when intercalating lithium ions.

The graphite structure is formed by graphene sheets linked by weak Van der Waals bonds. Lithium ions are inserted between the graphene sheets and in the defects of the sheets, this generates different insertion rates, which results in different potentials between 0 V and 0.25 V with respect to Li^+/Li [94]. Graphite-based anodes offer interesting performances, which depend on their crystal structure, size, morphology, specific surface, porosity, purity, and surface composition [95].

Nevertheless, the capacity of graphite remains limited, due to the small number of lithium ions that can intercalate in its crystalline structure. Other carbon structures, such as nanotubes, offer a high capacity of up to 1000 mAh/g, when the structure has several defects [96]. Despite their high capacity, these materials have the disadvantage of being expensive and highly irreversible during the first cycles.

The development of lithium-ion batteries, which have a high cyclability and thus a long lifetime with better performance, remains a challenge until today. Titanium dioxide as an anode material could be a potential candidate, to overcome the problems faced by other anode materials. Titanium oxide has several properties, which can improve the performance of lithium-ion batteries, it allows a reversible and more stable reaction with lithium compared to graphite, which promotes a long service life. Although TiO_2 as an anode provides some improvements to the performance of lithium-ion batteries, there are still some challenges. TiO_2 has the property of having a higher potential than graphite, which makes it a material of choice for low energy, long life applications such as laptops and smartphones. The insertion of lithium ions into the anode materials is done according to different mechanisms, with or without a significant volume variation. We can distinguish:

Intercalation materials:

In intercalation materials, lithium is inserted into the vacant sites of the crystal structure. The materials mentioned above, such as TiO_2, belong to this family of materials (figure 8).

Alloys:

Another mechanism of insertion of lithium ions into electrode materials is the formation of an alloy (Figure 8). Many metals and semiconductors react with lithium, and among these materials we can mention, tin, silicon, germanium, etc. [97-99].

Among the advantages of these materials, the ability to accommodate more lithium ion than intercalation materials, giving them a greater theoretical specific capacity. Silicon offers the highest theoretical capacity of 4200 mAh/g. Their insertion potential is generally slightly higher than that of graphite. This helps to reduce the risk of lithium metal deposition on the surface of the electrode and allows satisfactory voltages. Unfortunately, these materials have the disadvantage of a significant volume variation during the insertion of lithium ions and the formation of alloys (200 to 300%). This volume variation is accompanied by strong mechanical constraints, which results in the disintegration of the electrodes, a bad cyclability and a reduction of their lifetime.

TiO_2(B) accommodates Li^+ ions better, compared to other polymorphs, to form Li_xTiO_2(B), with, x, the maximum coefficient of intercalation of lithium ions by TiO_2, and which is between 0.70 and 0.82, and depends on the size of the nanoparticles and the range swept in potential [100-102]. Indeed, the structure of TiO_2(B) has infinite parallel chains of TiO_6 octahedra in the three crystallographic directions and which offer a space between the chains, which can accommodate lithium ions without significant distortion of the structure [103].

Conversion materials:

In the case of these materials [104-105], the mechanism of insertion of the lithium ions is done according to a conversion reaction (figure 8). This reaction consists in transforming the oxide into metal, of different nature and structure. Among these materials, we find the transition metal oxides, such as CoO, CuO and Fe_2O_3. The conversion reaction takes place according to the following reaction scheme:

$$MO + 2Li^{+} + 2e- \leftrightarrow M_0 + Li_2O$$

With M=Co, Cu, Ni, Fe. This reaction leads to the formation of metallic nanoparticles trapped in an amorphous matrix of Li_2O. The capacity of these materials can reach up to four times that of graphite. Even if these materials offer the possibility of having high capacities, they have the disadvantage of having slow reaction kinetics, which results in the appearance of a strong polarization of the system [106].

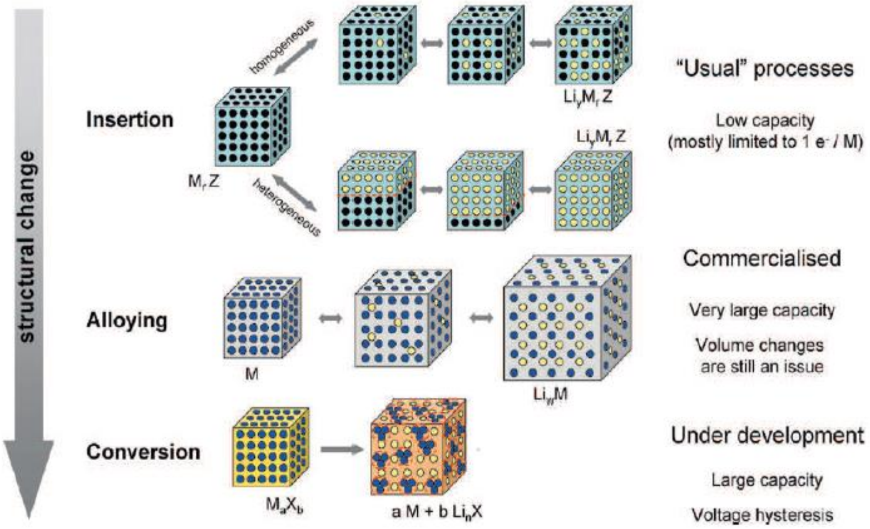

Figure 8 : Illustrative diagram of the different mechanisms of insertion of lithium ions in the electrode materials of a lithium-ion battery. The black circles represent the gaps in the crystal structure of the solid, the blue circles the metal atoms, and the yellow circles the lithium ions [107].

2.2. Operating principle of lithium-ion batteries

When an electronic device is powered by a lithium-ion battery, the battery undergoes a discharge process, during which lithium ions (Li^+) move from the negatively polarized anode to the cathode, which is more positively polarized (Figure 9). When the battery is discharged, the lithium ions are deintercalated at the anode and intercalated into the cathode material (Figure 9). The electrolyte, which has a good ionic conductivity, ensures the movement of lithium ions between the electrodes. In addition, electrons move from the anode to the cathode. In the case of the battery charging process, the phenomena are reversed, and the lithium ions move from the cathode to the anode, while the electrons move in the opposite direction.

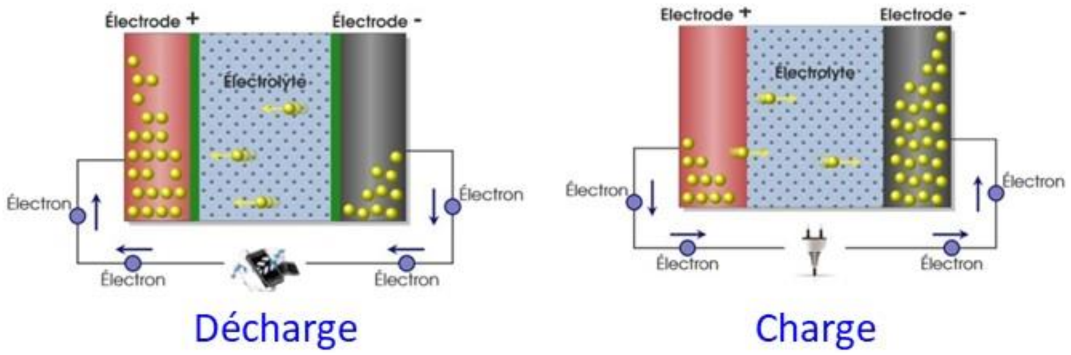

Figure 9 : Illustrative diagram of the operation of a lithium ion battery, during discharge (left) and charge (right).

During the discharge process, in the case of a graphite anode and a $LiCoO_2$ cathode, the electrochemical reactions at the electrodes are the following:

At the anode: The lithium metal trapped in the graphite is oxidized into Li^+ ion, which passes into the electrolyte (Eq. (1)).

$$LiC_6 = 6\ C + Li^+ + e^- \qquad \text{Eq (1)}$$

At the cathode: Lithium ions are reduced to lithium atoms and are inserted into the mixed oxide (Eq. (2)).

$$Li_{1\text{-}x}CoO_2 + x\ Li^+ + x\ e^- = LiCoO_2 \qquad \text{Eq (2)}$$

2.3. The electrical parameters characterizing the batteries

The characteristic quantities allowing to compare the performances of different cells are detailed below:

- The cell voltage (E), or electromotive force (e.m.f.): corresponds to the difference between the potential of the positive electrode and that of the negative electrode, and depends strongly on the materials of the two electrodes.
- The capacity (Q): corresponds to the quantity of charges that the battery can restore at a given current, it is usually expressed in Ampere-hour (Ah). The optimal functioning of a battery is reached when the capacities of the anode and the cathode are equal (same charge tank). The performance of the electrodes is evaluated by their specific capacity or mass capacity. The theoretical specific capacity depends on the number of electrons that can be exchanged during a single charge or discharge per mole of active material, as expressed by equation 3,

  $\text{Capacity}_{\text{Theoretical}} = (F \times n_{e^-\ \text{exchanged}}) / (3600 \times M)$ (in mAh.g^{-1} or Ah.kg^{-1}) Eq (3)

  With, M, the molar mass of the material, and, F, the Faraday constant.
- Energy: corresponds to the product of the electromotive force of the battery by its capacity and is expressed in Wh or kWh. In addition, it corresponds to the area under the voltage curve as a function of capacity, as shown in Figure 10. The energy density is the most commonly used, to compare different battery technologies, and is expressed in Wh/kg or Wh/L. As all the components of the battery are not electroactive, but contribute to its total mass and volume, the actual energy density is lower than the theoretical energy density, calculated taking into account only the electrode materials. In practice, capacity and energy are often reduced to the volume or mass of active material or the generator itself.
- Power: corresponds to the speed at which energy can be supplied or extracted from the battery, and is expressed as the ratio of energy to time.

- State of Charge: corresponds to the percentage of available capacity of the battery (SOC: State of Charge). If we compare the battery to a tank, the state of charge reflects the level of charge of the tank.
- The internal resistance: It evaluates the voltage drop when the current passes through the battery. To maintain the performance of the battery, it is necessary to reduce its internal resistance. It is a characteristic, which evolves according to the temperature and time because of the ageing of the battery.

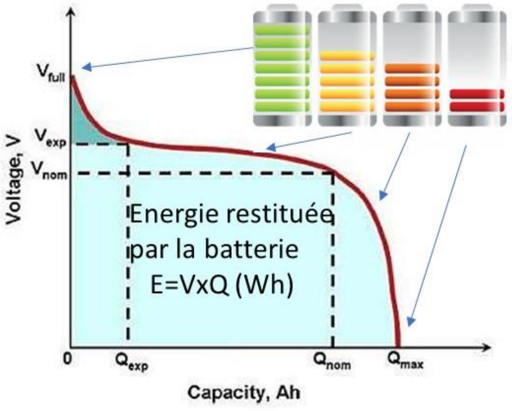

Figure 10 : Curve of the voltage versus the capacity characterizing the discharge of a battery.

- The cycling regime C/n: corresponds to the theoretical capacity obtained during the charge in n hours,

2.4. Parameters affecting battery performance

Often the lithiation/delithiation phenomena are accompanied by a volume expansion of the electrodes. The consequences of this variation in electrode volume are, on the one hand, the electrical disconnection of part of the electrode and, on the other hand, the delamination of part of the electrode from the current collector [108], which leads to a drop in the battery's capacity.

2.4.1 Effect of the electrodes nanostructuring

The nanostructuring of the electrode limits its degradation and improves its lifetime. Therefore the number of charge/discharge cycles is considerably increased, as long as the deposition of lithium metal on the electrode is not favored. Moreover, the operating temperatures are between less than 30°C and about 45°C, and the use of nanostructured materials does not increase the manufacturing cost of the electrodes.

By analyzing the Einstein equation (Eq. 4) we can see that one of the ways to reduce the diffusion time is to reduce the size of the materials.

$$t = d^2/(2D_{Li}) \quad (4)$$

With, d the diffusion length, t the diffusion time and, D_{Li} the diffusion coefficient, which is considered constant at a given temperature. It has been reported in the literature that a reduction in size from 100nm to 10nm, decreases the diffusion time from 300 to 3s for a diffusion coefficient of 10^{-13} cm^2/s [109]. Other works in the literature have confirmed this result, and have shown in the case of TiO_2 nanomaterials, that a decrease in size improves the insertion of lithium ions (Figure 11). This decrease in size is accompanied by an increase in the specific surface area, and makes it possible to reach capacities higher than that of the bulk material of the order of 165mAh/g corresponding to the insertion of 0.5 Li. The rate of intercalation in TiO_2 nanoparticles is increased in comparison with their massive form for brookite [110-111], rutile [112-113] and anatase [114-115].

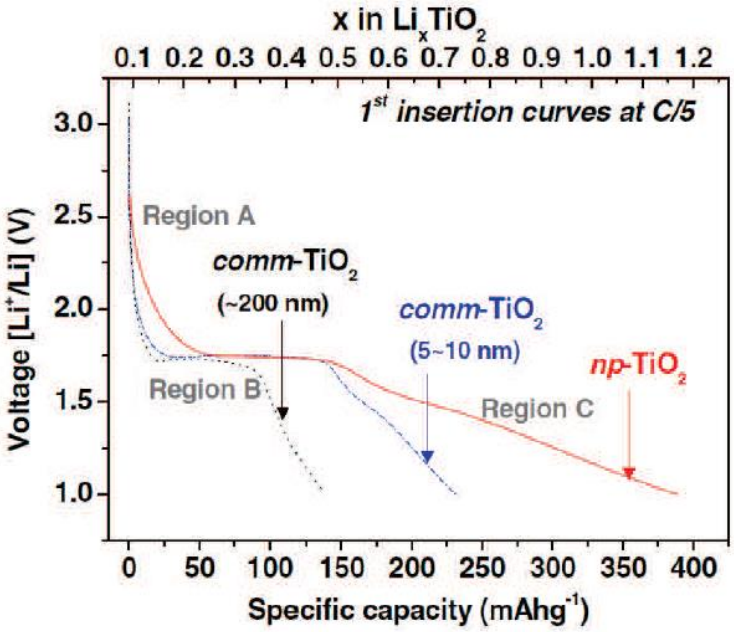

Figure 11 : The curves represent the first galvanostatic discharge, of a commercial TiO_2 anode with different nanoparticle sizes, and of a nanoporous TiO_2 anode [116].

It is very important to note that, if the nanostructuring of the electrodes improves the performances of the lithium-ion batteries, it allows the exposure of a very large surface of the active material to the electrolyte, which exalts the reactions of degradation of the latter [117].

2.4.2 Effect of electrode porosity

In addition to the reduction of the diffusion length, and the increase of the specific surface, brought by the nanostructuring of the electrodes, other parameters, such as the control of the porosity, can considerably improve the cyclability of the lithium-ion battery. Indeed, the porosity, in terms of pore size and distribution, favors the penetration of the electrolyte into the electrode materials, and allows to reach the majority of their surface. Moreover, this porosity created in the electrode, allows to reduce the diffusion length of the lithium ions, which also reduces the time of the charge and discharge cycles. In addition, the large specific surface of the electrode considerably improves the insertion of lithium ions, and therefore the capacity of the battery. The porosity also participates in the accommodation of the electrodes volume variation, during the cycles of insertion/desertion of the lithium ions. This improves the cyclability of the lithium-ion batteries. It has been reported in the literature that the coupling between, the increase of the diffusion rate of lithium ions in the interconnected network of pores, and the large surface of TiO_2 in contact with the electrolyte, participate to significantly improve the capacity and the lithiation/delithiation rate [118-119]. Other results have shown that the homogeneity of the size, shape and interconnectivity of the pores play a decisive role in improving the cyclability of the lithium-ion battery electrodes. It was also reported, that the mesoporosity of the electrodes gives better performance than the nanoporosity, and the capacity can reach 300mAh/g ($Li_{0.96}TiO_2$) [120].

Liu et al, reported that the advantage of a mesoporous TiO_2 structure to improve the energy density of lithium-ion batteries, lies in increasing the diffusion rate of lithium ions in the electrode material [121]. Very recently, other authors have shown that TiO_2 nanosheets, allowed to expect a capacity of 200mAh/g at 10C after 200 charge/discharge cycles [122].

2.4.3 Effect of electrode doping

The various TiO_2 polymorphs suffer from their very low conductivity (10^{-12} - 10^{-7} S/cm), which reduces their performance as battery insert materials. The low conductivity of TiO_2 is a consequence of its large band gap, and the absence of electron on the d-sub layer of Ti^{2+}.

Doping is used as one of the ways to improve the conductivity of TiO_2. Depending on the doping element and the doping technique used, the dopant can either insert itself in the gaps of the crystal lattice or substitute itself to an atom of the TiO_2 lattice. The doping elements insert intermediate energy levels in the energy band gap of TiO_2. This allows lower energy electronic transitions, which would improve the conductivity of TiO_2 [123-125]. The dopants used can be of type-p, with a valence lower than 4, that of Ti in TiO_2, and which behave like acceptor centers which capture the photoelectrons, and in a reverse way, the dopants of type-n with valence higher than 4, behave like donor centers [126-127]. These studies have shown that a small amount of dopant can significantly increase the conductivity of TiO_2. Different elements have been used to dope TiO_2, such as metal cations (transition or rare earth metals) [128-135] or anions (N, F, C ...) [136-154]

This way of doping to improve the conductivity of TiO_2 and thus the performance of lithium-ion batteries, will not be studied in this thesis work.

Conclusion

In the best-known titanium dioxide compounds, namely anatase, brookite, rutile and TiO_2(B), titanium forms an octahedral structure with oxygens at the apices. The crystal structure of these titanium polymorphs differs only in the arrangement of the titanium octahedra (TiO_6), which are assembled either through their edges, or through their vertices, or both.

In recent years, one of the most popular methods for the synthesis of TiO_2 nanomaterials is hydrothermal synthesis. This method has allowed the synthesis of various TiO_2 morphologies, and the "Kasuga" group was one of the pioneers to show the control of TiO_2 morphology, using a solvated TiO_2 precursor, in a concentrated NaOH solution. The participation of the hydroxo ligand in the solvation sphere of titanium, in a wide range of pH, strongly contributes to the condensation of titanium oxides. This chemistry is still poorly understood and remains an area of investigation for many researchers around the world. The condensation reaction can take place through two types of nucleophilic substitution reactions: olation which leads to the formation of a hydroxo bridge and oxolation which forms an oxo bridge between the metal cations. A modification of the chemical parameters such as the pH is sufficient to modify the condensation of the titanium oxides and leads to products, structurally and/or morphologically different.

Among the most synthesized TiO_2 morphologies are nanosheets, nanotubes, nanoribbons and nanowires. During the synthesis of TiO_2 in a concentrated solution of NaOH, two intermediates are formed: titanates and titanic acids. Immediately after synthesis, sodium titanates are formed with different morphologies as mentioned above, depending on the synthesis parameters. The sodium titanate is transformed into titanic acid, after a process of ion exchange in acid medium. The titanium dioxide TiO_2 is obtained, after annealing, and in general it is a mixture of phases. Through the different stages of synthesis, the phase changes but not the morphology. In the mechanisms of elaboration of these morphologies, several questions remain open and controversial in the literature and will be subject of interest in this thesis work.

Anode materials for lithium-ion batteries are one of the applications of TiO_2 materials. During the discharge process, TiO_2 materials allow the insertion of ions into the gaps formed by the TiO_2 structure. Therefore, the less dense TiO_2 polymorphs will be potential candidates for lithium ion battery applications. Among TiO_2 polymorphs, TiO_2(B) is the least dense, which makes it the most suitable polymorph for this application. TiO_2(B) nanomaterials offer several advantages for lithium-ion battery application, they allow to reduce the diffusion paths of lithium ions, they expose a large specific surface in contact with the electrolyte, which allows in addition to their structure a great capacity of lithium ion insertion. The advantages of TiO_2 as an anode material will be discussed in this thesis work.

References

1. Houdy, P., C. Brechignac, and M. Lahmani. "Les nanosciences. 2-Nanomatériaux et nanochimie." (2006).
2. Kreibig, Uwe, and Michael Vollmer. Optical properties of metal clusters. Vol. 25. Springer Science & Business Media, 2013.
3. Kittel, Charles. "Physical theory of ferromagnetic domains." Reviews of modern Physics 21, no. 4 (1949): 541.
4. Taleb, Al, V. Russier, A. Courty, and M. P. Pileni. "Collective optical properties of silver nanoparticles organized in two-dimensional superlattices." Physical Review B 59, no. 20 (1999): 13350.
5. https://fr.statista.com, consulté le 15/02/2021.
6. Zhao, Zhenhuan, Jian Tian, Yuanhua Sang, Andreu Cabot, and Hong Liu. "Structure, synthesis, and applications of TiO_2 nanobelts." Advanced materials 27, no. 16 (2015): 2557-2582.
7. Xu, Fang. "Review of analytical studies on TiO_2 nanoparticles and particle aggregation, coagulation, flocculation, sedimentation, stabilization." Chemosphere 212 (2018): 662-677.
8. Kim, Dong Hyun, Ha Sung Park, Kim Sun-Jae, and Kyung Sub Lee. "Synthesis of novel TiO_2 by mechanical alloying and heat treatment-derived nanocomposite of TiO_2 and $NiTiO_3$." Catalysis Letters 106, no. 1-2 (2006): 29-33.
9. Anuradha, T. V., and S. Ranganathan. "Nanocrystalline TiO_2 by three different synthetic approaches: A comparison." Bulletin of Materials Science 30, no. 3 (2007): 263-269.
10. Bedikyan, L., S. Zakhariev, and M. Zakharieva. "Titanium dioxide thin films: preparation and optical properties." Journal of Chemical Technology and Metallurgy 48, no. 6 (2013): 555-558.
11. Zhang, Feng, S. Jin, Yingjun Mao, Zhihong Zheng, Yu Chen, and Xianghuai Liu. "Surface characterization of titanium oxide films synthesized by ion beam enhanced deposition." Thin Solid Films 310, no. 1-2 (1997): 29-33.
12. Daviðsdóttir, Svava, Rajashekhara Shabadi, Aurelian Catalin Galca, Inge Hald Andersen, Kai Dirscherl, and Rajan Ambat. "Investigation of DC magnetron-sputtered TiO_2 coatings: Effect of coating thickness, structure, and morphology on photocatalytic activity." Applied surface science 313 (2014): 677-686.

13. Pradhan, Swati S., Sambita Sahoo, and Siddhartha Kumar Pradhan. "Influence of annealing temperature on the structural, mechanical and wetting property of TiO_2 films deposited by RF magnetron sputtering." Thin Solid Films 518, no. 23 (2010): 6904-6908.

14. Matsumoto, Y., M. Murakami, T. Hasegawa, T. Fukumura, M. Kawasaki, P. Ahmet, K. Nakajima, T. Chikyow, and H. Koinuma. "Structural control and combinatorial doping of titanium dioxide thin films by laser molecular beam epitaxy." Applied Surface Science 189, no. 3-4 (2002): 344-348.

15. Hansen, P. J., V. Vaithyanathan, Y. Wu, T. Mates, S. Heikman, U. K. Mishra, R. A. York, D. G. Schlom, and J. S. Speck. "Rutile films grown by molecular beam epitaxy on GaN and AlGaN / GaN." Journal of Vacuum Science & Technology B: Microelectronics and Nanometer Structures Processing, Measurement, and Phenomena 23, no. 2 (2005): 499-506.

16. Komiyama, Hiroshi, Takashi Kanai, and Hakuai Inoue. "Preparation of porous, amorphous, and ultrafine TiO_2 particles by chemical vapor deposition." Chemistry Letters 13, no. 8 (1984): 1283-1286.

17. Jung, S-C., B-H. Kim, S-J. Kim, Nobuyuki Imaishi, and Y-I. Cho. "Characterization of a TiO_2 photocatalyst film deposited by CVD and its photocatalytic activity." Chemical Vapor Deposition 11, no. 3 (2005): 137-141.

18. Djerdj, Igor, Anđelka M. Tonejc, Mirjana Bijelić, V. Vranes, and Aleksandra Turković. "Transmission electron microscopy studies of nanostructured TiO_2 films on various substrates." Vacuum 80, no. 4 (2005): 371-378.

19. Shinde, P. S., and C. H. Bhosale. "Properties of chemical vapour deposited nanocrystalline TiO_2 thin films and their use in dye-sensitized solar cells." Journal of Analytical and Applied Pyrolysis 82, no. 1 (2008): 83-88.

20. Sugimoto, Tadao, Xingping Zhou, and Atsushi Muramatsu. "Synthesis of uniform anatase TiO_2 nanoparticles by gel-sol method: 3. Formation process and size control." Journal of colloid and interface science 259, no. 1 (2003): 43-52.

21. Kanie, Kiyoshi, and Tadao Sugimoto. "Shape control of anatase TiO_2 nanoparticles by amino acids in a gel-sol system." Chemical Communications 14 (2004): 1584-1585.

22. Cozzoli, P. Davide, Andreas Kornowski, and Horst Weller. "Low-temperature synthesis of soluble and processable organic-capped anatase TiO_2 nanorods." Journal of the American Chemical Society 125, no. 47 (2003): 14539-14548.

23. Lin, Y., G. S. Wu, X. Y. Yuan, T. Xie, and L. D. Zhang. "Fabrication and optical properties of TiO_2 nanowire arrays made by sol-gel electrophoresis deposition into anodic alumina membranes." Journal of Physics: Condensed Matter 15, no. 17 (2003): 2917.

24. Lei, Y., L. D. Zhang, and J. C. Fan. "Fabrication, characterization and Raman study of TiO_2 nanowire arrays prepared by anodic oxidative hydrolysis of $TiCl_3$." Chemical Physics Letters 338, no. 4-6 (2001): 231-236.

25. Liu, Suqin, and Kelong Huang. "Straightforward fabrication of highly ordered TiO_2 nanowire arrays in AAM on aluminum substrate." Solar energy materials and solar cells 85, no. 1 (2005): 125-131.

26. Zhang, Qinghong, and Lian Gao. "Preparation of oxide nanocrystals with tunable morphologies by the moderate hydrothermal method: insights from rutile TiO_2." Langmuir 19, no. 3 (2003): 967-971.

27. Yang, Songwang, and Lian Gao. "Low-temperature synthesis of crystalline TiO_2 nanorods: mass production assisted by surfactant." Chemistry letters 34, no. 7 (2005): 964-965.

28. Yang, Songwang, and Lian Gao. "A facile and one-pot synthesis of high aspect ratio anatase nanorods based on aqueous solution." Chemistry letters 34, no. 7 (2005): 972-973.

29. Kim, Chung-Sik, Byung Kee Moon, Jong-Ho Park, Su Tae Chung, and Se-Mo Son. "Synthesis of nanocrystalline TiO_2 in toluene by a solvothermal route." Journal of crystal growth 254, no. 3-4 (2003): 405-410.

30. Li, Xiao-Lin, Qing Peng, Jia-Xiang Yi, Xun Wang, and Yadong Li. "Near monodisperse TiO_2 nanoparticles and nanorods." Chemistry–A European Journal 12, no. 8 (2006): 2383-2391.

31. Kasuga, Tomoko, Masayoshi Hiramatsu, Akihiko Hoson, Toru Sekino, and Koichi Niihara. "Formation of titanium oxide nanotube." Langmuir 14, no. 12 (1998): 3160-3163.

32. Fehse, Marcus, Florent Fischer, Cecile Tessier, Lorenzo Stievano, and Laure Monconduit. "Tailoring of phase composition and morphology of TiO_2-based electrode materials for lithium-ion batteries." Journal of power sources 231 (2013): 23-28.

33. Hernández-Alonso, María D., Sergio García-Rodríguez, Silvia Suárez, Raquel Portela, Benigno Sánchez, and Juan M. Coronado. "Highly selective one-dimensional TiO_2-based nanostructures for air treatment applications." Applied Catalysis B: Environmental 110 (2011): 251-259.

34. Nguyen, Cuong Ky, Hyun Gil Cha, and Young Soo Kang. "Axis-oriented, anatase TiO_2 single crystals with dominant {001} and {100} facets." Crystal growth & design 11, no. 9 (2011): 3947-3953.

35. Lim, Ying Wen L.; Tang, Yuxin; Cheng, Yu H.; Chen, Zhong: Morphology, crystal structure and adsorption performance of hydrothermally synthesized titania and titanate nanostructures. In: *Nanoscale* 2 (2010), 2751–2757.

36. Yoshida, Ryuhei; Suzuki, Yoshikazu; Yoshikawa, Susumu: Syntheses of TiO_2(B) nanowires and TiO_2 anatase nanowires by hydrothermal and post-heat treatments. In: *J. Solid State Chem.* 178 (2005), 2179–2185.

37. Bavykin, Dmitry V.; Parmon, Valentin N.; Lapkin, A; Walsh, Frank C.: The effect of hydrothermal conditions on the mesoporous structure of TiO_2 nanotubes. In: *J. Mater. Chem.* 14 (2004), 3370–3377.

38. Testino, Andrea, Ignazio Renato Bellobono, Vincenzo Buscaglia, Carmen Canevali, Massimiliano D'Arienzo, Stefano Polizzi, Roberto Scotti, and Franca Morazzoni. "Optimizing the photocatalytic properties of hydrothermal TiO_2 by the control of phase composition and particle morphology. A systematic approach." Journal of the American Chemical Society 129, no. 12 (2007): 3564-3575.

39. Xu, Yuanmei, Xiaoming Fang, Jian Xiong, and Zhengguo Zhang. "Hydrothermal transformation of titanate nanotubes into single-crystalline TiO_2 nanomaterials with controlled phase composition and morphology." Materials Research Bulletin 45, no. 7 (2010): 799-804.

40. Yin, Hengbo, Yuji Wada, Takayuki Kitamura, Shingo Kambe, Sadao Murasawa, Hirotaro Mori, Takao Sakata, and Shozo Yanagida. "Hydrothermal synthesis of nanosized anatase and rutile TiO_2 using amorphous phase TiO_2." Journal of Materials Chemistry 11, no. 6 (2001): 1694-1703.

41. Hernandez-Alonso, María D.; Garcia-Rodriguez, Sergio; Suarez, Silvia; Portela, Raquel; Sanchez, Benigno; Coronado, Juan M.: Highly selective one-dimensional TiO_2-based nanostructures for air treatment applications. In: *Applied Catalysis B: Environmental* 110 (2011), November, 251-259.

42. Zhou, Weijia, Guojun Du, Peiguang Hu, Guohong Li, Dongzhou Wang, Hong Liu, Jiyang Wang, Robert I. Boughton, Duo Liu, and Huaidong Jiang. "Nanoheterostructures on TiO_2 nanobelts achieved by acid hydrothermal method with enhanced photocatalytic and gas sensitive performance." Journal of Materials Chemistry 21, no. 22 (2011): 7937-7945.

43. Fehse, Marcus, Florent Fischer, Cecile Tessier, Lorenzo Stievano, and Laure Monconduit. "Tailoring of phase composition and morphology of TiO_2-based electrode materials for lithium-ion batteries." Journal of power sources 231 (2013): 23-28.

44. Cassaignon, Sophie, Magali Koelsch, and Jean-Pierre Jolivet. "Selective synthesis of brookite, anatase and rutile nanoparticles: thermolysis of $TiCl_4$ in aqueous nitric acid." Journal of Materials Science 42, no. 16 (2007): 6689-6695.

45. Sankapal, Babasaheb Raghunath, Shrikrishna Dattatraya Sartale, Martha Christina Lux-Steiner, and Ahmed Ennaoui. "Chemical and electrochemical synthesis of nanosized TiO_2 anatase for large-area photon conversion." Comptes Rendus Chimie 9, no. 5-6 (2006): 702-707.

46. Brown, Michael D., Teeraporn Suteewong, R. Sai Santosh Kumar, Valerio D'Innocenzo, Annamaria Petrozza, Michael M. Lee, Ulrich Wiesner, and Henry J. Snaith. "Plasmonic dye-sensitized solar cells using core-shell metal-insulator nanoparticles." Nano letters 11, no. 2 (2011): 438-445.

47. Xu, Qi, Fang Liu, Weisi Meng, and Yidong Huang. "Plasmonic core-shell metal-organic nanoparticles enhanced dye-sensitized solar cells." Optics express 20, no. 106 (2012): A898-A907.

48. Qi, Jifa, Xiangnan Dang, Paula T. Hammond, and Angela M. Belcher. "Highly efficient plasmon-enhanced dye-sensitized solar cells through metal@oxide core-shell nanostructure." ACS nano 5, no. 9 (2011): 7108-7116.

49. Sheehan, Stafford W., Heeso Noh, Gary W. Brudvig, Hui Cao, and Charles A. Schmuttenmaer. "Plasmonic enhancement of dye-sensitized solar cells using core-shell-shell nanostructures." The Journal of Physical Chemistry C 117, no. 2 (2013): 927-934.

50. Wu, Jin-Ming, Satoshi Hayakawa, Kanji Tsuru, and Akiyoshi Osaka. "Porous titania films prepared from interactions of titanium with hydrogen peroxide solution." Scripta Materialia 46, no. 1 (2002): 101-106.

51. Carp, Oana, Carolien L. Huisman, and Armin Reller. "Photoinduced reactivity of titanium dioxide." Progress in solid state chemistry 32, no. 1-2 (2004): 33-177.

52. Carp, Oana, Carolien L. Huisman, and Armin Reller. "Photoinduced reactivity of titanium dioxide." Progress in solid state chemistry 32, no. 1-2 (2004): 33-177.

53. Barnard, A. S., P. Zapol, and L. A. Curtiss. "Modeling the morphology and phase stability of TiO_2 nanocrystals in water." Journal of Chemical Theory and Computation 1, no. 1 (2005): 107-116.

54. Pottier, Agnes, Corinne Chanéac, Elisabeth Tronc, Léo Mazerolles, and Jean-Pierre Jolivet. "Synthesis of brookite TiO_2 nanoparticlesby thermolysis of $TiCl_4$ in strongly acidic aqueous media." Journal of Materials Chemistry 11, no. 4 (2001): 1116-1121.

55. Tang, H., F. Levy, H. Berger, and P. E. Schmid. "Urbach tail of anatase TiO_2." Physical Review B 52, no. 11 (1995): 7771.

56. Kasuga, Tomoko, Masayoshi Hiramatsu, Akihiko Hoson, Toru Sekino, and Koichi Niihara. "Titania nanotubes prepared by chemical processing." Advanced materials 11, no. 15 (1999): 1307-1311.

57. Bavykin, Dmitry V., Jens M. Friedrich, and Frank C. Walsh. "Protonated titanates and TiO_2 nanostructured materials: synthesis, properties, and applications." Advanced materials 18, no. 21 (2006): 2807-2824.

58. Morgan D. L.; Zhu H. -Y.; Frost R. L.; Waclawik E. R.; Determination of a morphological phase diagram of Titania/titanate nanostructures from alkaline hydrothermal treatment of Degussa P25, Chem. Mater.; 20(12) (2008) p3800.

59. Bavykin, Dmitry V., Jens M. Friedrich, and Frank C. Walsh. "Protonated titanates and TiO_2 nanostructured materials: synthesis, properties, and applications." Advanced materials 18, no. 21 (2006): 2807-2824.

60. Yao, B. D., Y. F. Chan, Xinyi Y. Zhang, W. F. Zhang, Z. Y. Yang, and N. Wang. "Formation mechanism of TiO_2 nanotubes." Applied physics letters 82, no. 2 (2003): 281-283.

61. Zhang, S., L-M. Peng, Q. Chen, G. H. Du, G. Dawson, and W. Z. Zhou. "Formation Mechanism of $H_2Ti_3O_7$ Nanotubes." Physical Review Letters 91, no. 25 (2003): 256103.

62. Ma, Renzhi, Yoshio Bando, and Takayoshi Sasaki. "Directly rolling nanosheets into nanotubes." The Journal of Physical Chemistry B 108, no. 7 (2004): 2115-2119.

63. Bavykin, Dmitry V., Valentin N. Parmon, Alexei A. Lapkin, and Frank C. Walsh. "The effect of hydrothermal conditions on the mesoporous structure of TiO_2 nanotubes." Journal of Materials Chemistry 14, no. 22 (2004): 3370-3377.

64. Zhao, Ji-Cheng. "Combinatorial approaches as effective tools in the study of phase diagrams and composition–structure–property relationships." Progress in materials science 51, no. 5 (2006): 557-631.

65. Lan, Yucheng, Yalin Lu, and Zhifeng Ren. "Mini review on photocatalysis of titanium dioxide nanoparticles and their solar applications." Nano Energy 2, no. 5 (2013): 1031-1045.

66. Fujishima, Akira, and Kenichi Honda. "Electrochemical photolysis of water at a semiconductor electrode." nature 238, no. 5358 (1972): 37-38.

67. Bonetta, Silvia, Sara Bonetta, Francesca Motta, Alberto Strini, and Elisabetta Carraro. "Photocatalytic bacterial inactivation by TiO_2-coated surfaces." AMB Express 3, no. 1 (2013): 1-8.

68. Maness, Pin-Ching, Sharon Smolinski, Daniel M. Blake, Zheng Huang, Edward J. Wolfrum, and William A. Jacoby. "Bactericidal activity of photocatalytic TiO_2 reaction: toward an understanding of its killing mechanism." Applied and environmental microbiology 65, no. 9 (1999): 4094-4098.

69. Saito, T., T. Iwase, J. Horie, and T. Morioka. "Mode of photocatalytic bactericidal action of powdered semiconductor TiO_2 on mutans streptococci." Journal of Photochemistry and Photobiology B: Biology 14, no. 4 (1992): 369-379.

70. Amezaga-Madrid, P., R. Silveyra-Morales, L. Cordoba-Fierro, G. V. Nevarez-Moorillon, M. Miki-Yoshida, E. Orrantia-Borunda, and F. J. Solıs. "TEM evidence of ultrastructural alteration on Pseudomonas aeruginosa by photocatalytic TiO_2 thin films." Journal of Photochemistry and Photobiology B: Biology 70, no. 1 (2003): 45-50.

71. Mitoraj, Dariusz, Agnieszka Jańczyk, Magdalena Strus, Horst Kisch, Grażyna Stochel, Piotr B. Heczko, and Wojciech Macyk. "Visible light inactivation of bacteria and fungi by modified titanium dioxide." Photochemical & Photobiological Sciences 6, no. 6 (2007): 642-648.

72. Blake, Daniel M., Pin-Ching Maness, Zheng Huang, Edward J. Wolfrum, Jie Huang, and William A. Jacoby. "Application of the photocatalytic chemistry of titanium dioxide to disinfection and the killing of cancer cells." Separation and purification methods 28, no. 1 (1999): 1-50.

73. Fujishima, A., T. N. Rao, and D. A. Tryk. "J Photochem, Photobiol, C Photochem." Rev 1 (2000): 1-21.

74. Pottier, Agnes, Sophie Cassaignon, Corinne Chanéac, Françoise Villain, Elisabeth Tronc, and Jean-Pierre Jolivet. "Size tailoring of TiO_2 anatase nanoparticles in aqueous medium and synthesis of nanocomposites. Characterization by Raman spectroscopy." Journal of Materials Chemistry 13, no. 4 (2003): 877-882.

75. Kočí, Kamila, Lucie Obalová, and Zdeněk Lacný. "Photocatalytic reduction of CO_2 over TiO_2 based catalysts." Chemical Papers 62, no. 1 (2008): 1-9.

76. Zhao, Xiao Kang, and Janos H. Fendler. "Size quantization in semiconductor particulate films." The Journal of Physical Chemistry 95, no. 9 (1991): 3716-3723.

78. Lee, Michael M. "Organic-inorganic hybrid photovoltaics based on organometal halide perovskites." PhD diss., Oxford University, UK, 2013.

79. Hanarp, Per, Duncan S. Sutherland, Julie Gold, and Bengt Kasemo. "Control of nanoparticle film structure for colloidal lithography." Colloids and Surfaces A: Physicochemical and Engineering Aspects 214, no. 1-3 (2003): 23-36.

80. Landi, Brian J., Matthew J. Ganter, Cory D. Cress, Roberta A. DiLeo, and Ryne P. Raffaelle. "Carbon nanotubes for lithium-ion batteries." Energy & Environmental Science 2, no. 6 (2009): 638-6

81. Chung, Geun-Chang, Hyung-Jin Kim, Seung-Il Yu, Song-Hui Jun, Jong-wook Choi, and Myung-Hwan Kim. "Origin of graphite exfoliation an investigation of the important role of solvent cointercalation." Journal of The Electrochemical Society 147, no. 12 (2000): 4391.

82. Shu, Z. X., R. S. McMillan, J. J. Murray, and I. J. Davidson. "Use of chloroethylene carbonate as an electrolyte solvent for a lithium-ion battery containing a graphitic anode." Journal of the Electrochemical Society 142, no. 9 (1995): L161.

83 Inaba, Minoru, Yutaka Kawatate, Atsushi Funabiki, Soon-Ki Jeong, Takeshi Abe, and Zempachi Ogumi. "STM study on graphite/electrolyte interface in lithium-ion batteries: solid electrolyte interface formation in trifluoropropylene carbonate solution." Electrochimica acta 45, no. 1-2 (1999): 99-105.

84. Chen, Zhaohui, and J. R. Dahn. "Effect of a ZrO_2 coating on the structure and electrochemistry of Li_xCoO_2 when cycled to 4.5 V." Electrochemical and Solid-State Letters 5, no. 10 (2002): A213.

85. Mladenov, Ml, R. Stoyanova, E. Zhecheva, and S. Vassilev. "Effect of Mg doping and MgO-surface modification on the cycling stability of $LiCoO_2$ electrodes." Electrochemistry Communications 3, no. 8 (2001): 410-416.

86. Cho, Jaephil, Yong Jeong Kim, and Byungwoo Park. "$LiCoO_2$ cathode material that does not show a phase transition from hexagonal to monoclinic phase." Journal of the electrochemical society 148, no. 10 (2001): A1110.

87. Kim, H-B., B-C. Park, S-T. Myung, K. Amine, Jai Prakash, and Y-K. Sun. "Electrochemical and thermal characterization of AlF_3-coated $Li[Ni_{0.8}Co_{0.15}Al_{0.05}]O_2$ cathode in lithium-ion cells." Journal of Power Sources 179, no. 1 (2008): 347-350.

88. Sun, Y-K., J-M. Han, S-T. Myung, S-W. Lee, and K. Amine. "Significant improvement of high voltage cycling behavior AlF_3-coated $LiCoO_2$ cathode." Electrochemistry communications 8, no. 5 (2006): 821-826.

89. Dahéron, Laurence, R. Dedryvère, Hervé Martinez, D. Flahaut, Michel Ménétrier, Claude Delmas, and Danielle Gonbeau. "Possible Explanation for the Efficiency of Al-Based Coatings on $LiCoO_2$: Surface Properties of $LiCo_{1-x}Al_xO_2$ Solid Solution." Chemistry of Materials 21, no. 23 (2009): 5607-5616.

90. Tarascon, J. M. "Histoire et Évolution Des Technologies d'accumulateurs." Chaire Développement durable Environnement, Énergie et Société (2011).

91. Vaughey, J. T., K. D. Kepler, R. Benedek, and M. M. Thackeray. "NiAs-versus zinc-blende-type intermetallic insertion electrodes for lithium batteries: lithium extraction from Li_2CuSn." Electrochemistry communications 1, no. 11 (1999): 517-521.

92. Kepler, Keith D., John T. Vaughey, and Michael M. Thackeray. "$Li_xCu_6Sn_5$ (0< x< 13): an intermetallic insertion electrode for rechargeable lithium batteries." Electrochemical and Solid-State Letters 2, no. 7 (1999): 307.

93. Winter, Martin, and Jürgen O. Besenhard. "Electrochemical lithiation of tin and tin-based intermetallics and composites." Electrochimica Acta 45, no. 1-2 (1999) 31-50.

94. A. Chagnes, 《Propriétés de transport dans les électrolytes concentrés à base de y-butyrolactone : application aux accumulateurs rechargeables au lithium》Ph.D. thesis, Université de Tours, France (2002).

95. Balbuena, Perla B., and Yi Xuan Wang, eds. Lithium-ion batteries: solid-electrolyte interphase. World Scientific, 2004.

96. Maurin, G., Ch Bousquet, F. Henn, P. Bernier, R. Almairac, and B. Simon. "Electrochemical intercalation of lithium into multiwall carbon nanotubes." Chemical physics letters 312, no. 1 (1999): 14-18.

97. Dey, A. N. "Electrochemical alloying of lithium in organic electrolytes." Journal of The Electrochemical Society 118, no. 10 (1971): 1547.

98. Rao, B. M. L., R. W. Francis, and H. A. Christopher. "Lithium-aluminum electrode." Journal of The Electrochemical Society 124, no. 10 (1977): 1490.

99. Lai, S-C. "Solid Lithium-Silicon Electrode." Journal of The Electrochemical Society 123, no. 8 (1976): 1196.

100. Armstrong, A. Robert, Graham Armstrong, Jesús Canales, and Peter G. Bruce. "TiO_2-B nanowires." Angewandte Chemie International Edition 43, no. 17 (2004): 2286-2288.

101. Brohan, Luc. "Physical Properties of M_xTiO_2 Bronzes (B)." Solid State Ionics 9 (1983): 419-424.

102. Armstrong, Graham, A. Robert Armstrong, Jesús Canales, and Peter G. Bruce. "TiO_2 (B) nanotubes as negative electrodes for rechargeable lithium batteries." Electrochemical and Solid-State Letters 9, no. 3 (2006): A139.

103. Nuspl, Gerhard, Kazunari Yoshizawa, and Tokio Yamabe. "Lithium intercalation in TiO_2 modifications." Journal of Materials Chemistry 7, no. 12 (1997): 2529-2536.

104. Poizot, P. L. S. G., S. Laruelle, S. Grugeon, L. Dupont, and J. M. Tarascon. "Nano-sized transition-metal oxides as negative-electrode materials for lithium-ion batteries." Nature 407, no. 6803 (2000): 496-499.

105. Cabana, Jordi, Laure Monconduit, Dominique Larcher, and M. Rosa Palacin. "Beyond intercalation-based Li-ion batteries: the state of the art and challenges of electrode materials reacting through conversion reactions." Advanced materials 22, no. 35 (2010): E170-E192.

106. Taberna, Pierre-Louis, Sayantanava Mitra, Philippe Poizot, Patrice Simon, and J-M. Tarascon. "High-rate capabilities Fe_3O_4-based Cu nano-architectured electrodes for lithium-ion battery applications." Nature materials 5, no. 7 (2006): 567-573.

107. Palacin, M. Rosa. "Recent advances in rechargeable battery materials: a chemist's perspective." Chemical Society Reviews 38, no. 9 (2009): 2565-2575.

108. Kasavajjula, Uday, Chunsheng Wang, and A. John Appleby. "Nano-and bulk-silicon-based insertion anodes for lithium-ion secondary cells." Journal of power sources 163, no. 2 (2007): 1003-1039.

109. Mukherjee, Rahul, Rahul Krishnan, Toh-Ming Lu, and Nikhil Koratkar. "Nanostructured electrodes for high-power lithium-ion batteries." Nano Energy 1, no. 4 (2012): 518-533.

110. Reddy, M. Anji, M. Satya Kishore, V. Pralong, U. V. Varadaraju, and B. Raveau. "Lithium intercalation into nanocrystalline brookite TiO_2." Electrochemical and Solid-State Letters 10, no. 2 (2006): A29.

111. Reddy, M. Anji, V. Pralong, U. V. Varadaraju, and B. Raveau. "Crystallite size constraints on lithium insertion into brookite TiO_2." Electrochemical and Solid-State Letters 11, no. 8 (2008): A132.

112. Baudrin, E., S. Cassaignon, M. Koelsch, J-P. Jolivet, L. Dupont, and J-M. Tarascon. "Structural evolution during the reaction of Li with nano-sized rutile type TiO_2 at room temperature." Electrochemistry communications 9, no. 2 (2007): 337-342.

113. Hu, Y-S., Lorenz Kienle, Y-G. Guo, and Joachim Maier. "High lithium electroactivity of nanometer-sized rutile TiO_2." Advanced Materials 18, no. 11 (2006): 1421-1426.

114. Wagemaker, Marnix, Wouter JH Borghols, and Fokko M. Mulder. "Large impact of particle size on insertion reactions. a case for anatase Li_xTiO_2." Journal of the American Chemical Society 129, no. 14 (2007): 4323-4327.

115. Hardwick, Laurence J., Michael Holzapfel, Petr Novák, Loïc Dupont, and Emmanuel Baudrin. "Electrochemical lithium insertion into anatase-type TiO_2: An in-situ Raman microscopy investigation." Electrochimica Acta 52, no. 17 (2007): 5357-5367.

116. Shin, Ji-Yong, Dominik Samuelis, and Joachim Maier. "Sustained lithium-storage performance of hierarchical, nanoporous anatase TiO_2 at high rates: Emphasis on interfacial storage phenomena." Advanced Functional Materials 21, no. 18 (2011): 3464-3472.

117. Mazouzi, Driss, David Reyter, Magali Gauthier, Philippe Moreau, Dominique Guyomard, Lionel Roué, and Bernard Lestriez. "Very high surface capacity observed using Si negative electrodes embedded in copper foam as 3D current collectors." Advanced Energy Materials 4, no. 8 (2014): 1301718.

118. Dylla, Anthony G., Graeme Henkelman, and Keith J. Stevenson. "Lithium insertion in nanostructured TiO_2 (B) architectures." Accounts of chemical research 46, no. 5 (2013): 1104-1112.

119. Shin, Ji-Yong, Dominik Samuelis, and Joachim Maier. "Sustained lithium-storage performance of hierarchical, nanoporous anatase TiO_2 at high rates: Emphasis on interfacial storage phenomena." Advanced Functional Materials 21, no. 18 (2011): 3464-3472.

120. Ren, Yu, Laurence J. Hardwick, and Peter G. Bruce. "Lithium intercalation into mesoporous anatase with an ordered 3D pore structure." Angewandte Chemie 122, no. 14 (2010): 2624-2628.

121. Liu, Hansan, Zhonghe Bi, Xiao-Guang Sun, Raymond R. Unocic, M. Parans Paranthaman, Sheng Dai, and Gilbert M. Brown. "Mesoporous TiO_2-B microspheres with superior rate performance for lithium-ion batteries." Advanced Materials 23, no. 30 (2011): 3450-3454.

122. Liu, Shaohua, Haiping Jia, Lu Han, Jiulin Wang, Pengfei Gao, Dongdong Xu, Jun Yang, and Shunai Che. "Nanosheet-constructed porous TiO_2-B for advanced lithium-ion batteries." Advanced Materials 24, no. 24 (2012): 3201-3204.

123. Ali, Zahid, Seung Nam Cha, Jung Inn Sohn, Imran Shakir, Changzeng Yan, Jong Min Kim, and Dae Joon Kang. "Design and evaluation of novel Zn doped mesoporous TiO_2 based anode material for advanced lithium-ion batteries." Journal of Materials Chemistry 22, no. 34 (2012): 17625-17629.

124. Wang, Yude, Bernd M. Smarsly, and Igor Djerdj. "Niobium doped TiO_2 with mesoporosity and its application for lithium insertion." Chemistry of materials 22, no. 24 (2010): 6624-6631.

125. Ryu, Myung-Hyun, Kyu-Nam Jung, Kyung-Hee Shin, Kyoo-Seung Han, and Sukeun Yoon. "High performance N-doped mesoporous carbon decorated TiO_2 nanofibers as anode materials for lithium-ion batteries." The Journal of Physical Chemistry C 117, no. 16 (2013): 8092-8098.

126. Sheppard, Leigh R., Thomas Dittrich, and Maria K. Nowotny. "The impact of niobium surface segregation on charge separation in niobium-doped titanium dioxide." The Journal of Physical Chemistry C 116, no. 39 (2012): 20923-20929.

127. Baumard, Jean Francois, and E. Tani. "Electrical conductivity and charge compensation in Nb doped TiO_2 rutile." The Journal of Chemical Physics 67, no. 3 (1977): 857-860.

128. El-Bahy, Zeinhom M., Adel A. Ismail, and Reda M. Mohamed. "Enhancement of titania by doping rare earth for photodegradation of organic dye (Direct Blue)." Journal of Hazardous Materials 166, no. 1 (2009): 138-143.

129. Štengl, Václav, Snejana Bakardjieva, and Nataliya Murafa. "Preparation and photocatalytic activity of rare earth doped TiO_2 nanoparticles." Materials Chemistry and Physics 114, no. 1 (2009): 217-226.

130. Umebayashi, Tsutomu, Tetsuya Yamaki, Hisayoshi Itoh, and Keisuke Asai. "Analysis of electronic structures of 3d transition metal-doped TiO_2 based on band calculations." Journal of Physics and Chemistry of Solids 63, no. 10 (2002): 1909-1920.

131. Asiltürk, Meltem, Funda Sayılkan, and Ertuğrul Arpaç. "Effect of Fe^{3+} ion doping to TiO_2 on the photocatalytic degradation of Malachite Green dye under UV and vis-irradiation." Journal of Photochemistry and Photobiology A: Chemistry 203, no. 1 (2009): 64-71.

132. Tian, Baozhu, Chunzhong Li, Feng Gu, Haibo Jiang, Yanjie Hu, and Jinlong Zhang. "Flame sprayed V-doped TiO_2 nanoparticles with enhanced photocatalytic activity under visible light irradiation." Chemical Engineering Journal 151, no. 1-3 (2009): 220-227.

133. Kumar, S. Girish, and L. Gomathi Devi. "Review on modified TiO_2 photocatalysis under UV/visible light: selected results and related mechanisms on interfacial charge carrier transfer dynamics." The Journal of physical chemistry A 115, no. 46 (2011): 13211-13241.

134. Rengaraj, S., and X. Z. Li. "Enhanced photocatalytic reduction reaction over Bi^{3+}-TiO_2 nanoparticles in presence of formic acid as a hole scavenger." Chemosphere 66, no. 5 (2007): 930-938.

135. Hu, Yin, Yuantao Cao, Peixian Wang, Danzhen Li, Wei Chen, Yunhui He, Xianzhi Fu, Yu Shao, and Yi Zheng. "A new perspective for effect of Bi on the photocatalytic activity of Bi-doped TiO_2." Applied Catalysis B: Environmental 125 (2012): 294-303.

136. Asahi, Ryoji, Takeshi Morikawa, Hiroshi Irie, and Takeshi Ohwaki. "Nitrogen-doped titanium dioxide as visible-light-sensitive photocatalyst: designs, developments, and prospects." Chemical reviews 114, no. 19 (2014): 9824-9852.

137. Teh, Chao Min, and Abdul Rahman Mohamed. "Roles of titanium dioxide and ion-doped titanium dioxide on photocatalytic degradation of organic pollutants (phenolic compounds and dyes) in aqueous solutions: A review." Journal of Alloys and Compounds 509, no. 5 (2011): 1648-1660.

138. S. In, A. Orlov, R. Berg, “Effective visible light activated B-doped and B/N-codoped TiO_2 photocatalysts,” *J. Am. Chem. Soc.*, vol. 129, no. 45, pp. 13790-13791, 2007.

139. S. Sakthivel and H. Kisch, “Daylight photocatalysis by carbon modified titanium dioxide,” *Angew. Chem. Int. Ed. Engl.*, vol. 42, no. 40, pp. 4908-4911, 2003.

140. Irie, Hiroshi, Yuka Watanabe, and Kazuhito Hashimoto. "Carbon-doped anatase TiO_2 powders as a visible-light sensitive photocatalyst." Chemistry Letters 32, no. 8 (2003): 772-773.

141. Yu, Jimmy C., Jiaguo Yu, Wingkei Ho, Zitao Jiang, and Lizhi Zhang. "Effects of F-doping on the photocatalytic activity and microstructures of nanocrystalline TiO_2 powders." Chemistry of materials 14, no. 9 (2002): 3808-3816.

142. Padmanabhan, Sibu C., Suresh C. Pillai, John Colreavy, Sivakumar Balakrishnan, Declan E. McCormack, Tatiana S. Perova, Yurii Gun'ko, Steven J. Hinder, and John M. Kelly. "A simple sol− gel processing for the

development of high-temperature stable photoactive anatase titania." Chemistry of materials 19, no. 18 (2007): 4474-4481.

143. Umebayashi, T., T. Yamaki, H. Itoh, and K. Asai. "Band gap narrowing of titanium dioxide by sulfur doping." Applied Physics Letters 81, no. 3 (2002): 454-456.

144. Hamadanian, M., A. Reisi-Vanani, and A. Majedi. "Preparation and characterization of S-doped TiO_2 nanoparticles, effect of calcination temperature and evaluation of photocatalytic activity." Materials Chemistry and Physics 116, no. 2-3 (2009): 376-382.

145. Hong, Xiaoting, Zhengpeng Wang, Weimin Cai, Feng Lu, Jun Zhang, Yanzhu Yang, Na Ma, and Yingjun Liu. "Visible-light-activated nanoparticle photocatalyst of iodine-doped titanium dioxide." Chemistry of Materials 17, no. 6 (2005): 1548-1552.

146. Lin, Li, Wei Lin, Yuexiang Zhu, Biying Zhao, and Youchang Xie. "Phosphor-doped titania-a novel photocatalyst active in visible light." Chemistry Letters 34, no. 3 (2005): 284-285.

147. Dozzi, Maria Vittoria, Cosimo D'Andrea, Bunsho Ohtani, Gianluca Valentini, and Elena Selli. "Fluorine-doped TiO_2 materials: photocatalytic activity vs time-resolved photoluminescence." The Journal of Physical Chemistry C 117, no. 48 (2013): 25586-25595.

148. Li, Fa-tang, Xiao-jing Wang, Ye Zhao, Ji-xing Liu, Ying-juan Hao, Rui-hong Liu, and Di-shun Zhao. "Ionic-liquid-assisted synthesis of high-visible-light-activated N-B-F-tri-doped mesoporous TiO_2 via a microwave route." Applied Catalysis B: Environmental 144 (2014): 442-453.

149. Wu, Zhongbiao, Fan Dong, Weirong Zhao, and Sen Guo. "Visible light induced electron transfer process over nitrogen doped TiO_2 nanocrystals prepared by oxidation of titanium nitride." Journal of Hazardous Materials 157, no. 1 (2008): 57-63.

150. Ghicov, Andrei, Jan M. Macak, Hiroaki Tsuchiya, Julia Kunze, Volker Haeublein, Lothar Frey, and Patrik Schmuki. "Ion implantation and annealing for an efficient N-doping of TiO_2 nanotubes." Nano Letters 6, no. 5 (2006): 1080-1082.

151. Balcerski, William, Su Young Ryu, and Michael R. Hoffmann. "Visible-light photoactivity of nitrogen-doped TiO_2: photo-oxidation of HCO_2H to CO_2 and H_2O." The Journal of Physical Chemistry C 111, no. 42 (2007): 15357-15362.

152. Ku, Young, W. Chen, and W. Hou. "Photocatalytic decomposition of Methylene Blue with nitrogen-doped TiO_2 under visible light irradiation." vol 23 (2013): 15-21.

153. Livraghi, Stefano, Maria Cristina Paganini, Elio Giamello, Annabella Selloni, Cristiana Di Valentin, and Gianfranco Pacchioni. "Origin of photoactivity of nitrogen-doped titanium dioxide under visible light." Journal of the American Chemical Society 128, no. 49 (2006): 15666-15671.

154. Amadelli, Rossano, L. Samiolo, M. Borsa, M. Bellardita, and L. Palmisano. "N-TiO_2 Photocatalysts highly active under visible irradiation for NO_X abatement and 2-propanol oxidation." Catalysis today 206 (2013): 19-25.

CHAPTER II: Large-Scale Synthesis Route of TiO_2 Nanomaterials with Controlled Morphologies Using Hydrothermal Method and TiO_2 Aggregates as Precursor.

Nanomaterials**,** 2021**,** 11, 365.

Summary

In this work, we have highlighted the possibility of preparing titanium dioxide nanoparticles of different morphologies, using hydrothermal synthesis and an alkaline NaOH solution. Among the parameters of the synthesis, which we have varied, are the temperature, the reaction time in the reactor (autoclave), and the nature of the TiO_2 precursor used for the synthesis. The nature of the latter in the form of TiO_2 aggregate, is original compared to the literature and has helped to better control the morphology of the powders and to understand the mechanisms of formation of TiO_2 nanotubes and nanoribbons.

In a first step, we used the $TiOSO_4$ precursor for the synthesis of TiO_2 nanopowders based on anatase phase aggregates of controlled size. The different characterizations have shown that the aggregates are formed by TiO_2 nanoparticles, whose size varies from 4 to 10 nm. Depending on the synthesis conditions we obtained nanosheets, nanotubes, nanoribbons and nanourchins. For the different morphologies, the synthesis time was lower or equal to 6 h, which is a record compared to those reported in the literature for other precursors.

Moreover, the synthesis involves two intermediates: sodium titanates and titanic acids, and it takes place in three steps. First, the synthesis takes place in an autoclave, then the powder obtained undergoes ion exchange and the sodium titanate is transformed into titanic acid, which undergoes a heat treatment in the last step. For reaction times of 6h and at the temperature of 100°C or 150°C, we observed the formation of nanourchins. The formation of this morphology, we explained it by a mechanism of exfoliation/coalescence and disordered assembly of TiO_2 nanosheets. At the temperature of 200°C and for a time of 6h, we observed the formation of nanoribbons of small thickness (<10nm) and a diameter of 50 to 100nm. For the temperature of 200°C and for the short times of 15min and 180min, we observed TiO_2 nanosheets and nanotubes respectively. By a high resolution electron microscopy analysis, we have highlighted the coiling of nanosheets, which evolves in a later time to a nanotube morphology. Moreover, we observed a coexistence of nanosheets of the size of TiO_2 nanoparticles with nanosheets of slightly larger diameter. These different morphologies are probably the different stages of formation of the same nanoribbon morphology. Indeed, probably during the synthesis in alkaline medium, there is insertion of sodium ions in the structure of TiO_2 aggregates and their exfoliation in a second step, to form the nanosheets of larger size by coalescence. Our different observations are in the direction of an exfoliation and coalescence, and not in the direction of a dissolution and precipitation of the nanoparticles through the formation of TiO_2 octahedra, which will assemble afterwards to form the nanosheets. Our suggestion of an exfoliation/coalescence mechanism was supported by other experiments. Using precursors of different sizes of TiO_2 aggregates, we have shown that nanoribbons of different sizes are obtained in the same direction of trend as the aggregates.

Moreover, as the nanoribbons are obtained at longer times under the same conditions as the nanotubes, prove that there is a morphological evolution of the latter by a process of coalescence.

Concerning the phases of the different TiO_2 morphologies, we have shown that nanosheets, nanotubes and nanourchins crystallize under the TiO_2(B) phase, while nanoribbons in the form of a phase mixture that depends on the synthesis temperature of the precursor and thus on the size of the TiO_2 nanoparticles in the precursor. For a synthesis temperature of 100°C of the precursor, we observed a phase mixture with a predominance of the Brookite phase over the anatase phase. For a synthesis temperature of 200°C, we observed a TiO_2(B)/anatase phases mixture with a predominance of the TiO_2(B) phase.

Large-Scale Synthesis Route of TiO_2 Nanomaterials with Controlled Morphologies Using Hydrothermal Method and TiO_2 Aggregates as Precursor

Wenpo Luo [1] and Abdelhafed Taleb [1,2,*]

[1] PSL Research University Chimie ParisTech - CNRS, Institut de Recherche de Chimie Paris– 75005, Paris, France Wenpo.Luo@chimieparistech.psl.eu, abdelhafed.taleb@chimieparistech.psl.eu

[2] Sorbonne université, 75231, Paris, France

* Correspondence: abdelhafed.taleb@sorbonne-universite.fr;
Tel.: +33-1-85-78-41-97

Abstract: TiO_2 of controlled morphologies have been successfully prepared hydrothermally using TiO_2 aggregates of different sizes. Different techniques were used to characterize the prepared TiO_2 powder such as XRD, XPS, FEGSEM, EDS, and HRTEM. It was illustrated that the prepared TiO_2 powders are of high crystallinity with different morphologies such as nanobelt, nanourchin, and nanotube depending on the synthesis conditions of temperature, time, and additives. The mechanism behind the formation of prepared morphologies is proposed involving nanosheet intermediate formation. Furthermore, it was found that the nanoparticle properties were governed by those of TiO_2 nanoparticles aggregate used as a precursor. For example, the size of prepared nanobelts was proven to be influenced by the aggregates size used as a precursor for the synthesis.

Keywords: TiO_2 nanoparticles; aggregates; morphologies

1. Introduction

Recently, tremendous efforts have been devoted to developing innovative strategies to synthesize nanomaterials with the desired morphologies and properties. Particularly the one-dimensional (1D) structure of TiO_2 nanomaterials exhibits interesting properties compared to other TiO_2 nanoparticles: it has lower carrier recombination rate and higher charge carrier mobility, thanks to the grain boundaries and junctions absence. In fact, the electron diffusion takes place through the junctions between nanoparticles, inducing slower charge transfer by several orders of magnitude [1]. In addition, it favors light scattering in the photoanode, which increases the light harvesting [2]. Among the studied morphologies and materials, semi conducting nanostructured materials such as nanowires, nanobelts, and nanotube have received particular attention, due to their use as photoanaode for potential applications in different areas such as photovoltaic [2], photo catalysis [3], gas sensing [4], and water photo-splitting [5].

Tuning the size and the morphology of materials is becoming a challenging goal in materials science. Over the past few years, various synthesis methods and protocols have been developed to control the semi-conducting nanomaterials morphology, including vapor–liquid–solid (VLS) [6], solution–liquid–solid (SLS) [7], template-based synthetic approaches [8,9], arc discharge [10], laser ablation [11], chemical vapor deposition [12], microwave [13,14], and sol–gel [15]. Among these synthesis methods, which mostly brought contamination to the synthesis products, the hydrothermal technique has been proven to be a simple and straightforward method using noncomplex apparatus, scalable for large production, with high chemical purity, allowing a large rang of nanomaterial sizes and morphologies [16-17]. Furthermore, the morphology of prepared TiO_2 nanomaterials by using hydrothermal method was demonstrated to depend on the concentration of alkaline solution, the synthesis temperature and time, the material precursor used [17-18], additives, Pressure, pH, and the reaction medium [19-25].

Additionally, the hydrothermal method allows the control of the nanoparticle's aggregation [26]. The most reported strategy to control the morphology of oxide nanomaterials is based on using organic surfactant, which adsorbs on a selected crystallographic plan of growing nucleus, leading to a change of its orientation and growth rate. This results in controlling the morphology of the obtained nanomaterial at the final growth stage [27,28]. Additionally, strategies based on aggregation/coalescence of nanomaterials were reported and demonstrated to be efficient in controlling the morphology of the final synthesized powder [29]. The exfoliation step was also reported to be a crucial step in the formation mechanism of prepared morphologies [29]. Most of the studies are based on nanomaterials aggregation/coalescence processes, and to the best of our knowledge, very few are based on exfoliation/aggregation/coalescence processes to explain synthesized morphologies. In the case of TiO_2 nanomaterials, there is still a misunderstanding of the mechanism behind the formation of reported morphologies and particularly nanotube, nanobelt, and nanourchin. Some authors claimed that the $Na_2Ti_3O_7$ nanosheets exfoliation step is the crucial step in the mechanism formation of different morphologies, whereas other authors stated that it is the dissolution of TiO_2 nanoparticles into TiO_6 octahedra, followed by $Na_2Ti_3O_7$ nucleation and growth, forming a nanosheet in a later stage [29]. Furthermore, it is well accepted that different polymorphs of TiO_2 nanomaterials are formed by different arrangements of TiO_6 octahedra. In fact, the growth of anatase tetragonal polymorph proceeds through face sharing arrangements of TiO_6

octahedras, whereas the rutile tetragonal phase growth takes place through edge-sharing arrangements. Furthermore, the Brookite phase is obtained by TiO_6 octahedra assembly, sharing their edge and corner; whereas in Ti_2O (B) (bronze) phase, Ti^{4+} ion form two distinct geometries with oxygen: octahedron in one case and a square pyramidal in the other. In addition, to homogeneous size and morphology, prepared TiO_2 nanomaterials using hydrothermal method exhibit several characteristics such as high crystallinity, an accurate control of different crystallinity phases from anatase to rutile depending on the synthesis and annealing temperatures, and high specific surface [30]. It is well accepted that the anatase polymorph possesses a higher band gap energy (3.3 eV) than that of the rutile polymorph (3 eV).

In the present work, different morphologies of TiO_2 have been successfully prepared hydrothermally using TiO_2 aggregates made of TiO_2 nanoparticles as a precursor. The mechanism behind the morphology control of prepared nanomaterials was discussed. It was found that the prepared TiO_2 nanomaterials properties were governed by those of TiO_2 nanoparticles aggregate. By controlling TiO_2 nanoparticles and aggregate sizes, it has been demonstrated that it is possible to control the TiO_2 nanobelt sizes.

2. Materials and Methods

2.1. Synthesis of TiO_2 Nanoparticles

For the synthesis of TiO_2 nanoparticles, titanium (IV) oxysulfate hydrate ($TiOSO_4$, Sigma Aldrich, St. Louis, MO, USA) precursor was used. Furthermore, the synthesis of TiO_2 aggregates has been performed using a hydrothermal synthesis technique. The $TiOSO_4$ precursor solution was prepared by dissolving 6.4 g of $TiOSO_4$ (2.5 M) in 16 mL of distilled water under constant stirring of 750 r/min and temperature of 45 °C for 2 h to get a clear solution. Then the solution of $TiOSO_4$ was transferred into a Teflon-lined stainless-steel autoclave of 25 mL capacity. The heating rate was of 2.5 °C/min, and during the synthesis, the temperature was maintained at different temperatures of 100, 200 and 220 °C for 6 h depending on the aggregate size required. After this synthesis in autoclave, a white TiO_2 powder was obtained and was washed six times in distilled water and two times in ethanol. Then the powder was dried overnight in the oven and annealed in air at temperature of 500 °C for 30 min with the heat rate of 5 °C/min. For nanourchin, nanotube, and nanobelt synthesis, 0.5 g powder of TiO_2 aggregate was introduced in a Teflon-lined autoclave of 25 mL capacity. Then, the autoclave was filled with 10 M NaOH solution up to 80% of the autoclave capacity. During the synthesis, the temperature was maintained at different temperatures of 100, 150, and 220 °C with the heating rate of 2.5 °C/min and the synthesis time of 360, 180, and 15 min, depending on the required morphology. Afterwards, synthesis nanobelt particles are subjected to the washing and annealing protocols to obtain at the end of these processes: sodium titanate. The latter product was washed many times with diluted HCl solution to attain a pH value of 1. After that, the suspension was washed with distilled water several times to reach a pH value of 7. Finally, the obtained powder was dried overnight in the oven, and annealed in air at temperature of 500 °C for 30 min, with the heat rate of 5 °C/min.

All the chemicals are of analytical grade and used without further purification. The water used in all the experiments was purified by Milli Q System (Millipore, electric resistivity 18.2 MΩ.cm).

2.2. The Characterizations of TiO_2 Films

The morphological investigations of the prepared films were achieved with a high-resolution Ultra 55 Zeiss FEG scanning electron microscope (FEGSEM) operating at an acceleration voltage of 10 kV and the high-resolution transmission electron microscope HRTEM using JEOL 2100 Plus microscope.

The crystalline structure of TiO_2 was determined by an X-ray diffractometer (Siemens D5000 XRD unit) in 2θ range from 20° to 80° by 0.07° s^{-1} increasing steps operating at 40 KV accelerating voltage and 40 mA current using Cu Kα radiation source with λ = 1.5406Å.

The chemical compositions of all the samples were determined by the FEGSEM using a Princeton Gamme-Tech PGT, USA, spirit energy dispersive spectrometry EDS system, and by X-ray photoelectron spectroscopy XPS realized with X-ray photoelectron spectroscopy (XPS), and for the measurements we used a Thermo K Alpha analyzer system equipped with an AL Kα X-ray source (hυ = 1486.6 eV; spot size 400 μm).

3. Results and Discussion

Various powders were prepared using the alkali hydrothermal synthesis method and varying synthesis temperatures and reaction times. To prepare these powders, TiO_2 aggregates of spherical shape and different sizes were prepared and used as precursors. The FEG-SEM characterization of precursor powders are shown in Figure 1, and it can be observed that the sizes of spherical aggregates are ranging from 50 to 200 nm.

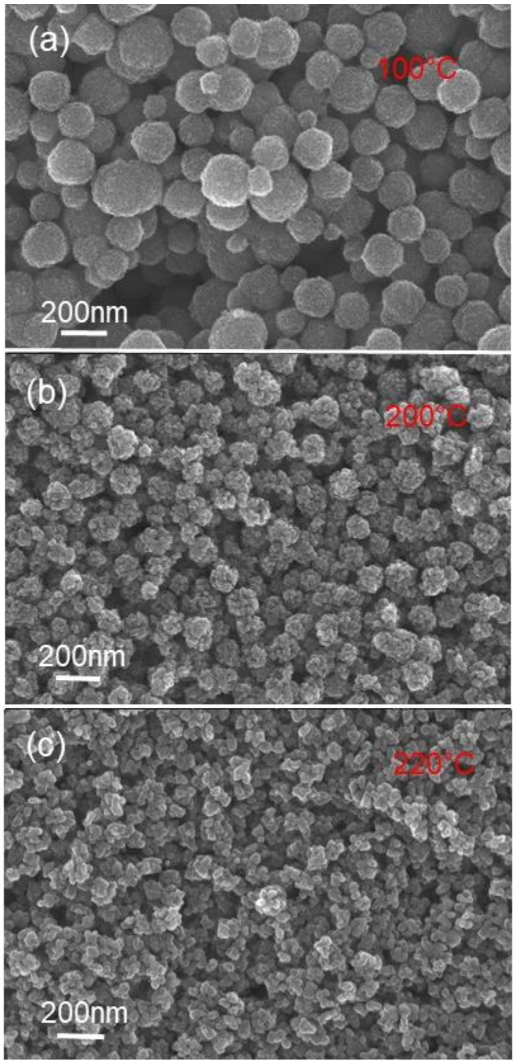

Figure 1 . FEGSEM images of TiO_2 aggregates obtained at different synthesis temperatures: (**a**) 100, (**b**) 200, and (**c**) 220 °C.

The XRD method was used to characterize the crystalline phase of TiO_2 aggregate precursors, and the obtained results are depicted in Figure 2. Several well-resolved peaks were observed and are all assigned to TiO_2 anatase phase (JCPDS No. 21-1272), which is proof of the high purity of the prepared precursor powders. Additionally, Scherer analysis was used to calculate the average crystallite sizes at the half-maximum width of the intense peak corresponding to (101) crystallographic plane, and were found to be 9.8, 24.7, and 30.4 nm, for the synthesis temperatures of 100, 200, and 220 °C, respectively.

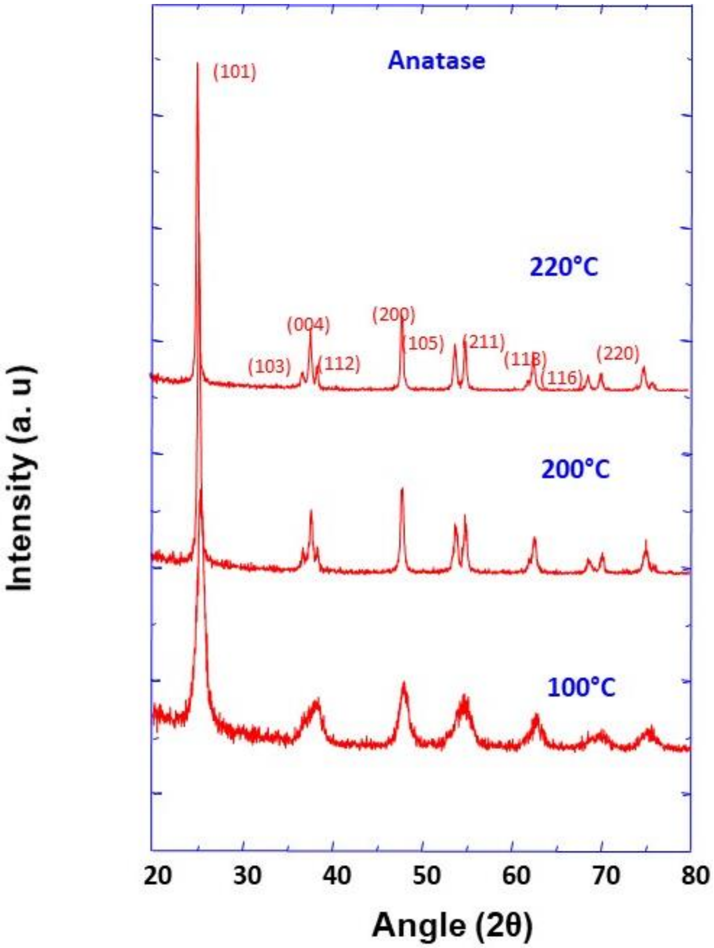

Figure 2 . XRD pattern of TiO_2 nanoparticle aggregates prepared at different synthesis temperatures as indicated.

White powders were obtained using TiO_2 aggregate precursors whatever the preparation conditions, and their corresponding morphologies are depicted in Figure 3. As it can be observed, at the synthesis temperature of 100 °C, the morphology of the prepared powder is nanourchin-like with a stretched sheet-like network (Figure 3a), whereas at a temperature of 150 °C, the morphology is still nanourchin-like but with a more rolled nanosheet-like network (Figure 3b). From these experiments, it is clear that the temperature increase favors the nanosheet scrolling. This could be explained by the fact that the crystallization enhanced by the temperature increase tends to induce the microstructure to change into rolled nanosheet structure. In fact, to reduce the surface energy of rolled structure, nanosheets reduce the defects and the distortion energy [32]. At a higher temperature of about 200 °C, the FEGSEM characterization of prepared white powder is depicted in Figure 3c,d. It can be observed that TiO_2 powder is of nanobelt-like and nanotube morphologies, with monodisperse size. The insert of Figure 3d shows a sticking of several distinguishable nanobelts along their axis direction, forming bundles of nanobelts as a building unit. It can also be observed that their thickness is homogeneous and it is of about 10 nm, their diameter is ranging from 50 to 100 nm with length of around 10 mm. In addition, the nanobelt surface is smooth at the magnification scale, and no contamination was observed. As indicated in Figure 3d, some curved nanobelts were observed, which gives an indication about their high elasticity. From the described experiments, it is clear that the synthesis temperature is an important parameter in the morphology control of TiO_2 nanomaterials.

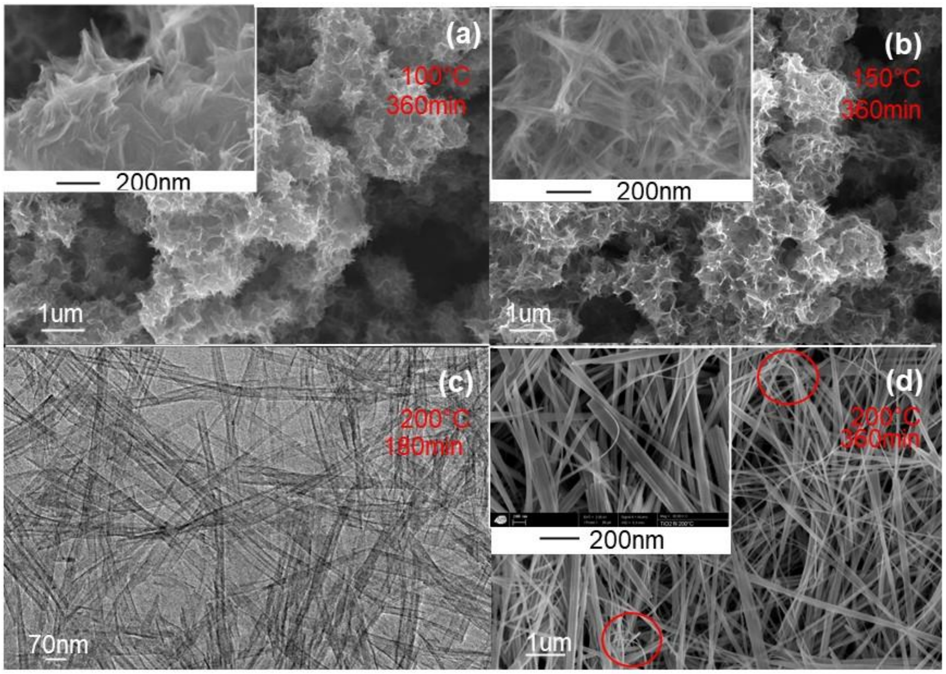

Figure 3 . FEGSEM images of TiO_2 nanoparticles with different morphologies obtained at different synthesis times and temperatures: (**a**) Nanourchin prepared at conditions of 100 °C and 360 min, (**b**) Nanourchin prepared at conditions of 150 °C and 360 min, (**c**) TEM image of Nanotube prepared at conditions of 200 °C and 180 min, and (**d**) Nanobelts prepared at conditions of 200 °C and 360 min.

The crystalline structure and phase of prepared TiO_2 nanobelt, nanotube, and nanourchin-like powders were studied by the X-ray diffraction method. The obtained XRD patterns are presented in Figure 4, and they show well-resolved peaks in the case of nanourchin and nanotube mophologies attributed to (-511) and (020) crystallographic planes of pure TiO_2(B) phase (JCPDS No. 35-0088) (Figure 4a–c). In the case of TiO_2 with nanobelt morphology, the observed XRD peaks indicates that the prepared powder is a mixture of anatase (JCPDS 21-1272) and brookite (JCPDS 29-1360) phases (Figure 4d).

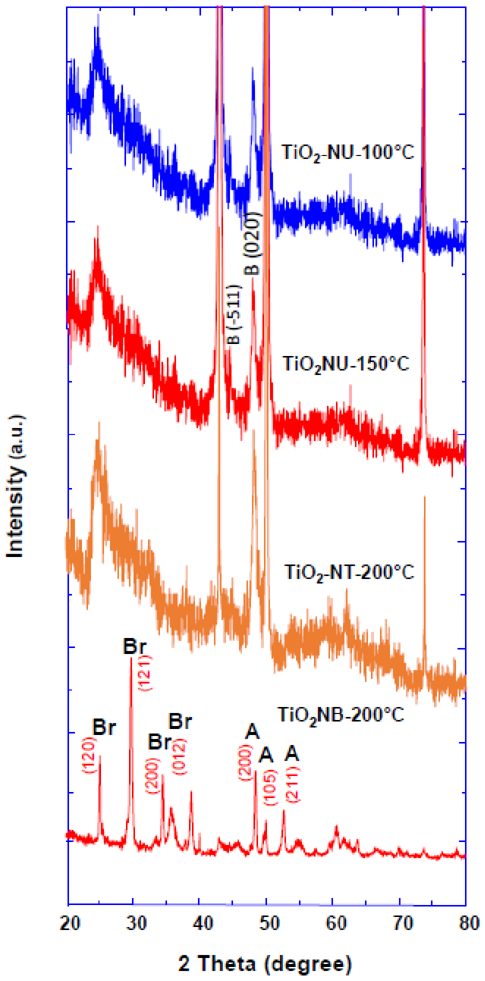

Figure 4 . XRD pattern of TiO_2 nanoparticles with different morphologies prepared at different synthesis temperatures as indicated, (a) nanourchin 100°C, (b) nanourchin 150°C, (c) nanotube 200°C and (d) nanobelt 200°C (Br: Brookite; A: Anatase; B: TiO_2-B).

Additionally, among all the peaks, the most intense is the one corresponding to (121) crystallographic plane of brookite. Further details of crystallinity are provided by HRTEM depicted in Figure 5, clearly well resolved lattice planes are shown, and the insert electron diffraction shows well resolved spots (Figure 5b). These spots are the signature that the individual nanobelt is a single crystal. The interplanar distance of about 0.88 nm measured from HRTEM image is assigned to

(100) crystallographic plane of brookite, indicating that the growth takes place along the (100) crystallographic plane, which is in good agreement with the result from XRD experiments in terms of brookite formation.

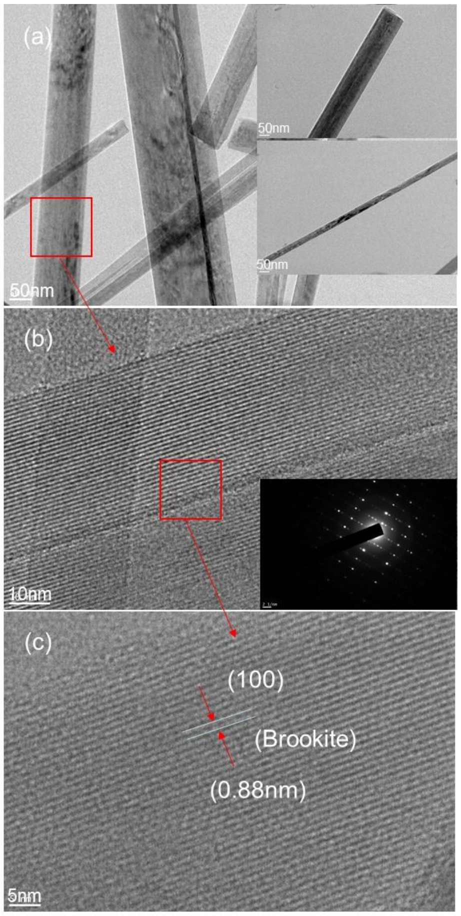

Figure 5 . (**a**) TEM images of TiO_2 nanobelt obtained at synthesis temperature of 200 °C a synthesis time of 6 h at different magnifications; (**b**) the corresponding HRTEM showing inter atomic crystallographic planes and the insert show the corresponding electron diffraction; (**c**) another magnification of TiO_2 nanobelt.

Furthermore, the chemical composition of the powder was provided by XPS analysis, and the obtained spectra are depicted in Figure 6. The XPS survey spectrum in Figure 6a of TiO_2 aggregates precursor shows intense peaks corresponding to O1s and Ti2p core levels, and the very weak intensity of the peak corresponding to Na1s. However, the XPS survey spectrum corresponding to TiO_2 nanobelt-like and nanourchin-like powders (Figure 6b) shows intense and well resolved peak, corresponding to the core level of Na1s, which is a signature of the formation of sodium titanate ($Na_2Ti_3O_7$), in addition to those of O1s and Ti2p. It was reported that $Na_2Ti_3O_7$ is constituted by corrugated strips of edge-sharing TiO_6 octahedra [29]. The width of each strips is about three-octahedra, and they are connected through their corner to form stepped layers. Within the sticking layers, sodium cations are located at the positions between the layers.

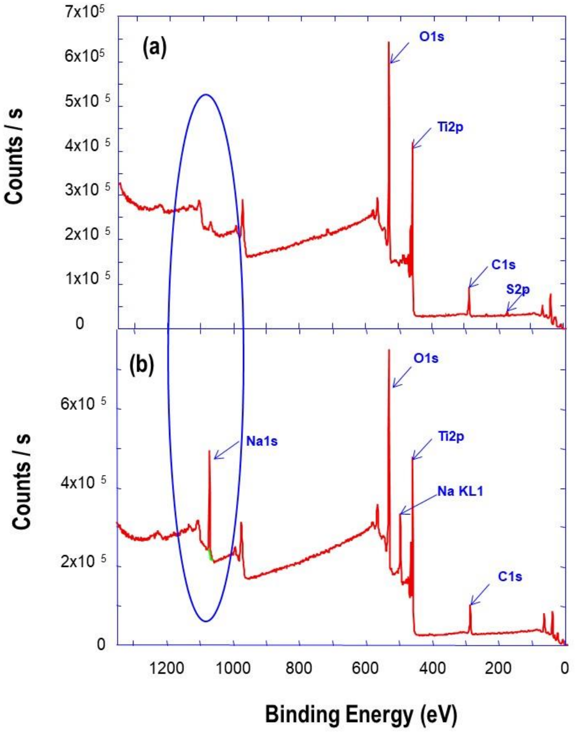

Figure 6 . XPS survey spectra of prepared TiO_2 (**a**) aggregate precursor (**b**) nanobelts after synthesis.

In Figure 7a, it is important to note that nanourchin-like nanoparticles show more enrolled nanosheet with more dense structure, as a consequence of the annealing process. The EDS analyses have been performed to determine the chemical composition of TiO_2 nanoparticles, after just synthesis, or after washing and annealing processes. In Figure 7 the obtained EDS spectra are depicted; it should be noted that, on the EDS spectrum of TiO_2 nanoparticles, after synthesis shows the presence of Na peak Figure 7b, whereas it is absent in the spectrum after the washing and annealing processes in Figure 7c. In fact, during the washing processes of $Na_2Ti_3O_7$ by HCl, Na^+ ions were exchanged by H^+ ions. These results are a clear evidence of the important role played by Na^+ ions in the formation of TiO_2 nanobelts, nanotube, and nanourchin morphologies.

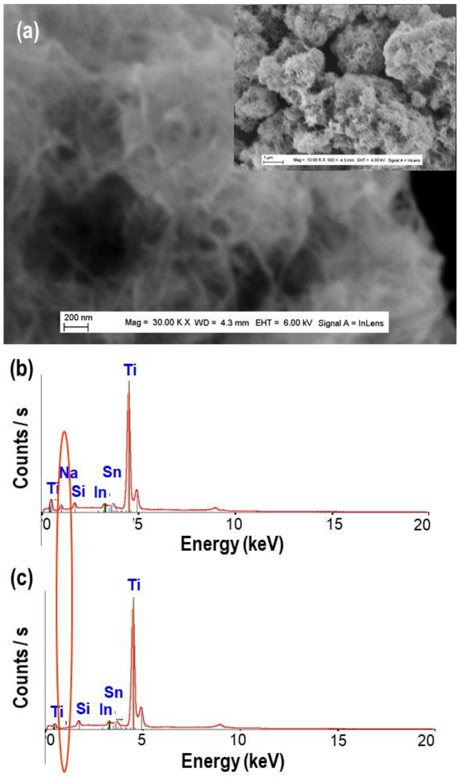

Figure 7. (**a**) FEGSEM images of TiO_2 nanourchin obtained at synthesis temperatures of 150 °C, after washing and annealing; (**b**,**c**) the corresponding EDS spectrum obtained just after synthesis and after washing and annealing processes, respectively.

The details of TiO_2 nanobelt and nanotube formation mechanisms are further investigated by using high resolution transmission electron microscopy (HRTEM). The influence of hydrothermal reaction time on the morphology of prepared TiO_2 nanomaterials is studied at 15, 180, and 360 min. At short reaction time of about 15 min, the morphology of prepared powder is mainly stretched nanosheet-like, with some minor rolled sheet. Closer analysis of prepared powder (Figure 8) shows different stages of the same formation mechanism.

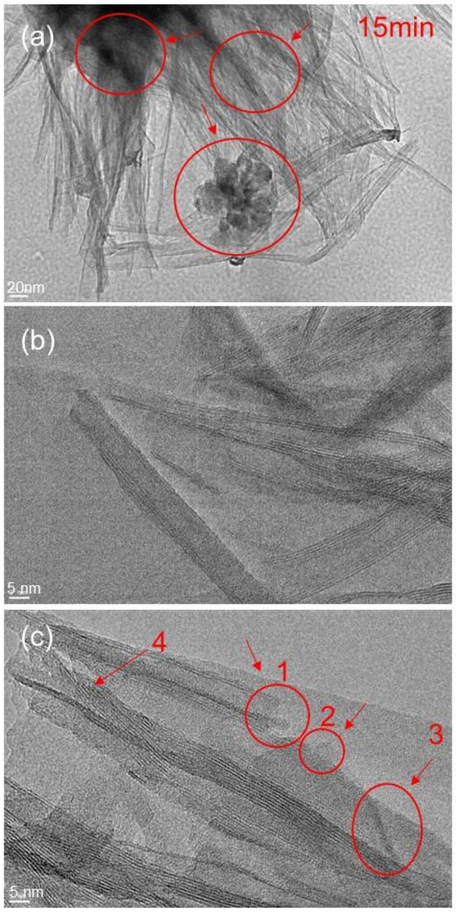

Figure 8 . HRTEM images with different magnifications (**a**–**c**) of TiO_2 nanotube prepared at synthesis temperature of 200 °C and synthesis time of 15 min.

In fact, the observed nucleation stage can be considered as an integrated growth process of nanobelt structure, from aggregates made of nanoparticles of about 20 nm diameter to nanobelt of several micrometers in length. Similar evolution was observed by other authors [4,29]. Thus, we may assume that the morphologies shown in Figures 8 and 9 represent different stages of the nanobelt growth process.

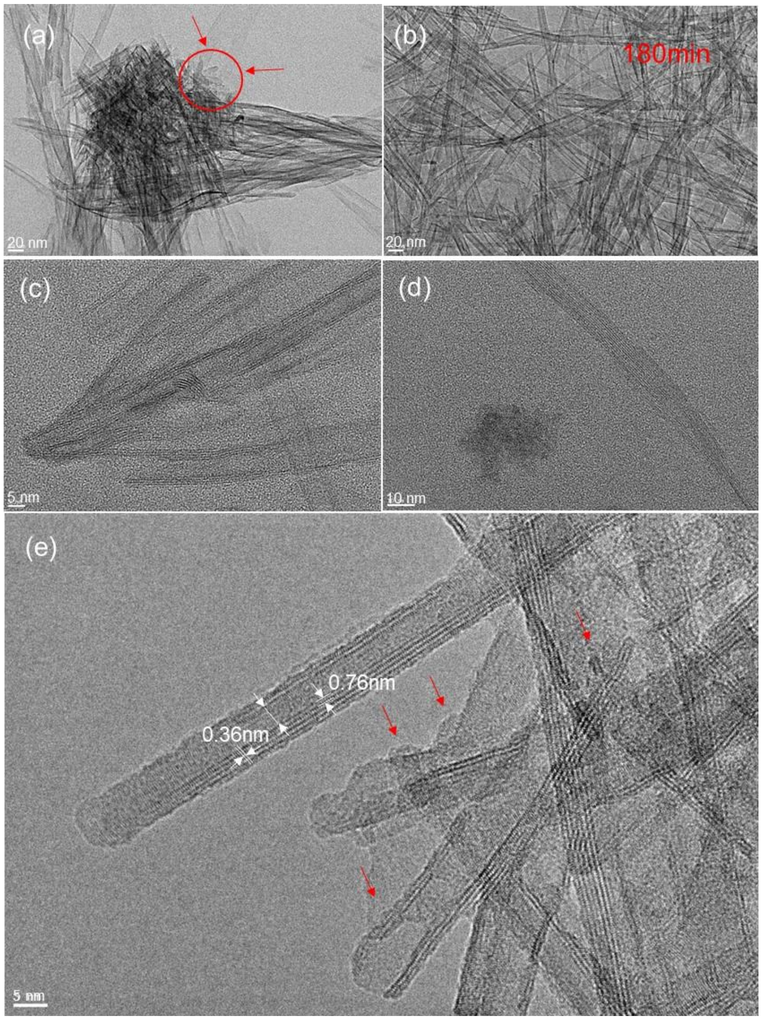

Figure 9 . HRTEM images with different magnifications (**a**–**e**) of TiO_2 nanotube prepared at synthesis temperature of 200 °C and synthesis time of 180 min.

It can be observed that at the earlier stage (reaction time of 15 min) of the nanobelt growth process, coalesced nanoparticles coexist with nanosheet like particles, indicated by zones in Figure 8a,c. Nanoparticles were located at the nanotube edges (region 1 and 2 in Figure 8c), and beside this simple attachment, an alignment of coalesced nanoparticles takes place (region 3 in Figure 8c). In addition, the nanosheet shows both stretched and rolled structures. The indicated region 4 in Figure 8c shows the starting process of nanosheet rolling. However, all these steps are a consequence of different nanobelt growth stages, which will evolve in a later stage to a nanotube structure observed in Figure 9 and nanobelt structure shown in Figure 10. However, at closer inspection of the nanosheet structure at an earlier stage, with a synthesis time of 15 min, we find that it presents an assembly of nanoparticles, whose sizes range from 5 to 20 nm, as indicated in selected region of Figure 8a, c. This proves that these nanoparticles and aggregates are the primary building units for the nanosheet formation process. Furthermore, it is well accepted in the literature that the key point for the formation of nanobelt-like structure is the formation of sodium titanate nanobelt intermediate, in which the sodium ion (Na^+) is inserted into space between TiO_6 octahedra layers, balancing their negative charges [4,29]. From the present experiments, it can be inferred that the aggregate of TiO_2 nanoparticles split up into nanosheets as a consequence of Na^+ insertion and their rolling in a second stage to form nanotube in an intermediate stage. Typical TEM and HRTEM patterns of TiO_2 nanotube are depicted in Figure 9, with similar structure of nanotube obtained using TiO_2 nanoparticles in terms of asymmetrical walls. It can be seen that the nanotube exhibits four layers on one side and two layers on the other (Figure 9e), which indicates that the nanotubes are formed by the scrolling of several layers of nanosheet, as previously observed by other authors. The interplane on both sides is of 0.36 nm, which corresponds to the (010) crystallographic plane, and is the characteristic of monoclinic $H_2Ti_3O_7$. It was reported for the same materials that the nanotube growth takes place along the (010) direction. Additionally, the interlayer distance between rolled nanosheets is about 0.76 nm closer to different reported values [29].

From XPS and EDX analysis in Figures 6 and 7, it is clearly demonstrated that the sodium ions are incorporated in the TiO_2 nanobelt, nanotube, and nanourchin, which suggest that it plays a role in their formation mechanisms. These observations indicate that nanobelts are formed by an orderly sticking of nanosheet and their coalescence in later stage; whereas nanourchins are formed by random assembly of the nanosheets.

The size dependence of the TiO_2 nanobelt on the size of TiO_2 aggregate precursor was demonstrated. Different sizes of TiO_2 aggregate precursors were used to prepare TiO_2 nanobelt, and the obtained results are depicted on Figure 10. It can be observed that the nanobelt length tends to increase with the increasing of the TiO_2 aggregate precursor size. Additionally, Figure 1). This confirms that TiO_2 nanoparticles play a role in the formation of different observed morphologies. In fact, if we assume that the formation of observed morphologies goes through the TiO_2 dissolution and precipitation, the TiO_2 nanoparticles size will not have any effects on the final nanoparticle size. Additionally, the observation of TiO_2 nanoparticles during the nanotube formation supports the mechanism through which sodium ions (Na^+) induce exfoliation of TiO_2 aggregates by insertion into the space between TiO_6 octahedra layers and their coalescence to form nanosheets at later stage. Furthermore, the present results provide additional arguments to support some reported works in the literature and contradict others [30,31], in which it was claimed that during the hydrothermal synthesis process, TiO_2 is dissolved through Ti–O–Ti bonds breaking and formation of sodium titanate nanosheet [29], which is converted to hydrogen titanate during the washing step and at a later stage to TiO_2 nanobelt after the annealing process.

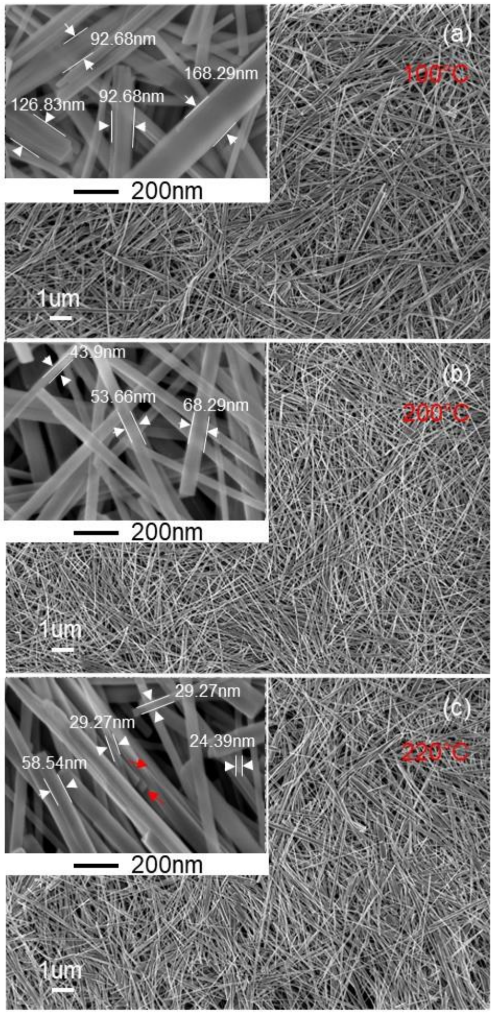

Figure 10 . FEGSEM images of TiO_2 nanobelts prepared at synthesis temperature of 200 °C and using TiO_2 aggregate precursors of different sizes prepared at temperatures of (a) 100°C, (b) 200°C, and (c) 220 °C, respectively.

It can be seen from the XRD results that the nanobelt powder, at different synthesis stages (Figure 11), shows a changing of crystalline structure. The TiO_2 aggregates precursor is of anatase phase, with tetragonal structure, in which TiO_6 octahedra are sharing their face and get stacked in a one-dimensional zigzag chain. During the synthesis of $Na_2Ti_3O_7$ nanobelts, a crystalline transition takes place, and TiO_2 anatase phase is transformed into an orthorhombic structure. In fact, the formation of sodium titanate nanobelt intermediate is obtained through the insertion of sodium ion (Na^+) into the space between TiO_6 octahedra layers, inducing the distortion of the initial structure.

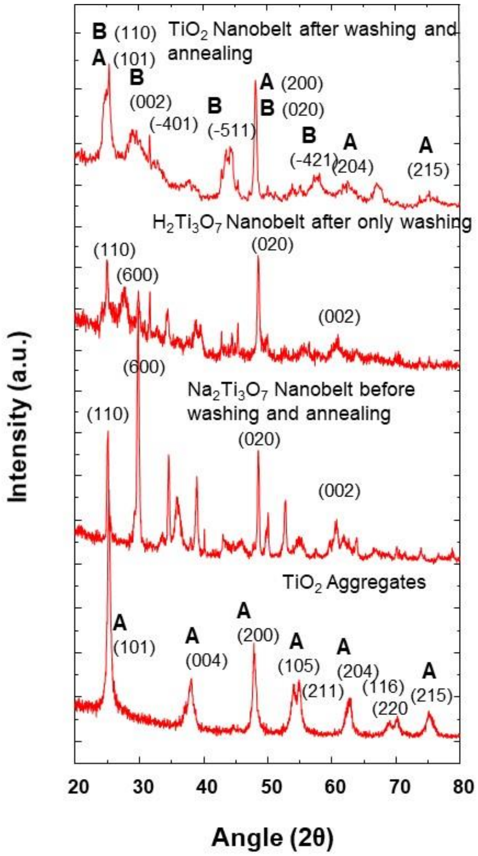

Figure 11 . XRD pattern of TiO_2 nanobelt at different synthesis stages as indicated and at the synthesis temperature of 100 °C (A: Anatase; B: TiO_2-B).

From these XRD results obtained at the synthesis temperature of 100 °C, it can be inferred that the anatase TiO_2 aggregate structure changes are a consequence of Na^+ insertion and a strong repulsion between Na^+ ions, which induces a distortion of the anatase crystalline structure. Similar behavior is observed with the insertion of Na^+ ion in the case of Na ion batteries charging/discharging cycles [33]. However, after the washing step with hydrochloric acid solution, the $H_2Ti_3O_7$ nanobelts are obtained as a consequence of proton exchange processes of sodium trititanate. From Figure 11, it can be seen that this exchanging of steps and the resulting orthorhombic structure of $H_2Ti_3O_7$ (JCPDS Card No. 47-0124) are accompanied by some XRD peak modifications, in terms of the intensity enhancement of some peaks, and their decrease for some others [34,35]. These modifications indicate the distortion of the initial structure after ion exchanges. Additionally, after the annealing process and the removal of protons, a mixture of anatase (JCPDS 21-1272) and TiO_2-B (JCPDS 35-0088) phases is obtained at the synthesis temperature of 100 °C. The obtained XRD pattern is similar to that obtained for the same mixture by Beuvier et al. [36]. A phase transition was observed when the morphology changed from nanotube to nanobelt, but with different compositions than those obtained at the synthesis temperature of 200 °C. It was reported by Zhang et al. that the TiO_2 nanoparticle size has a strong impact on the phase transformation during the growth of coalesced nanoparticles [37]. In addition, the temperature also plays an important role in the phase transformation of TiO_2 nanoparticles [26]. However, as when the temperature is changed the coalescence and/or growth of TiO_2 nanoparticles take place, both the temperature and the size contribute to the phase transformation and a formation of different phase mixtures depending on the used synthesis temperature 100 and 200 °C. Furthermore, as it can be observed from Figures 4 and 10, the peaks corresponding to the anatase phase are of lower intensity, which indicates that both of the latter synthesis temperatures produce a lower proportion of anatase, in agreement with different reported works in the literature [36]. During the synthesis process at a given temperature, the phase is also changed due to the insertion of different ions, and it is not necessary to dissolve and precipitate TiO_2 octahedra. Furthermore, from these results, it is worth noting that the synthesis temperature plays a crucial role in the phase control of prepared nanobelt powders.

4. Conclusions

Different morphologies of TiO_2 nanoparticles have been synthesized, in a large scale using hydrothermal synthesis technique and TiO_2 aggregate as a precursor. Both nanotube, nanourchin-like, and nanobelt-like nanoparticles were obtained at low temperatures and over short times. Furthermore, it is demonstrated that a morphology control of prepared TiO_2 powders could be achieved through the tuning of the synthesis temperature and time. The mechanisms formation of TiO_2 nanobelt-like, nanourchin-like, and nanotube nanoparticles are illustrated to involve TiO_2 nanoparticles coalescence and nanosheet intermediate, formed thanks to Na^+ ions exfoliation. Furthermore, it was found that the prepared TiO_2 nanomaterials properties were governed by those of TiO_2 nanoparticles aggregate. It has been demonstrated that it is possible to tune the nanobelt size by using different TiO_2 aggregates precursor sizes. Additionally, it was shown that the synthesis temperature enables the tuning of the phase's composition of the nanobelt powders. The investigation of prepared powders performance, as anode material for Li-ion batteries, is under progress in our group.

Funding: This research was funded by the European Union′s Horizon 2020 research and innovation program under the Marie Sklodowska-Curie grant agreement No. 734276.

Acknowledgments: The authors would like to thank Pierre Dubot from Université Paris Est Créteil, CNRS, ICMPE, UMR 7182, 2-8 rue Dunant F-94320 Thiais, France; for the XPS experiments. The authors would like also to thank the Chinese Scholar Council for supporting W.L. with a scholarship.

Conflicts of Interest: The authors declare no conflict of interest. The funders had no role in the design of the study; in the collection, analyses, or interpretation of data; in the writing of the manuscript; or in the decision to publish the results.

References

1. Fisher, A.C.; Peter, L.M.; Ponomarev, E.A.; Walker, A.B.; Wijiayantha, K.G.U. Intensity Dependence of the Back Reaction and Transport of Electrons in Dye-Sensitized Nanocrystalline TiO_2 Solar Cells, *J. Phys. Chem. B***.** **2000**, *104*, 949–958.
2. Tan, B.; Wu, Y. Dye-sensitized solar cells based on anatase TiO_2 nanoparticle/nanowire composites. *J. Phys. Chem. B.* **2006**, *110*, 15932–15938.
3. Schneider, J.; Matsuoka, M.; Takeuchi, M.; Zhang, J.; Horiuchi, Y.; Anpo, M.; Bahnemann, D.W. Understanding TiO_2 Photocatalysis: Mechanisms and Materials. *Chem. Rev.* **2014**, *114*, 9919–9986.
4. Zhao, Z.; Tian, J.; Sang, Y.; Cabot, A.; Liu, H. Structure, Synthesis, and Applications of TiO_2 Nanobelts. *Adv. Mater.* **2015**, *27*, 2557–2582.
5. Sun, B.; Shi, T.; Peng, Z.; Sheng, W.; Jiang, T.; Liao, G. Controlled fabrication of Sn/TiO_2 nanorods for photoelectrochemical water splitting. *Nanoscale Res. Lett.* **2013**, *8*, 1–8.
6. Trentler, T.J.; Hickman, K.M.; Goel, S.C.; Viano, A.M.; Gibbons, P.C.; Buhro, W.E. Solution-liquid-solid growth of crystalline III-V semiconductors: An analogy to vapor-liquid-solid growth. *Sci.* **1995**, *270*, 1791.
7. Wang, F.; Dong, A.; Buhro, W.E. Solution–Liquid–Solid Synthesis, Properties, and Applications of One-Dimensional Colloidal Semiconductor Nanorods and Nanowires. *Chem. Rev.* **2016**, *116*, 10888–10933.

8. Martin, C.R. Nanomaterials: A membrane-based synthetic approach. *Sci*. **1994**, *266*, 1961–1966.
9. Xu, G.R.; Wang, J.N.; Li, C.J. Template direct preparation of TiO_2 nanomaterials with tunable morphologies and their photocatalytic activity research. *Appl. Surf. Sci.* **2013**, *279*, 103–108.
10. Choi, Y.C.; Kim, W.S.; Park, Y.S.; Lee, S.M.; Bae, D.J.; Lee, Y.H.; Kim, J.M. Catalytic Growth of β-Ga_2O_3 Nanowires by Arc Discharge. *Adv. Mater.* **2000**, *12*, 746–750.
11. Morales, A.M.; Lieber, C.M. A laser ablation method for the synthesis of crystalline semiconductor nanowires. *Sci*. **1998**, *279*, 208.
12. Duan, X.; Lieber, C.M. General synthesis of compound semiconductor nanowires. *Adv. Mater.* **2000**, *12*, 298–302.
13. Li, L.; Qin, X.; Wang, G.; Qi, L.; Du, G.; Hu, Z. Synthesis of anatase TiO_2 nanowire by modifying TiO_2 nanoparticles using the microwave heating method. *Appl. Surf. Sci.* **2011**, *257*, 8006–8012.
14. Wang, H.E.; Zheng, L.X.; Liu, C.P.; Liu, Y.K.; Luan, C.Y.; Cheng, H.; Bello, I. Rapidmicrowave synthesis of porous TiO_2 spheres and their applications in dye sensitized solar cells. *J. Phys. Chem. C* **2011**, *115*,10419–10425.
15. Crippa, M.; Callone, E.; D'Arienzo, M.; Müller, K.; Polizzi, S.; Wahba, L.; Scotti, R. TiO_2 nanocrystal grafted on macroporous silica: A novel hybrid organic-inorganic sol-gel approach for the synthesis of highly photoactive composite material. *Appl. Catal. B*. **2011**, *104*, 282–290.
16. Poudel, B.; Wang, W.Z.; Dames, C.; Huang, J.Y.; Kunwar, S.; Wang, D.Z.; Ren, Z.F. Formation of crystallized titania nanotubes and their transformation into nanowires. *Nanotechnology* **2005**, *16*, 1935–1940.
17. Asiah, M.N.; Mamat, M.H.; Khusaimi, Z.; Abdullah, S.; Rusop, M.; Qurashi, A. Surfactant-free seed-mediated large-scale synthesis of mesoporous TiO_2 nanowires. *Ceram. Int.* **2015**, *41*, 4266–4266.
18. Cui, L.; Hui, K.N.; Hui, K.S.; Lee, S.K.; Zhou, W.; Wan, Z.P.; Thuc, C.N.H. Facile microwave-assisted hydrothermal synthesis of TiO_2 nanotubes. *Mater. Lett.* **2012**, *75*, 175–178.
19. Byrappa, K.; Adschiri, T. Hydrothermal technology for nanotechnology. *Prog. Cryst. Growth Charact. Mater.* **2007**, *53*, 117–166.

20. Yu, J.; Su, Y.; Cheng, B.; Zhou, M. Effects of pH on the microstructures and photocatalytic activity of mesoporous nanocrystalline titania powders prepared via hydrothermal method. *J. Mol. Catal. A Chem.* **2006**, *258*, 104–112.
21. Mamaghani, A.H.; Haghighat, F.; Lee, C.S. Role of titanium dioxide (TiO_2) structural design/morphology in photocatalytic air purification. *Appl. Catal. B Environ.* **2020**, *269*, 118735.
22. Hoang, S.; Guo, S.; Hahn, N.T.; Bard, A.J.; Mullins, C.B. Visible light driven photoelectrochemical water oxidation on nitrogen modified TiO_2 nanowires. *Nano Lett.* **2012**, *12*, 26–32.
23. Pan, X.; Zhao, Y.; Liu, S.; Korzeniewski, C.L.; Wang, S.; Fan, Z. Comparing graphene-TiO_2 nanowire and graphene-TiO_2 nanoparticle composite photocatalysts. *ACS Appl. Mater. Interface* **2012**, *4*, 2944–3950.
24. Chen, J.Z.; Ko, W.Y.; Yen, Y.C.; Chen, P.H.; Lin, K.J. Hydrothermally processed TiO_2 nanowire electrodes with antireflective and electrochromic properties. *ACS Nano.* **2012**, *6*, 6633–6639.
25. Kasuga, T.; Hiramatsu, M.; Hoson, A.; Sekino, T.; Niihara, K. Formation of titanium oxide nanotube, *Langmuir* **1998**, *14*, 3160–3163.
26. Taleb, A.; Mesguich, F.; Hérissan, A.; Colbeau-Justin, C.; Yanpeng, X.; Dubot, P. Optimized TiO_2 nanoparticle packing for DSSC photovoltaic applications. *Sol. Energy Mater. Sol. Cells.* **2016**, *148*, 52–59.
27. Wang, Y.D.; Zhang, S.; Ma, C.L.; Li, H.D. Synthesis and room temperature photoluminescence of ZnO/CTAB ordered layered nanocomposite with flake-like architecture. *J. Lumin.* **2007**, *26*, 661.
28. Wang, H.X.; Li, X.X.; Tang, L. Effect of surfactants on the morphology and properties of TiO_2. *Appl. Phys. A.* **2020**, *126*, 448.
29. Wu, D.; Liu, J.; Zhao, X.; Li, A.; Chen, Y.; Ming, N. Sequence of events for the formation of titanate nanotubes, nanowire and nanobelts. *Chem. Mater.* **2006**, *18*, 547–553.
30. Mamaghani, A.H.; Haghighat, F.; Lee, C.S.Photocatalytic oxidation technology for indoor environment air purification: The state-of-the-art. *Appl. Catal. B Environ.* **2017**, *203*, 247–269.
31. Diebold, U.; Ruzycki, N.; Herman, G.S.; Selloni, A. One Step towards Bridging the Materials Gap: Surface Studies of TiO_2 Anatase. *Catal. Today.* **2003**, *85*, 93–100.

32. Ding, L.; Chen, J.; Dong, B.; Xi, Y.; Shi, L.; Liu, W.; Cao, L. Organic macromolecule assisted synthesis of ultralong carbon&TiO_2 nanotubes for high performance lithium-ion batteries. *Electrochem. Acta* **2016**, *200*, 97–105.

33. Massaro, A.; Munoz-Garc, A.B.; Maddalena, P.; Bella, F.; Meligrana, G.; Gerbaldi, C.; Pavone, M. First-principles study of Na insertion at TiO_2 anatase surfaces: New hints for Na-ion battery design, *Nanoscale Adv*. **2020**, *2*, 274.

34. Yao, B.D.; Chan, Y.F.; Zhang, X.Y.; Zhang, W.F.; Yang, Z.Y.; Wang, N. Formation mechanism of TiO_2 nanotubes. *Appl. Phys. Lett.* **2003**, *82*, 281.

35. Wang, W.; Varghese, O.K.; Paulose, M.; Grimes, C.A.; Wang, Q.; Dickey, E.C. A study on the growth and structure of titania nanotubes. *J. Mater. Res*. **2004**, *19*, 417.

36. Beuvier, T.; Richard-Plouet, M.; Mancini-Le Granvalet, M.; Brousse, T.; Crosnier, O.; Brohan, L. TiO_2(B) Nanoribbons as negative electrode material for lithium-ion batteries with high-rate performance. *Inorg. Chem*. **2010**, *49*, 8457–8464.

37. Zhang, H.; Banfield, J. Understanding polymetric phase transformation behavior during growth of nanocrystalline aggregates: Insights from TiO_2. *J. Phys. Chem. B* **2000**, *104*, 3481–3487.

CHAPTER III: Influence of TiO_2 nanoparticle morphologies on the performance of lithium-ion batteries

Summary

In this work, we used TiO_2 powders of different morphologies described in the previous chapter, as anode materials for lithium-ion batteries, and we evaluated their performance in terms of specific capacity and cyclability. Our results showed that the morphology has an influence on the capacity only during the first discharge/charge cycles of the lithium-ion battery. During the following cycles, the capacity decreases to stabilize in a second time. By scanning electron microscopy, we have shown that the different morphologies are transformed into aggregates, during the first cycles by a disintegration process. During the lithiation/delithiation process of lithium ions, a volume variation occurs, and it is at the origin of the disintegration phenomenon. The difference between the capacities of the different morphologies, during the first cycle of charge and discharge, can be explained both by the specific surface of the aggregates and by the properties of their porosity in terms of pore size and connectivity. Furthermore, we have also shown that changes in morphology during battery preparation can be taken into account to explain variations in specific capacity. During the following cycles, as all the TiO_2 morphologies transform into aggregates of TiO_2 nanoparticles, we can assume that the pore connectivity is the same for all the powders, and that the specific capacity of the powders is mainly influenced by the specific surface area and by the pore size.

Influence of TiO_2 nanoparticle morphologies on the performance of lithium-ion batteries

Wenpo Luo[1], Juliette Blanchard[2], Abdelhafed Taleb[1,2 *]

[1] *PSL Research University, Chimie ParisTech - CNRS, Institut de Recherche de Chimie Paris, 75005, Paris, France*, abdelhafed.taleb@chimieparistech.psl.eu (A. T), WenpoLuo@outlook.com (W.L)

[2] *Sorbonne université, 4 place Jussieu, 75231 - Paris France*

[3] *LRS - Laboratoire de Réactivité de Surface*, juliette.blanchard@sorbonne-universite.fr

Abstract: TiO_2 nanoparticles of different morphologies were prepared successfully using the hydrothermal method, and were characterized by different techniques, such as X-ray diffraction (DRX), scanning electron microscopy (FEGSEM) and N_2-sorption. Prepared TiO_2 nanoparticles were used as anode materials for the lithium-ion batteries (LIB), and their electrochemical properties were tested using charging/discharging measurements. The results demonstrated that the nanoparticles morphology plays a major role in the batteries performance, and that a better capacity was obtained for TiO_2 nanobelts morphology. A mechanism, behind the capacity decreasing with the number of cycling, was suggested and discussed.

Keywords: Titania, nanoparticles, aggregates, morphologies, Li-ion batteries

---

*Corresponding author. Tel.: +33155426378; fax: +331442767 50
E-mail address: abdelhafed.taleb@chimieparistech.psl.eu (A. Taleb).

1. Introduction:

The renewable energies are increasingly becoming an alternative solution to overcome the problems of fossil energies pollution and the increasing energy demand of human activities. However, at present, the storage of renewable energies is one of the issues which limits its use when it is required, and still need to be addressed. This concern motivated the development of different storage systems, such as batteries [1-2], and supercapacitors [3-4]. Among the energy storage technologies, the batteries appear to be the prominently promising.

Nowadays, over all the secondary batteries, lithium-ion batteries (LIB) are the most used technology, which drew a tremendous attention from the scientific community. This is due to their performance such: compactness, high power, high density of energy and high cyclability. LIB are the most popular secondary batteries used as source of energy in portable technologies and electric vehicles [5-6]. Whereas in plants of solar and wind energy it plays a role of storage energy systems [7]. Research to overcome the LIB limitations challenges and improve its performance is a hot topic in material science. Even if some limitations were overcome, some of them are still under investigation. Recent progress is mainly devoted to prepare innovative anode materials with optimized properties, which allow the alleviation of it volume variation during the batteries cycles. It is well accepted that the electrode materials play a major role in determining the efficiency of batteries. The main consequence of the expansion and shrinkage of the anode material volume during the lithiation and delithiation is the anode cracking, which could induce the LIB explosion due to overcharging [8-9].

Different strategies were reported to overcome the reduction of the anode volume expansion, with among them, a better choice of the materials composition and/or architecture. Regarding the material composition, TiO_2 polymorphes were used for LIB application, and have been shown to have a low volume variation, of less than 4%, during Li^+ lithiation/delithiation [10-11]. TiO_2 polymorphs have additional advantages, which make them a convenient candidate for LIBs application, such as high mechanical and chemical stability, environmental friendliness, low cost, high cyclability, relatively high theoretical capacity of 335 mAh g^{-1} (anatase phase), and a flat working potential [12-13].

Furthermore, nanoparticles agglomeration has also proven to be a promising approach to obtain materials with the desired architecture to alleviate the volume variation during LIB charging/discharging cycles [14]. The assemblies of nanoparticles with different sizes offer a large number of possibilities to tailor the porosity of agglomerated materials, in terms of size and size distribution. In addition, the nanoparticle assemblies give rise to several cases of pores connectivity [15]. This kind of materials architecture is more flexible, allowing to combine several material properties, even if they are of conflicting nature [16]. For LIB application, agglomeration of nanoparticles offers the possibility to accommodate the structure stress of the anode material, induced by the lithium insertion, which enhances the recycling stability of LIBs. Furthermore, agglomerated material provides high interface area in contact with the electrolyte, which strongly reduces the Li^+ ions diffusion paths in the material network.

In the present work, TiO_2 materials with micro- and nano- structures made by TiO_2 nanoparticles of different morphologies, as building unit, have been prepared using the hydrothermal method. The obtained results revealed that the nanoparticle morphologies have a great influence on the performance. Furthermore, on the light of the LIB literature and the present results, the capacity decreasing with the number of charging and discharging cycles was discussed in terms of the morphology evolution of TiO_2 nanoparticles, and in turn the properties of their assembly with the LIB cycles.

2. Experimental.

2.1. Synthesis of TiO_2 nanoparticles and aggregates

For TiO_2 nano-urchin, nanotube and nanobelt nanoparticles synthesis, the hydrothermal method was used. TiO_2 aggregates were used as a precursor and prepared according to previously published protocols [17].

For the nanoparticle synthesis, 0.5 g powder of TiO_2 aggregate precursor was introduced in a Teflon-lined autoclave with the capacity of 25 mL. After, the autoclave was filled with 10 M NaOH solution up to 80% of the autoclave capacity. Depending on the desired morphology, the synthesis temperature was maintained at different temperatures of 100, 150, and 220 °C with the heating rate of 2.5 °C/min and the synthesis time of 360, 180, and 15 min. Afterwards, obtained nanoparticle powders are subjected to the washing and annealing protocols to obtain at the final stage of these processes: sodium titanate. This latter product was washed many times with diluted HCl solution to reach a pH value of 1, and then with distilled water to attain a pH value of 7. At the final stage of the synthesis process, the obtained powder was dried overnight in the oven, and annealed in air at temperature of 500 °C for 30 min, with the heat rate of 5 °C/min. All the used chemicals are of analytical grade and used as purchased without further purification. The used water was purified by Milli Q System (Millipore, electric resistivity 18.2 MΩ.cm).

Four powders were prepared with different morphologies depending on the synthesis temperature and time. The powders are named namely TiO_2-NU-100°C (nanourchin nanoparticles prepared at synthesis temperature of 100°C), TiO_2-NU-150°C (nanourchin nanoparticles prepared at synthesis temperature of 150°C), TiO_2-NT-200°C (nanotube nanoparticles prepared at synthesis temperature of 200°C and synthesis time of 15 min) and TiO_2-NT-200°C (nanobelt nanoparticles prepared at synthesis temperature of 200°C and synthesis time of 360 min).

2.2. Characterization of prepared of TiO_2 nanoparticles and aggregates

The morphological investigations of the prepared TiO_2 nanoparticles and aggregates were achieved with a high-resolution Ultra 55 Zeiss FEG scanning electron microscope (FEGSEM) operating at an acceleration voltage of 10 kV.

The crystalline structure of TiO_2 was determined by an X-ray diffractometer (Siemens D5000 XRD unit) in 2θ range from 20° to 80° by $0.07^{\circ}\ s^{-1}$ increasing steps operating at 40 KV accelerating voltage and 40 mA current using Cu $K\alpha$ radiation source with λ= 1.5406 Å.

Nitrogen adsorption - desorption isotherms were measured at liquid nitrogen temperature on a BelSorp Max apparatus. Before analysis, the samples were degassed at 120°C for 10 hours. The specific surface area (SBET) was evaluated using the Brunauer-Emmett-Teller (BET) method in the P/P° range of 0.05-0.25. The pore size distribution was determined from the desorption branch of the isotherm using the NLDFT method (cylindrical pores; oxide materials). The total pore volume was determined from the amount of N_2 adsorbed up to P/P°=0.98.

The chemical compositions of all the samples were determined by the FEGSEM using a Princeton Gamme-Tech PGT, USA, spirit energy dispersive spectrometry EDS system. The chemical compositions of all the samples (TiO_2 nanoparticles and aggregates) were determined by X-ray photoelectron spectroscopy (XPS), For the measurements we used a RIBER MACII analyzer system equipped with a Al Kα X-ray source (hυ = 1486.6 eV; spot size 20 mm, power = 11 kVx50 w). Charges effects were corrected by setting the lowest energy carbon peak (C1s) at 285.0eV.

The electrochemical tests were performed in Teflon Swagelok half-cells, where TiO_2 composite was used as a working electrode and a Li metal foil (Sigma Aldrich) as a reference and a counter electrode in a battery grade electrolyte having the composition: 1M $LiPF_6$ ethylene carbonate, propylene carbonate and dimethyl carbonate (1:1:1, v/v/v) with 1%wt vinylene carbonate, purchased from Solvionic, France). The TiO_2 composite electrode was prepared using a mortar, from a mixture of prepared TiO_2 active material (80 wt %), 7 wt % of mesoporous carbon, 7% of graphite powder and 6 wt % of poly(tetrafluoroethylene) (PTFE). The prepared homogenous mixture is uniformly pressed onto a stainless-steel foil substrate with pression of 125bar. Thirdly, this electrode was dried in the oven for the whole night at temperature of 80℃. Glass microfiber filter (Grade GF/D (Whatman)) 0.67 mm thick, with a pore size of 2.7 um (GmF) was used as a separator. The Swagelok cells were assembled in the MBraun Glove Box (with H_2O < 1 ppm and

$O_2 < 1$ ppm). Assembled batteries were galvanostatically cycled in the voltage range between 3 - 1.0 V vs Li/Li^+ at a charge/discharge rate of C/10 (full charge or discharge in 10 h), using a VMP3 Biologic multi-channel potentiostat/galvanostat.

3. Results and discussion.

Using different synthesis protocols, white powders were obtained, and were characterized using different techniques.

The morphology of the prepared powders was characterized by FEGSEM, and the obtained morphologies are shown in Figure. 1. At higher synthesis temperature of 200°C, Figure. 1(a) and 1(b), it is shown that TiO_2 powder is of nanotube morphology at short synthesis time of 180min, and nanobelt like morphology at a longer synthesis time of 360min, respectively. The insert of Figure. 1 (b) shows a bundle of several nanobelts stacking along their long axis direction. It can also be observed that the prepared nanobelts are of homogeneous thickness of about 10 nm, with a diameter ranging from 50 to 100 nm, and a length of more than 10 micrometers. At higher magnification scale, the nanobelts show smooth surface without any contamination. Furthermore, the indicated regions in Figure. 1(b), shows curved nanobelts, which illustrate their high elasticity. At the synthesis temperature of 100°C, prepared powder is of urchin like morphology, with connected stretched sheet like, to form a randomly connected network (Fig. 1(c)). At the synthesis temperature of 150°C, the morphology is similar to that obtained at a temperature of 150°C, but with more rolled nanosheet (Fig. 1(d)).

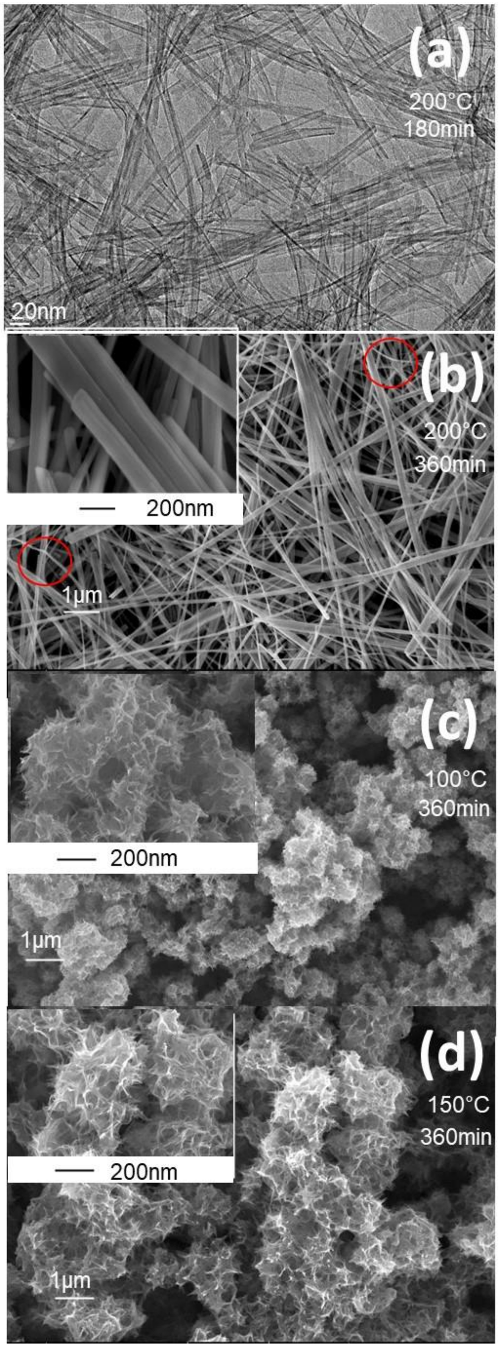

Figure 1: FEGSEM and TEM images of TiO_2 powder of different morphologies prepared at different synthesis time and temperature. (a) TEM image of TiO_2-NT-200°C powder prepared at synthesis temperature of 200°C, over 180min, (b) FEGSEM image of TiO_2-NB-200°C powder prepared at synthesis temperature of 200°C over 360min, (c) FEGSEM image of TIO_2-NU-100°C powder prepared at synthesis temperature of 100°C, over 360min and (d) FEGSEM image of TiO_2-NU-150°C powder prepared at synthesis temperature of 150°C, over 360min. the insert are the high magnifications.

The EDS spectrometry was used to analyze the chemical composition of prepared TiO_2 powders with different morphologies after synthesis (Fig. 2(a)) and after washing and annealing steps (Fig. 2(b)). The EDS spectra, shows the peak corresponding to Na just after synthesis Fig. 2(a), whereas after washing and annealing steps the Na peak is completely absent Fig. 2(b), which indicate the complete exchange of Na^+ ions by H^+ during the washing step.

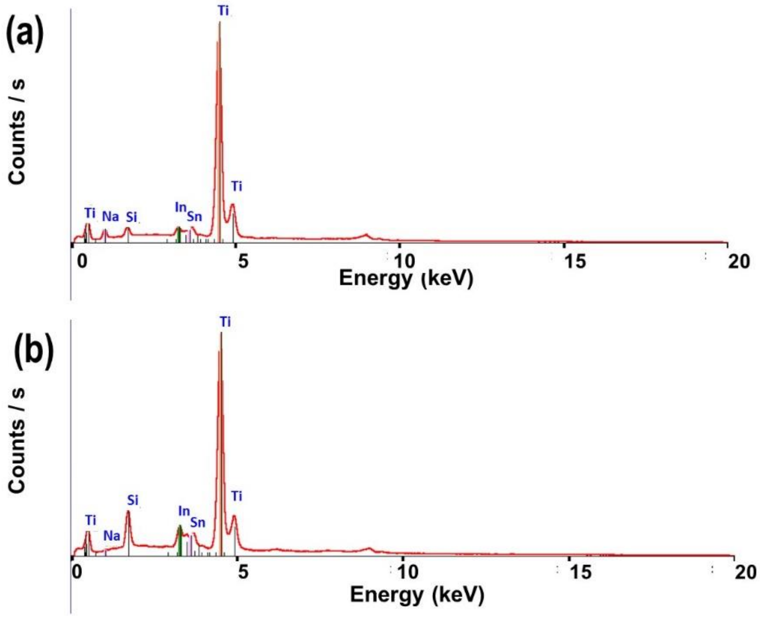

Figure 2: EDS spectrum images of prepared TiO_2 powders (a) just after synthesis and (b) after washing and annealing processes.

The crystalline structure and phase of prepared TiO_2 powder with different morphologies were investigated by XRD method, and the obtained patterns are depicted in Figure. 3. In the case of TiO_2 nano-urchin and nanotube morphologies (TiO_2-NT-200°C, TiO_2-NU-150°C and TiO_2-NU-100°C), a well pronounced peaks were observed and were assigned to (-511) and (020) crystallographic planes of pure TiO_2 (B) phase (JCPDS No. 35-008) (Fig. 3). In the case of TiO_2

nanobelt morphology (TiO_2-NB-200°C), the well resolved XRD peaks were attributed to a mixture of anatase (JCPDS 83-2243) and TiO_2-B (JCPDS 35-0088) phases (Fig. 3).

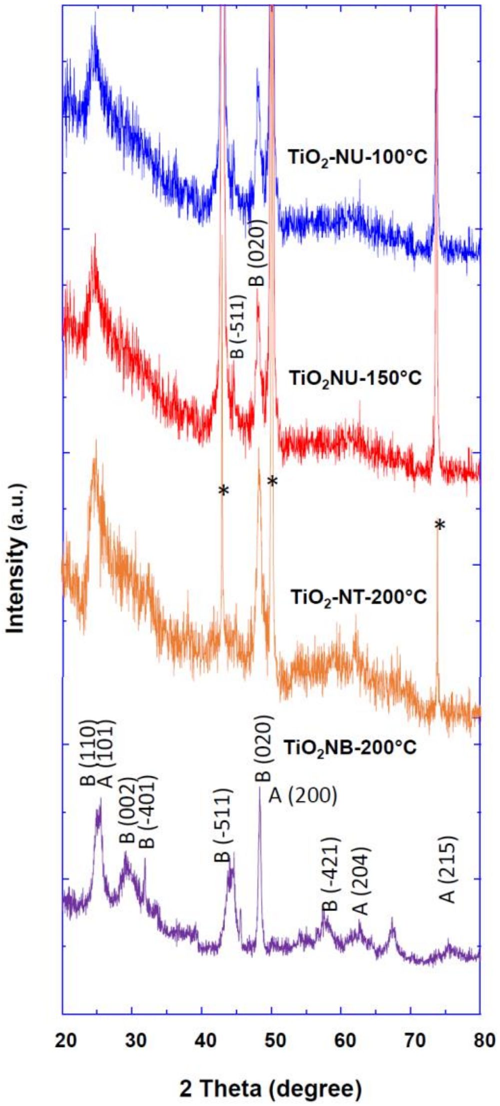

Figure 3: XRD pattern of TiO_2 powders with different morphologies prepared at different synthesis temperatures as indicated. The peaks with stars correspond to the substrate.

The properties of prepared TiO_2 powders in terms of specific surface area, and the average pore size, were evaluated by analyzing the nitrogen adsorption/desorption isotherms. From the isotherm curves (Fig.4), the specific surface areas (BET model) were calculated to be 270 m^2g^{-1}, 329 m^2g^{-1}, 434 m^2g^{-1} and 335 m^2g^{-1}, for respectively the TiO_2 powder morphology of nanobelt (TiO_2-NB-200°C), nanotube (TiO_2-NT-200°C), nano-urchin (TiO_2-NU-100°C) and (TiO_2-NU-150°C). For most of the samples a multiscale porosity is observed: the smaller pores (2.5-3 nm) are likely due to the intrinsic porosity of the particles (porosity of the tubes, belt or sheet), while the porosity leading to the second maximum in the pore size distribution (about 5 nm) is probably related to pores resulting from the aggregation of the primary particles. Lastly, the larger pores (between 10 and 20 nm) could result from the flexible porosity formed between particles that are not chemical link. It is worth noting that the porosity of TiO_2-NU-150°C is similar to that of TiO_2-NT-200°C, which is consisting with the fact that the nanotube particles are obtained by nanosheets enrolling as reported previously [17]. It is commonly accepted that the large surface area enhances the material contact surface with the electrolyte and the large pore size favors fast diffusion and transfer toward the material surface [18]. These characteristics favor the improvement of LIB rate capability.

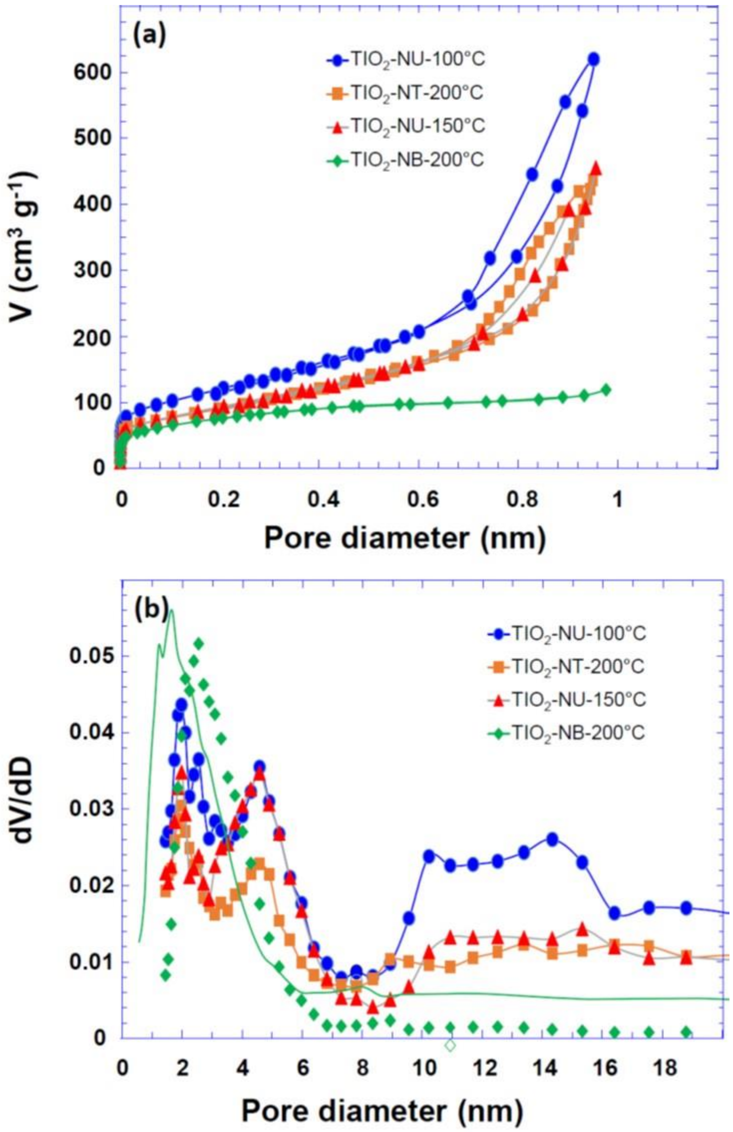

Figure 4: (a): N_2 physisorption isotherm of TiO_2 powders with different morphologies as indicated; (b) : the corresponding pore size distribution (NLDT).

The electrochemical characterizations of prepared TiO_2 powders with different morphologies were performed. The obtained discharging/charging curves at a current rate of C/10 are shown in Fig. 5.

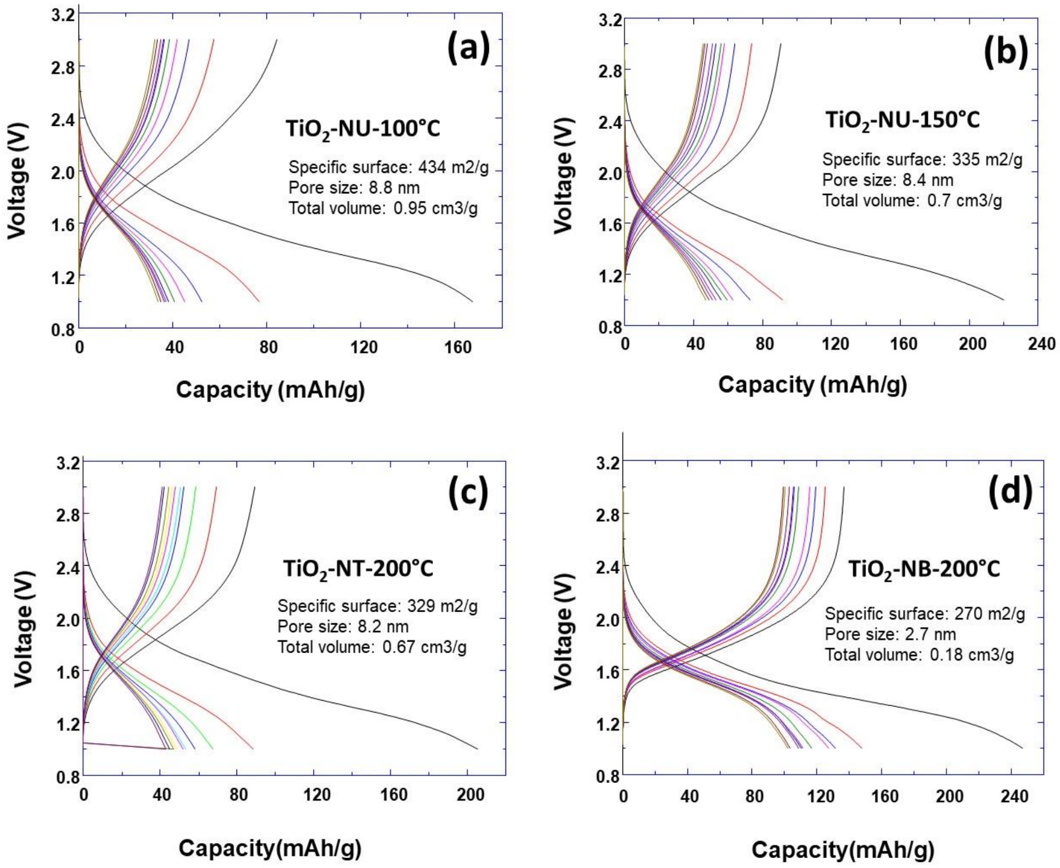

Figure 5: the potential-capacity curves corresponding to discharge/charge cycles of the 10 first cycles for different TiO_2 powder morphologies.

It can be observed that the specific capacity decreases as a function of the number of discharging/charging cycles (Fig. 6). At the first initial discharging process, the highest capacity of about 250 mAh/g was observed for the nanobelt morphology. For the other morphologies, this initial capacity was about 210 mAh/g, 170 mAh/g and 220 mAh/g for respectively the TiO_2 powder morphologies of nanotube (TiO_2-NT-200°C), and nanourchin (TiO_2-NU-100°C and TiO_2-NU-150°C). One could expect that higher capacities are associated to materials with a higher specific surface, which provide a higher contact surface area with the electrolyte. For example, on can be observed that TiO_2 powders of nanotube and nano-urchin150 morphologies show similar specific capacity, which could be explained by their similar specific surface area. Moreover, TiO_2 powder with nano-urchin morphology shows more enrolled nanosheets (TiO_2-NU-150°C) which resembles that of the nanotube morphology. However, the TiO_2-NU-100°C powder has a higher specific surface than TiO_2-NU-150°C (434 vs 335 m^2/g), and should, normally, exhibit a higher capacity. The electrochemical measurements show actually a lower capacity, which is very surprising, if only the specific surface parameter is considered.

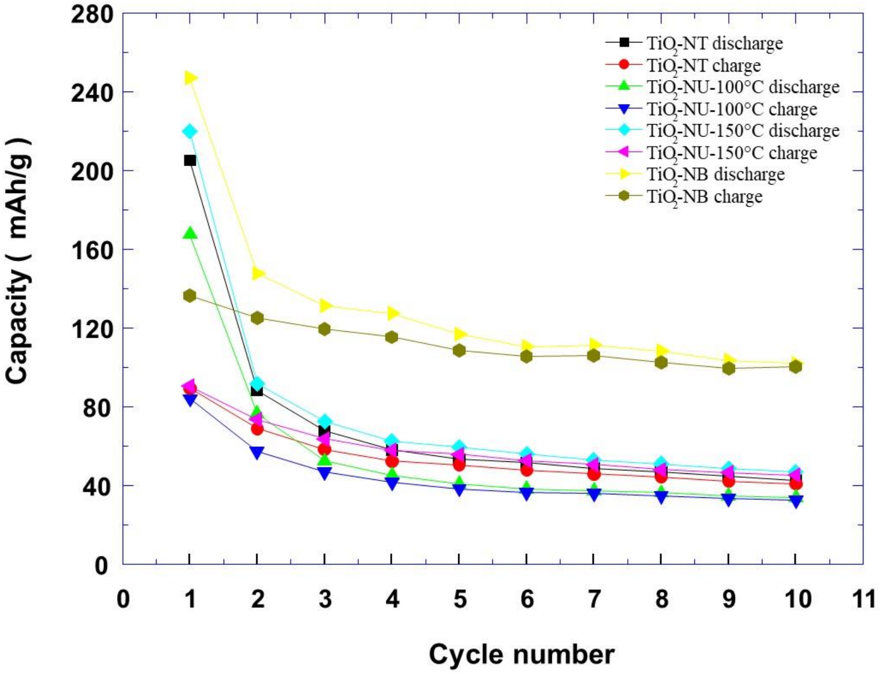

Figure 6: The curves of specific capacity versus the number of discharge/charge of the 10 first cycles for different TiO_2 powder morphologies.

After the first discharging step, the specific capacity decreases very fast for all prepared TiO_2 powder morphologies, and it reaches a plateau after a few numbers of discharging/charging cycles. To understand this behavior, another phenomenon of individual nanoparticles should be discussed to explain the observed variation of the specific capacity versus the number of discharging/charging cycles. In fact, it was reported that the anode material expansion and shrinkage during the lithiation/dilithiation induces the formation of cracks, and the initial TiO_2 particles disintegration into small nanoparticles. This in turn provokes the electric disconnection between the current collector and the anode materials. This lowers the LIB cycling stability and specific capacity [19]. Hereafter, we will discuss how the control over the TiO_2 powder morphology may be used to improve the Li ion batteries performance. It is well accepted that the pore size and the specific surface depend on the prepared TiO_2 powder morphology and it plays a crucial role in the optimization of the Li ion batteries specific capacity. To understand how these parameters are behind the observed decreasing of the specific capacity, versus the discharging/charging cycles, we must investigate the evolution of the TiO_2 powder morphology during the cycling process. To check this point, the FEGSEM characterization was performed just after preparation of the anode for batteries testing and after 10 discharging/charging cycles. The results are presented in Figure 7, 8 and 9, for prepared TiO_2 powders with different morphologies. The TiO_2-NU-100°C powder, with stretched nanosheets, starts to collapse during the preparation of the anode electrode (Fig. 7(a) and 7(b)), inducing the decrease of the anode specific surface. After the 10th discharging cycle, it can be observed that the nanosheets of nano-urchin morphology did mostly collapse, to form aggregates of around 100nm diameter (Fig. 7(c) and (d)). The observed peculiarity with the TiO_2-NU-100°C powder, in terms of low specific capacity (Fig. 6), despite that it is characterized by the highest specific surface, could be explained by the fact that the stretched sheet forming nano-urchin morphology are easy to collapse, during the battery's fabrication process. After their preparation, the nano-urchin morphology evolves to a denser structure with a lower specific surface than that of nanobelt morphology. Similar nanosheets collapse behavior was previously observed with TiO_2 powders of nano-urchin morphology by Tian Hui et al [20]. Similar

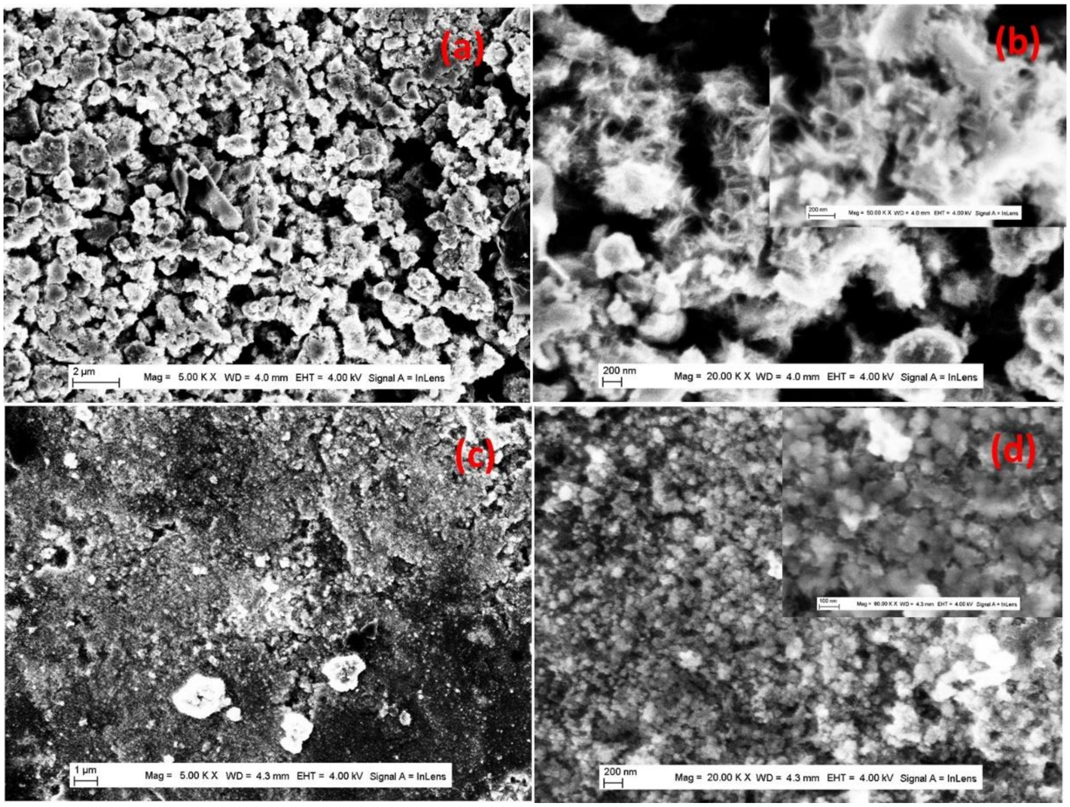

Figure 7: FEGSEM images of TiO_2 powder with nano-urchin100 morphology (a) and (b) different magnifications of the anode materials after preparation (c) and (d) different magnification de anode materials after 10 discharging/charging cycles. The inserts are the corresponding high magnification.

behavior was observed with TiO_2-NB-200°C powder, in terms of strong decreasing of the LIB specific capacity between the first and the 10th discharging cycle (Fig. 6). To understand this behavior in the case of nanobelt morphology, we analyzed closely the FEGSEM characterization before batteries testing, and after the 10th discharging cycle (Fig. 8). Just after the preparation of the anode, the TiO_2 powder keep its nanobelt morphology as it can be clearly identified in the FEGSEM pattern of Figure 8(a) and 8(b). After the 10th cycle, only the aggregates with diameter ranging from 50nm to 200nm could be observed, in addition to a few nanobelts (Fig. 8(c)-8(g)). Further analysis of the observed nanobelt shows its transformation into aggregates of nanoparticles (Fig. 8(d)-8(g)).

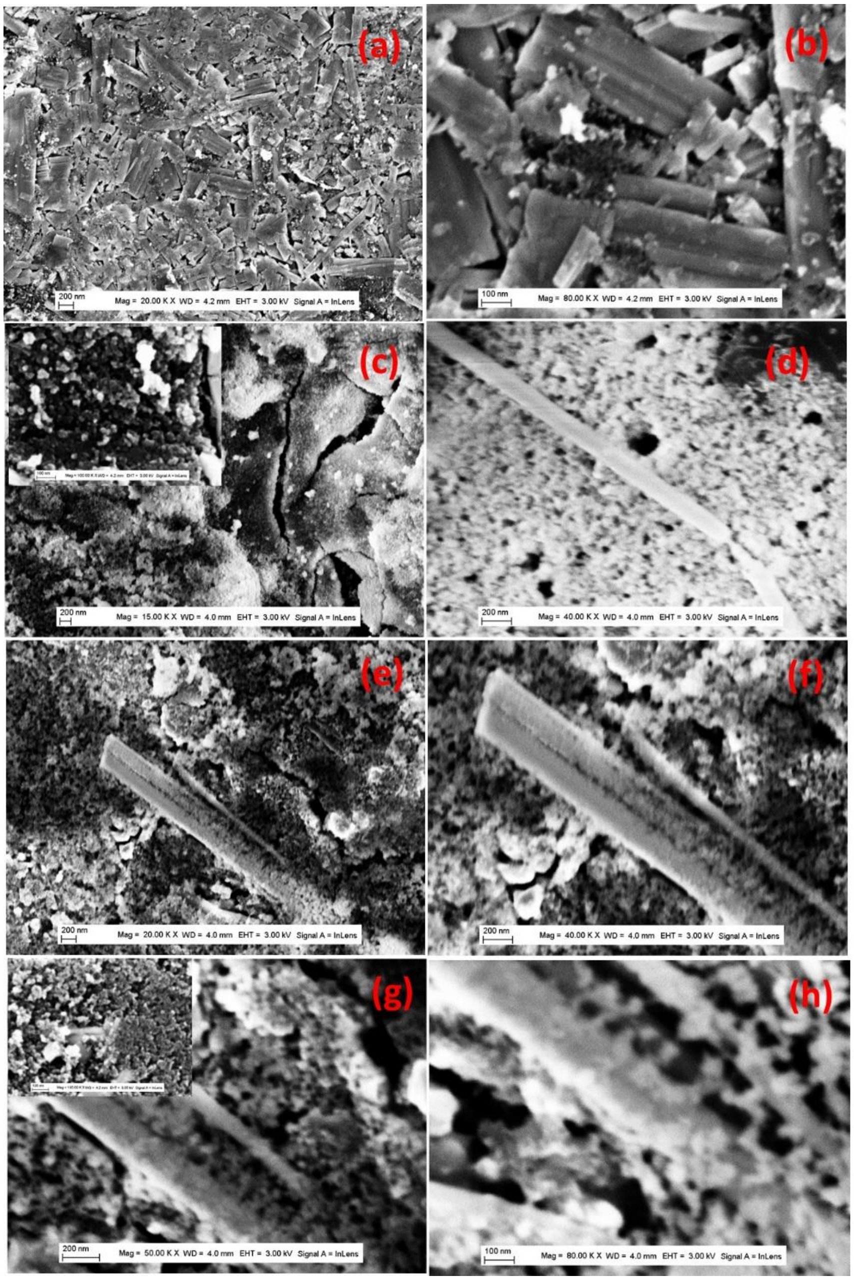

Figure 8: FEGSEM images of TiO_2 powder with nanobelt morphology (a) and (b) different magnifications of the anode materials after preparation (c)-(h) different magnifications de anode materials after 10 discharging/charging cycles. The inserts are the corresponding high or low magnification.

In fact, it is well known that lithium storage capacity in the anode material induces its expansion during the lithium insertion, which can provoke mechanical fracture in individual nanobelts, and its disintegration into aggregates. With TiO_2-NT-200°C powder, aggregates are formed during the battery's fabrication process (Fig. 9(a) and 9(b)). At high magnification in Figure 9(b) and the insert, TiO_2 nanotubes could be observed. After the 10th cycle, cracks are formed (Fig. 9(c) and 9(d)), and aggregates of nanotubes could be observed with the diameter ranging from 20nm to 50nm (Fig. 9(e) and 9(f)). TiO_2-NU-150°C powder, also collapses, but this collapse is less pronounced than that of nano-urchin100 morphology, due to its nanosheet enrolled structure, which provides more resistance to the change of the powder's morphology during the fabrication process. Regarding TiO_2 nanotube powder, their aggregation yields to surface reduction, which explain its lower capacity compared to that of nanobelt powder.

It is well known that nanoparticles aggregate is a porous material characterized by pore size, size distribution, connectivity and specific surface. Furthermore, it is well accepted that these parameters affect the Li ion diffusion within the LIB electrode. This result is very surprising if only we take into account the fact that the reduction of the pore size induces the enhancement of the specific surface, and in turn the specific capacity as previously observed by Lin et al [21].

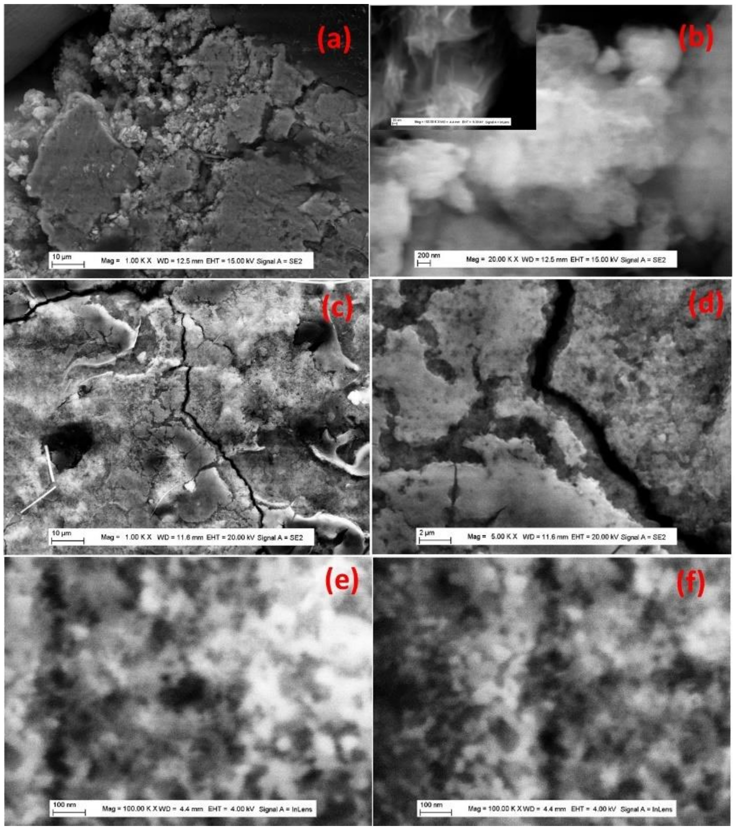

Figure 9: FEGSEM images of TiO_2 powder with nanotube morphology (a) and (b) different magnifications of the anode materials after preparation (c) - (f) different magnification de anode materials after 10th discharging/charging cycles. The inserts are the corresponding high magnification.

In addition, the pores connectivity should play an important role in the optimization of energy storage of porous electrodes [22]. However, during the first discharging cycle, the TiO_2 powders are still keeping different morphologies and probably different connectivity, which could explain partly the observed difference in specific capacities for all the TiO_2 powders. The observed plateaus in Figure 6, can be explained by the fact that, for all the samples, the shapes and sizes of the nanoparticles and their connectivities (and, a consequence their specific surface areas) are similar after 10 charging-discharging cycles. In addition, the very low variation of the specific capacity could be explained by the less variation of the powder shape and size with the discharging/charging cycles.

These results were confirmed by XRD experiments (Tab. 1), which show that the crystallite size decreases between the 1st and the 10th cycle. This confirms that during the discharging/charging cycles, large particles are disintegrated into small ones. Furthermore, by comparing the crystallite size after the 10th cycle, we note that the nanobelt morphology show small crystallite, which should have high specific surface, explaining the corresponding high specific capacity. In addition, the other morphologies show more or less the same crystallite size, which explains their closer specific capacity.

Table 1: Crystallite sizes (nm) of TiO_2 powders after preparation of the anode electrode and after 10 discharging/charging cycles.

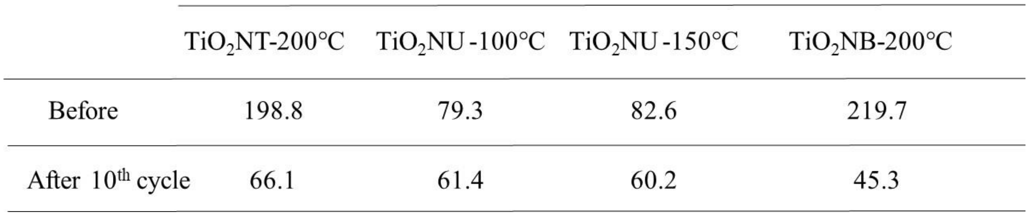

	TiO_2NT-200°C	TiO_2NU-100°C	TiO_2NU-150°C	TiO_2NB-200°C
Before	198.8	79.3	82.6	219.7
After 10th cycle	66.1	61.4	60.2	45.3

4. Conclusion

The large variation of the LIB capacity between the first and the 10th cycle, was demonstrated to be attributed to the morphology evolution during the discharging/charging process, which also indicates that the pores connectivity is also playing a major influence on the LIB capacity. This in addition to the formation of cracks, which provoke the disintegration of individual particles into smaller ones. Furthermore, the observed plateau in the capacity versus the number of discharging/charging cycle is attributed to the properties of formed aggregates in terms of pores size and specific surface, which probably will vary very slowly.

These results will contribute significantly to the understanding of LIB cyclability and the variation of its specific capacity versus the number of discharging/charging cycles, which could enable the improvement of lithium-ion batteries performance.

Acknowledgement: The authors would like also to thank the Chinese Scholar Council for supporting W. L with a scholarship. This research was funded by the European Union′s Horizon 2020 research and innovation program under the Marie Sklodowska-Curie grant agreement No 734276,

Conflicts of Interest: The authors declare no conflict of interest. The funders had no role in the design of the study; in the collection, analyses, or interpretation of data; in the writing of the manuscript, or in the decision to publish the results”

References.

1. J. Qu, J. Ding, N. Yuan, The synthesis of four morphologies of TiO_2 through temperature control and their electrochemical performance, Int. J. Elecrochem. Soci. 10 (2015) 8385-8394.
2. J. Lu, Z. Chen, F. Pan, Y. Cui, K. Amine, High-Performance anode materials for rechargeable lithium-ion batteries, Electrochemical Energy Reviewers 1 (2018) 35-53.
3. Z. Zhao, J. Tian, Y. Sang, A. Cabot, H. Liu, Structure, synthesis, and applications of TiO_2 nanobelts, Adv. Mater. 27 (2015) 2557-2582.
4. C. Xiang, M. Li, M. Zhi, A. Manivannan, N. Wu, J. Mater. Chem. 22 (2012) 19161.
5. J. M. Tarascon, M. Armand, Issues and challenges facing rechargeable lithium batteries, Nature 41 (2001) 359-367.
6. B. Scrosati, Challenge of portable power, Nature 373 (1995) 557-558.
7. Y. Liu, X. Wu, J. Du, Z. Song, G. Wu, Optimal sizing of wind-energy storage system considering battery life, Renewable Energy 147 (2020) 247-2483.
8. R. Yazami, Surface chemistry and lithium storage capability of the graphite lithium electrode. Electrochemica acta, 45(1-2) 1999 87-97.
9. A. Pupus, J. Varna, modeling mechanical stress and exfoliation damage in carbon fiber electrodes subjected to cyclic intercalation/deintercalation of lithium ions, Comp Part B, 65 2014 69-79.
10. X. Li, Y. Zhang, T. Li, Q. Zhong, H. Li, and J. Huang, Graphene nanoscrolls encapsulated TiO_2 nanowires for lithium storage, Journal of power sources, 268, 2014, 372-378.
11. J. Jin, S. Z. Huang, J. Liu et al., Design of new anode materials based on hierarchical three-dimensional ordered macro mesoporous TiO_2 for high performance lithium-ion batteries, journal of materials chemistry A, 2(25) 2014, 9699-9708.

[12] H. Ming, Y. Yan, J. Ming, X. Li, Q. Zhou, H. Huang, J. Zheng, RSC Adv. 4 (2014) 12971.

13. D. Deng, M. G. Kim, J. Y. Lee, J. Cho, Energ. environ. Sci. 2 (2009) 818.

14. Z. Liu, M. Zheng, B. Zhao, G. Wang, L. Pu, Y. Shi, Influence of the pore structure parameters of mesoporous anatase microsphereson their performance in Lithium-ion batteries, J. Solid state Electrochem, 18 (2014) 1673-1681.

15. O. A. Vasilyev, A. A. Kornyshev, S. Kondrat, Connections Matter: On the importance of pore percolation for nanoporous supercapacitors, ACS Appl. Energy Mater. 2 (2019) 5386-5390.

16. A. Taleb, F. Mesguich, A. Hérissan, C. Colbeau-Justin, Y. Xue, P. Dubot, Optimized TiO_2 nanoparticle packing for DSSC photovoltaic applications, Solar Energy Materials & Solar Cells 148 (2016) 52-59.

17. W. Luo, A. Taleb, Hydrothermal Synthesis of TiO2 Aggregates and Their Applications as Negative Electrodes for Lithium-ion Batteries: The Conflicting Effects of Specific Surface and Pore Size,, Nanomaterials 11 (2021) 365.

18. J. M. Tarascon, M. Armand, Issues and challenges facing rechargeable lithium batteries, Nature 414 (2001) 359-367.

19. J. Lu, Z. Chen, F. Pan, Y. Cui, K. Amine, High-Performance anode materials for rechargeable lithium-ion batteries, Electrochemical Energy Reviewers 1 (2018) 35-53.

20. Z. Tian-Hui, P. Ling-Yu, Z. Su-ling, X. Zheng, W. Qian, K. Chao, application of TiO_2 with different structures in soar cells, Chin. Phys. B, 21 (2012) 118401.

21. Z. Lin, M. Zheng, B. Zhao, G. Wang, L. Pu, Y. Shi, Influence of the pore structure parameters of mesoporous anatase microspheres on their performance in lithium-ion batteries, J. Solid State Electrochem 18 (2014) 1673-1681

22. Z. Lin, W. Yue, D. Huang, J. Hu, X. Zhang, Z. Yuan, X. Yang, Pore length control of mesoporous Co_3O_4 and its influence on the capacity of porous electrodes for lithium-ion batteries, RSC Advances, 2 (2012) 1794-1797.

CHAPTER IV: Synthesis of TiO_2 nanorods decorated with TiO_2 nanoaggregates and their use as anode materials for Lithium-ion batteries

Summary

In this work we have performed the synthesis of TiO_2 nanorods decorated on the surface by TiO_2 aggregates, using the hydrothermal method. By varying the temperature, we have shown that it is possible to control the coverage rate of the nanorods by the aggregates. This results in varying the specific surface of the prepared powders and modifying their connectivity. Moreover, we used these powders as anode materials for lithium-ion batteries. The electrochemical results of the discharge/charge cycles of the battery showed that both the highest capacity and the best cyclability were observed for the synthesis temperature of 230°C. This was explained by the large specific surface area of these powders, as well as the connectivity of their pores.

Indeed, the large specific surface of the powders allows to reduce the diffusion paths of the lithium ions, and to increase considerably the surface of the active material in contact with the electrolyte and thus with the lithium ions. This results in an improvement of the speed of the discharge/charge cycles, and the specific capacity of the battery. Moreover, the variation of the coverage rate of the nanorods by the aggregates, probably also allows to modify the connectivity of the pores within the anode materials, which allows to optimize its accommodation to the volume variations during the cycling. Normally, this volume variation is at the origin of the formation of cracks, which causes the disconnection of pieces of the active material and therefore the loss of cyclability and the decrease of the specific capacity.

Synthesis of TiO_2 nanorods decorated with TiO_2 nanoaggregates and their use as anode materials for Lithium-ion batteries

Wenpo Luo[1], Juliette Blanchard[2], Abdelhafed Taleb[1,2] *

[1] *PSL Research University, Chimie ParisTech - CNRS, Institut de Recherche de Chimie Paris, 75005, Paris, France,*
abdelhafed.taleb@chimieparistech.psl.eu (A. T), WenpoLuo@outlook.com (W.L)
[2] *Sorbonne université, 4 place Jussieu, 75231 – Paris, France*
[3] *LRS - Laboratoire de Réactivité de Surface, Sorbonne université, 4, place Jussieu, 75231 – Paris, France,*
juliette.blanchard@sorbonne-universite.fr

Abstract: A mixture of TiO_2 aggregates and nanorods were prepared using easy and scalable hydrothermal method at various temperatures of 170 °C, 190 °C, 210 °C and 230 °C. It was demonstrated that the synthesis temperature is a key parameter to tune the proportion of the two morphologies. Prepared TiO_2 aggregates and nanorods were used to design anode materials, in which the aggregates regulate the pore size and the connectivity of interconnected nanorods structure. The electrochemical measurements of TiO_2 samples were carried out by using the galvanostatic technique. It was clearly found that the pores connectivity and the specific surface area have a striking impact on the Li insertion behavior, lithium storage capability and cycling performance of batteries. The first irreversible capacity was shown to increase with the specific surface area. When the pore size is larger, the ability of the mesoporous anatase to release deformation stress was stronger, and thus shows a good cycling stability. TiO_2 samples electrode prepared at high temperature 230 °C showed the highest discharging and charging capacities (203.3

mAh/g and 140.8 mAh/g) and a good cycling stability, due to its very large specific surface area and pore size.

Keywords: Mesoporous TiO_2, pores architecture, specific surface area, Lithium-ion batteries

1. Introduction

This last century, global warming is becoming a very concerning issue, which threatens our ecosystem equilibrium. Furthermore, it is well accepted that the fossil energy contributes strongly to this global warming, and that the renewable energy sources could be a serious candidate to replace the fossil energy. The issue is how to stock this renewable energy, and to use it when needed, has been driving the industrial and the scientific communities into the development of energy storage devices. Batteries [1-2] and supercapacitors [3-4] have attracted much focus, due to their portability, low cost and energy storage effectiveness. Furthermore, another motivation of batteries development is the emergence of electric vehicles [5,6] as a potential candidate to replace the petrol vehicles which are considered a tremendous source of pollution.

Lithium-ion batteries (LIBs) are one of the most popular energy storage systems for the portable electronic devices in the last century [5,7-11], and this is mainly due to their high energy density, high life cycle and safety. Lithium-ion batteries are composed of positive and negative electrodes separated by the electrolyte usually made of polypropylene-polyethylene and dissociated salts of Li in alkyl organic carbonates. The two electrodes are isolated by a separator, which allows the Li diffusion during the charging and discharging process. For the cathode which is a positive electrode, the commonly used materials are based on transition metals oxides or phosphates such as $LiMnO_2$ [12], $LiCoO_2$ [13], $LiNiO_2$ [14], $LiFePO_4$ [15], $LiMnPO_4$ [16] etc. For the negative electrode (anode), graphite is the commonly used active material, because of its cyclability at high C-rates. However, its mean drawbacks are the low power density, the low C-rate and the safety concerns [17,18].

However, there is an urgent need for the development of alternative anode materials with high-capacity and high lithium-ion diffusion rate that could help improve the energy and power densities of LIB. Titanium dioxide (TiO_2) has been successfully demonstrated to be a promising material for energy storage applications [19-21], thanks to its excellent electrochemical performance as non-hazardous handling, low cost, low toxicity, good life cycling, appropriate insertion potential (~2.0V) and low volume expansion (3-4%) during lithium insertion [22-24]. TiO_2 exists in different phases: rutile [25], anatase [26] and brookite [27]. Anatase phase is the most studied as a host material for electroactive Li-insertion [28-30]. However, due to its lower ionic diffusion and electronic conductivity, large TiO_2 anatase particles demonstrate unsatisfactory performances, which do hinder their practical application. To improve the performance of TiO_2 anatase particles, different approaches were used including the tuning of their crystallinity, size, morphology and specific surface area [31-34]. In particular, TiO_2 nanomaterials with large specific surface area allow the enhancement of lithium storage capability, and rate cyclability, due to the short diffusion pathway [28-31]. The TiO_2 nanomaterials specific surface area is usually tuned by the pore size and their connectivity. Furthermore, the Li ion diffusion is also controlled by the pore length as a consequence of the particles size and morphology [35]. It was reported that the pore length has a strong influence on the capacity and the rate cyclability of mesoporous Co_3O_4 as a cathode material for LIB, which increases when the nanoparticles size decreases [36]. It is well accepted that with mesoporous material, the high specific surface area favors the Li ion diffusion, which leads to a higher specific capacity and rate cyclability.

In this study, mesoporous nanostructures of TiO_2 aggregates and nanorods mixture have been successfully prepared hydrothermally. The synthesis temperature has been pointed out to be a crucial parameter to tune the TiO_2 powders composition. The performance of LIB using prepared TiO_2 powders as anode materials, has been discussed in terms of its pores size and architecture.

2. Experimental

2.1. Synthesis of TiO_2 samples

All of the used chemical reagents were purchased from Sigma Aldrich Chemical Reagent Co. Ltd. and used without further purification unless otherwise stated. The TiO_2 powders were prepared according to the scheme 1 using a typical hydrothermal method synthesis.

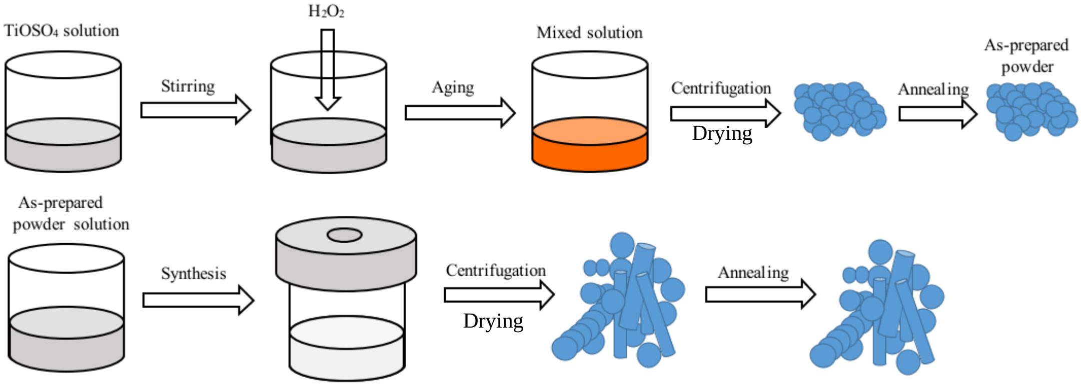

Scheme 1. Schematic illustration of different steps of TiO_2 powder synthesis.

To prepare the precursor solution, 0.64 g of $TiOSO_4$ and 16 ml of deionized water were mixed, and then followed by the addition of 1.266 g of H_2O_2 under stirring at 25 °C. After 24h aging at room temperature, the precipitate was collected by centrifugation, washed with deionized water six times, and then with ethanol two times, and dried overnight in the oven at later stage. The obtained powder was subjected to thermal annealing at a temperature of 500 °C for 1h. A solution was prepared by dissolving 0.2 g of prepared TiO_2 powder in 16 ml of cold deionized water under ultrasonic bath for 15 min. Then the solution was placed in a PTFE lined autoclave (volume 25 ml) and heated with a rate of 2.5 °C/min. During the synthesis, the temperature was maintained at different levels (170, 190, 210 and 230 °C) for 16h. Then by centrifugation, the obtained TiO_2 powder is precipitated and washed six times in deionized water, two times in ethanol, and dried overnight in the oven. Finally, the dried powders were annealed in air at 500 °C for 1h.

2.2. Structure and morphology characterization

The morphological investigations of the prepared powders were achieved with a high-resolution Ultra 55 Zeiss FEG scanning electron microscope (FEGSEM) operating at an acceleration voltage of 10 kV.

The crystalline structure of TiO_2 powders was determined by an X-ray diffractometer (Siemens D5000 XRD unit) in 2θ range from 20° to 80° by 0.07° s^{-1} increasing steps operating at 40 kV accelerating voltage and 40 mA current using Cu Kα radiation source with $\lambda = 1.5406$ Å.

Nitrogen adsorption-desorption isotherms were measured at liquid nitrogen temperature on a Micromeritics ASAP 2020 apparatus. Before analysis, all the samples were degassed at 120 °C for 10 h. The specific surface area (SBET) was evaluated using the Brunauer-Emmett-Teller (BET) method in the P/P° range of 0.05-0.25. The pore size distribution was determined from the desorption branch of the isotherm using the Barret-Joyner-Halender (BJH) method. The total pore volume was determined from the amount of N_2 adsorbed up to $P/P^{\circ} = 0.98$.

2.3. Electrochemical measurements

Electrodes were fabricated by intimately mixing the active material (80 wt%) with carbon mesoporous (~7wt%), graphite (~7wt%) and binder PTFE (~7wt%). The resulting mixture was then compressed onto stainless steel foil and allowed to dry at 80 °C for the overnight. Swagelok cells were assembled in a glove box under a dry argon atmosphere using lithium metal as a counter electrode and a Celgard 2400 membrane with glass fiber as a separator. Cells were kept in a glovebox for 12 h before electrochemical measurements. The electrolyte was prepared by dissolving 1 M $LiPF_6$ in a 1:1:1 volume ratio of ethylene carbonate (EC), diethyl carbonate (DEC) and dimethyl carbonate (DMC). All cells were tested vs. Li/Li^+ at room temperature in the range between 1 and 3.0 V using a program-controlled Battery Test system (EC-Lab, France) at a current rate of 0.12C.

3. Result and discussion

3.1. Phase and microstructure characterization

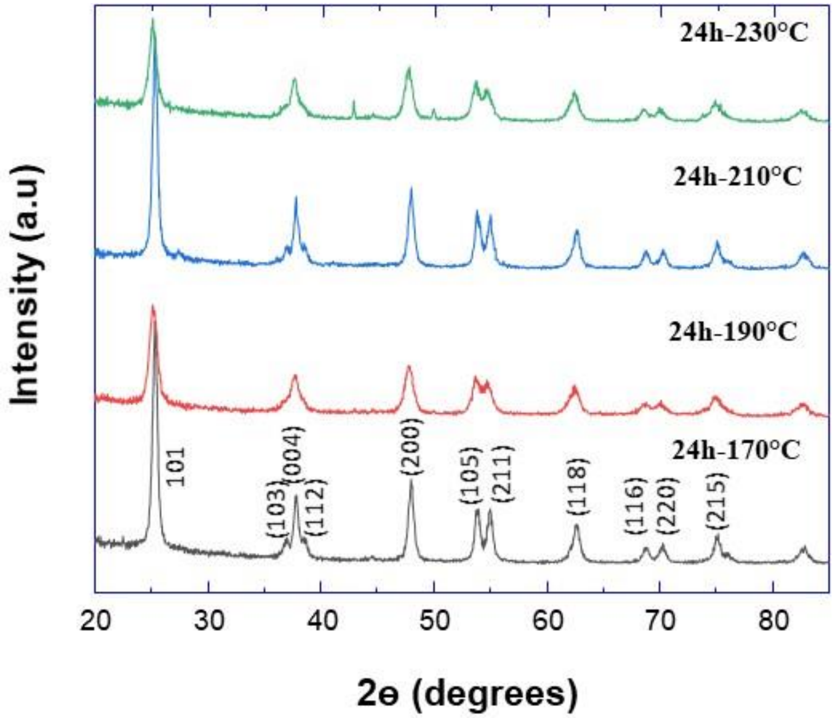

Figure 1. XRD pattern of TiO_2 nanostructures prepared at the different temperatures as indicated.

The structural characterization of obtained powders at various temperatures was investigated using XRD experiments, and the obtained patterns are depicted in Figure. 1. It is revealed that the powders are of crystalline structure with all the peaks assigned to TiO_2 anatase phase (JCPDS No. 89-4921), with no other detected phases. The average TiO_2 crystallite sizes were calculated using Scherer formula: ($D = 0.9\lambda / B \cos\theta$), and the analysis of the full width at half maximum of the intense peak corresponding to (101) crystallographic plane [37]. The crystallite size (D) of TiO_2 powders at different temperatures is given in Table 1. It was clearly found that the crystalline size decreases with the synthesis temperature increasing.

Table 1. Crystallite size of TiO_2 powders prepared at various synthesis temperatures.

temperature (°C)	Crystallite size (nm)
170	17.9
190	17.7
210	15.7
230	14

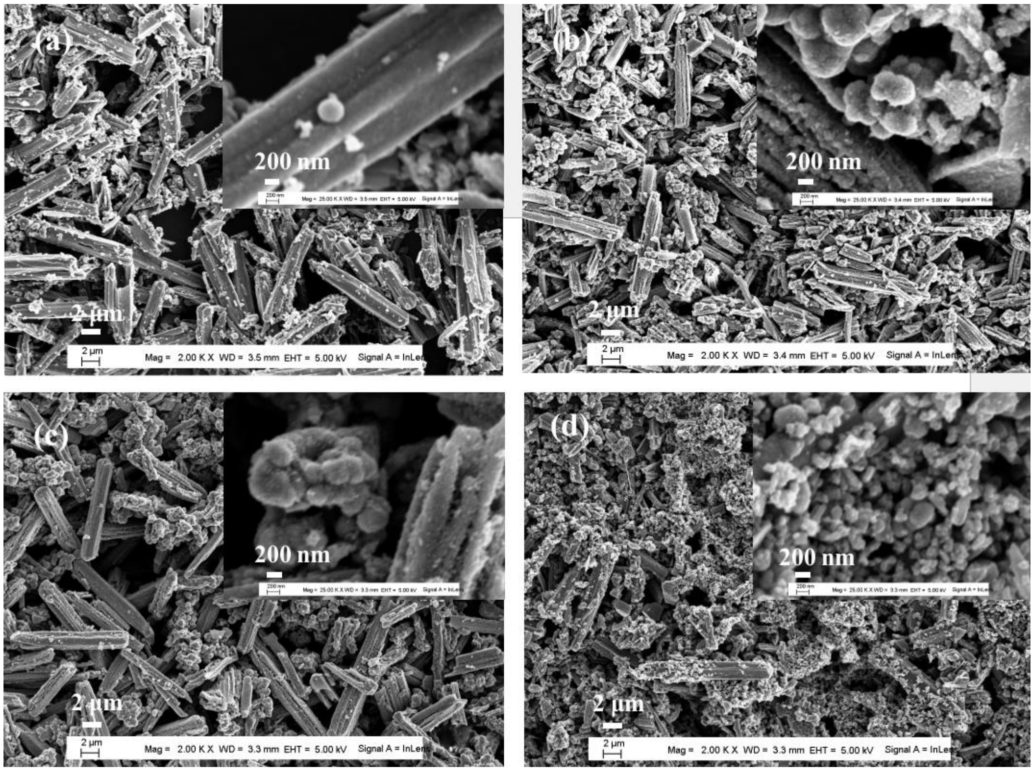

Figure 2. FEGSEM images of prepared TiO_2 powders at various synthesis temperatures: (a)170°C; (b) 190°C; (c) 210°C; and (d) 230°C.

The morphology characterization of prepared TiO_2 powders is shown in figure 2. It is worth noting that depending on the synthesis temperature, various mixtures of TiO_2 powders were obtained. Both nanorods and aggregates resulting from the spontaneous aggregation of TiO_2 nanoparticles could be observed. Furthermore, the number of nanoparticles and their aggregation is increasing with the synthesis temperature.

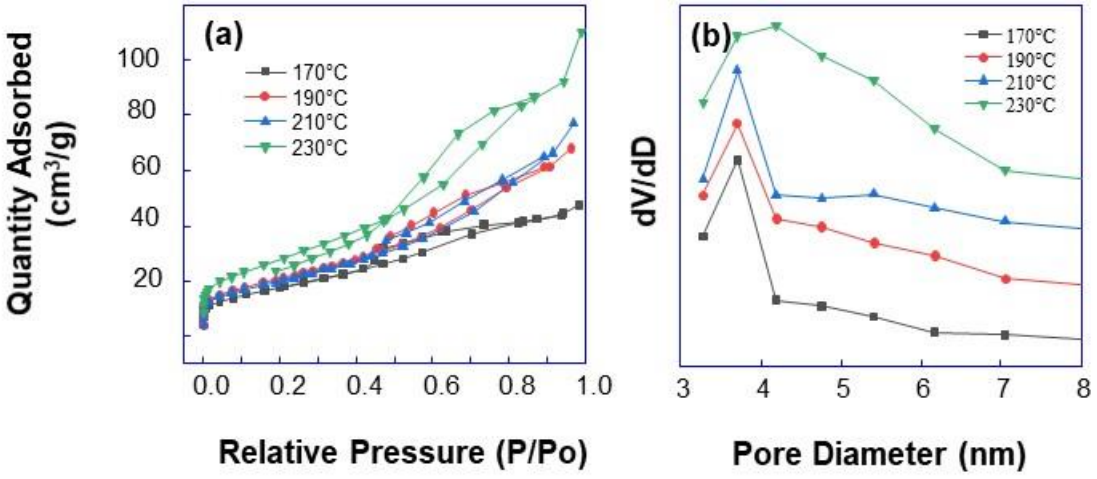

Figure 3. (a) N_2 adsorption-desorption isotherms and (b) BJH pore size distribution curves obtained from the adsorption branch of the prepared TiO_2 powders at various synthesis temperature as indicated.

Table 2. BET-specific surface area, mean pore diameter and pore volume of the prepared TiO_2 powders at various synthesis temperatures.

Powder	BET-specific surface area (m^2/g)	Average pore diameter (nm)	Pore volume (cm^3/g)
TiO_2-170°C	65	4.0	0.07
TiO_2-190°C	75	4.0	0.11
TiO_2-210°C	77	4.5	0.12
TiO_2-230°C	103	4.5	0.26

The results of the nitrogen adsorption-desorption analysis are shown in Figure 3, and the standard multipoint Brunauer-Emmett-Teller (BET) method was used to calculate the specific surface area. However, the pore size distributions were obtained from the isotherm adsorption branches based on the Barrett-Joyner-Halenda (BJH) model. Furthermore, nitrogen adsorption/desorption isotherms (Fig. 3(a)) of all prepared TiO_2 powders show a hysteresis loop, indicating that the prepared powders exhibit high mesoporous structure [38]. The pronounced hysteresis is well believed to be connected to the capillary condensation at large pore channels, which can also be associated to the modulation of the channel structure [39]. From the BJH pore size distribution (Fig. 3(b)), the powder average diameters were calculated and shown to be ranging from 4 nm to 6 nm. The obtained results for the prepared TiO_2 powders in terms of specific surface area, average pore diameter, and pore volume are summarized in Table 2. It can be observed that the specific surface area and the pore size increase with the synthesis temperature, which is consistent with the transition from nanorod powder with low to high-rate of aggregates coverage on their surface (Figure 2). In fact, the porous TiO_2 aggregates on the surface of the nanorod powder enhances their specific surface area and their pore size, and it could also change the pores connectivity, and thus the channel structure. It is worth mentioning that the structures with high pore diameter enable a rapid filling of pores by the electrolyte during the electrochemical charging/discharging cycles, which enhances the rate capability of the anode materials [30]

3.2. Electrochemical performance

The electrochemical properties of prepared powders at various temperatures were tested as anode materials for LIBs. The insertion of Li^+ into anatase powders is well accepted to be accompanied by a phase transition from tetragonal TiO_2 (space group I41/amd) to orthorhombic $Li_{0.5}TiO_2$ (space group Imma), whose reaction equation is expressed as follows:

$$TiO_2+xLi^++xe^- \leftrightarrow Li_xTiO_2 \quad (1)$$

Where, x is the amount of inserted Li^+ in the anatase, which depends both on the crystallographic and microstructure properties of used materials [40]. Although anatase possesses a theoretical specific capacity of 335 mAh/g, the only half of this capacity is usually observed, and this is mainly due to the strong Li-Li repulsions in the Li_xTiO_2 lattice at greater insertion ratios ($x > 0.5$) [41-42]. The main redox reaction behind the TiO_2 electrochemical activity is that corresponding to the interconversion of Ti^{4+}/Ti^{3+} during discharging/charging cycles.

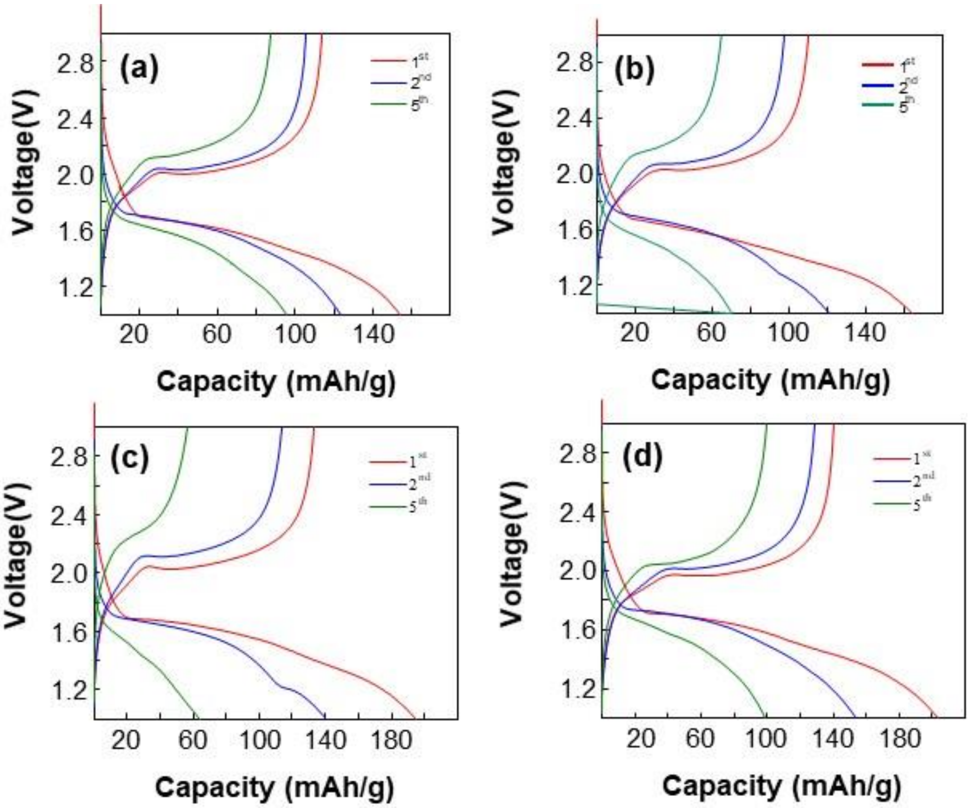

Figure 4. Charging/discharging curves of TiO_2 powders prepared at various synthesis temperatures:(a) 170° C; (b) 190°C; (c) 210°C; and (d) 230°C, and cycled between 1.0 and 3.0 V at a constant current rate of 0.12C.

In Figure 4, the shown 1st, 2nd and 5th charging/discharging cycles correspond to synthesized TiO_2 powders at the temperature of 170°C, 190°C, 210°C and 230°C. The electrochemical cycling was performed at the voltages ranging from 1.0 to 3.0V, and at a constant current rate of 0.12C. The curves show similar patterns with clear plateaus near ~1.75V for both discharging and charging cycles, and it is similar to other reported values for the same systems [43-44]. It is worth noting that the capacity increases with the temperature, and the highest discharging and charging capacities (203.3 mAh/g and 140.8 mAh/g, respectively) were obtained for the prepared powder at higher synthesis temperature of 230 °C. The observed irreversible capacity during the first cycle was mainly attributed to three phenomena: the formation of a solid solution [45-46], the irreversible lithium insertion in the crystal lattice defects or on the electrode surface sites [47], and the reduction of electrolyte on the electrode surface [48]. The highest capacity observed for the electrode prepared with TiO_2 powder synthesized at temperature of 230 °C was explained by the higher specific surface area and a larger pore size, which offers a high contact area between the active material and the electrolyte.

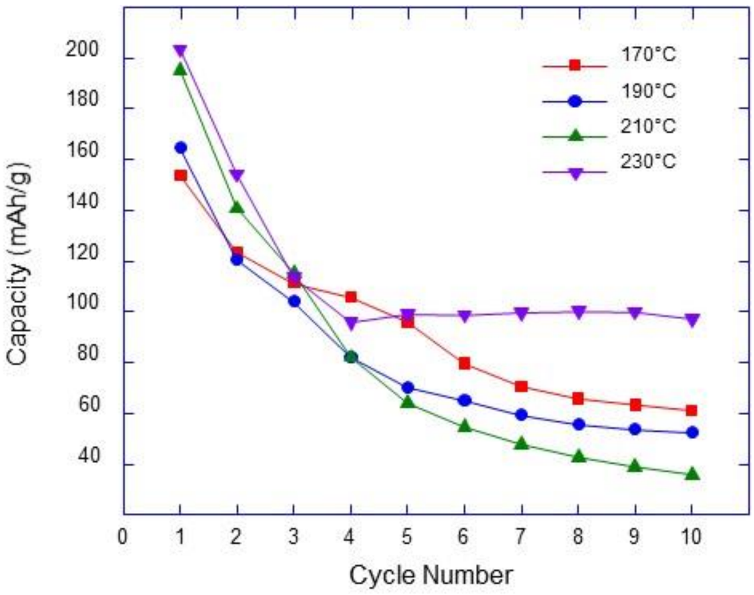

Figure 5. Cycling performance at constant current rate (0.12C) of TiO_2 powders prepared at different indicated temperatures as anode materials for LIB.

In Figure 5 the cycling performance of LIBs using prepared TiO_2 powders at various temperatures as anode materials is presented. TiO_2 powder at the synthesis temperature of 230 °C has shown the best cycling performance with very slow decrease of the capacity. This TiO_2 powder is characterized by high-rate coverage of TiO_2 aggregates on the surface of the nanorods. These aggregates not only increase the specific surface of prepared powder, but also change the pores size and their connectivity. When the temperature increases, both the specific surface and capacity increases (Tab. 2). This trend doesn't explain the capacity behavior versus the temperature of the powders prepared at the synthesis temperature of 170°C, 190°C and 210°C. The results corresponding to these powders show clearly that when the pores size increases, the specific surface increases also. These results are in contradiction with the ones obtained for the spherical nanoparticles, in which the specific surface increases, when the size of nanoparticles and the pores between them decrease. To explain this peculiarity, it is crucial to assume that the nanorods play a major role in fixing the pores size, and the aggregates on its surface increase the pores size between nanorods and change the pores connectivity. For mesoporous materials, the internal mesoporous structure accommodated the volume expansion during the lithium insertion and released the deformation stress. The pore volume of prepared TiO_2 powder at synthesis temperature of 230 °C was much higher than that of other three TiO_2 powders, and correspond to more flexible pores connectivity, with a better capability of releasing deformation stress. This TiO_2 powder, with micro and meso porous structures, better accommodate the volume variation during the discharging/charging cycles, which explain the observed roughly constant capacity (Fig. 5), resulting in a much better cycling performance than the other three samples. With other TiO_2 powders, the enhancement of nanoparticles aggregation on the nanorods surface with the temperature, reduces the pores length, leading to a higher specific surface. This in turn will enhance the exposed surface area for Li ion intercalation, which will favor the capacity increase. However, the new pores connectivity and structure is less flexible and is not willing to accommodate the deformation stress due to the anode volume change during discharging/charging cycles, which provokes the formation of cracks and electrical disconnection of active material piece, reducing strongly the batteries capacity with discharging/charging cycles. This effect is enhanced by the temperature as it can observed for the temperatures of 170°C, 190°C and 210°C, which probably is due to the promotion of porous structure with less capability to accommodate the volume variation during the discharging/charging cycles.

To check if other parameters are behind the observed behavior, the powders are characterized by XRD and FEGSEM after the 10th cycle. It can be observed from the FEGSEM characterization (Figure 6) that only aggregates could be observed and nanorods are completely absent. This could be explained by the nanorods disintegration during the cycling processes, and their transformation into aggregates (indicated zone in Figure 6). In fact, as a consequence of volume variation, stress within the materials takes place and cracks appear provoking the materials disintegration. This hypothesis was confirmed by XRD experiments, and it can be observed in table 3 that the TiO_2 crystallites size decreases after the 10th cycle, which confirms the disintegration of the powder took place during the cycling processes. After the nanorods are transformed into aggregates, and the batteries specific capacity is controlled by the specific surface and the pore size as previously demonstrated [49].

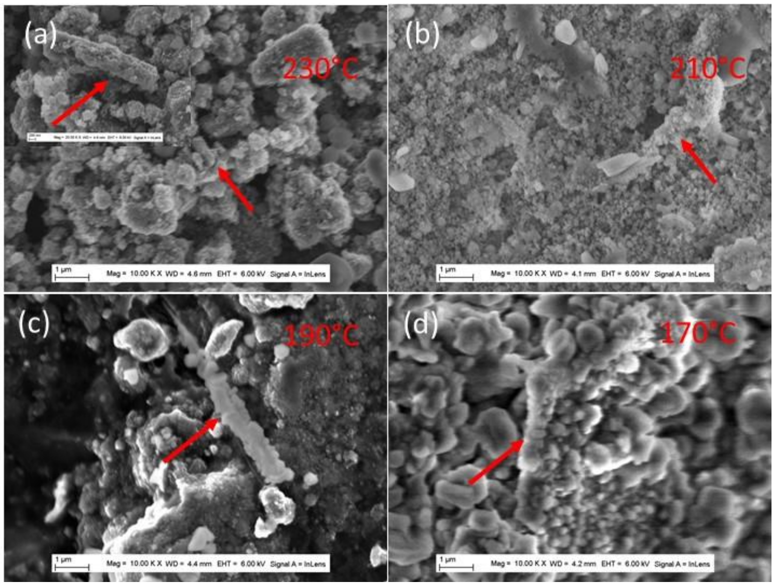

Figure 6. FEGSEM pattern after 10th cycle at constant current rate (0.12C) of TiO_2 powders prepared at different indicated temperatures as anode materials for LIB.

Table 3: Crystallite size of TiO_2 powders prepared at various synthesis temperatures.

TiO_2-24h crystallite size	170°C	190°C	210°C	230°C
After synthesis	17.9nm	17.0	15.7	14
After 10th cycle	14.7	11.6	11.5	9.6

4. Conclusions

Different powders of TiO_2 nanoparticles, aggregates and nanorods mixture, were prepared using the hydrothermal method at various synthesis temperatures of 170 °C, 190 °C, 210 °C and 230 °C. It was shown that the temperature is a crucial parameter to control the prepared TiO_2 powders properties in terms of specific surface areas, and pore size distributions. By increasing the synthesis temperature, it was demonstrated that the TiO_2 powders morphology change from nanorod, with low to high-rate coverage of aggregates on their surface. The electrochemical measurements showed that the TiO_2 powder synthesized at a temperature of 230 °C exhibits the highest discharging and charging capacities (203.3 mAh/g and 140.8 mAh/g), and the best cycling performance. This was explained by the higher specific surface area of this TiO_2 powder, and by the pore's connectivity and structure, which could better accommodate the volume expansion, and in turn enables to release the deformation stress. In fact, TiO_2 electrode materials, with a large active surface area, allow a high electrochemical reaction rates per unit of volume, and enhances the diffusion kinetics by reducing the diffusion pathway for electronic and ionic transport. Additionally, the cycling performance of TiO_2 powder synthesized, at a temperature of 230 °C, was influenced by the pore volume and the pore's connectivity. When the pore size increases, the ability of the TiO_2 mesoporous powder to release the deformation stress is stronger, which favors a good cycling stability.

Acknowledgement: The authors would like also to thank the Chinese Scholar Council for supporting W. L with a scholarship. This research was funded by the European Union′s Horizon 2020 research and innovation programme under the Marie Sklodowska-Curie grant agreement No 734276.

References

1. J. Qu, J. Ding, N. Yuan, The synthesis of four morphologies of TiO_2 through temperature control and their electrochemical performance, Int. J. Elecrochem. Soci. 10 (2015) 8385-8394.
2. J. Lu, Z. Chen, F. Pan, Y. Cui, K. Amine, High-Performance anode materials for rechargeable lithium-ion batteries, Electrochemical Energy Reviewers 1 (2018) 35-53.
3. Z. Zhao, J. Tian, Y. Sang, A. Cabot, H. Liu, Structure, synthesis, and applications of TiO_2 nanobelts, Adv. Mater. 27 (2015) 2557-2582.
4. C. Xiang, M. Li, M. Zhi, A. Manivannan, N. Wu, J. Mater. Chem. 22 (2012) 19161.
5. Yang Z, Zhang J, Kintner-Meyer M C W, et al. Electrochemical energy storage for green grid[J]. Chemical reviews, 2011, 111(5): 3577-3613.
6. Armand M, Tarascon J M. Building better batteries[J]. nature, 2008, 451(7179): 652-657.
7. Whittingham M S. Ultimate limits to intercalation reactions for lithium batteries, J. Chemical reviews, 2014, 114(23): 11414-11443.
8. Xu K. Nonaqueous liquid electrolytes for lithium-based rechargeable batteries[J]. Chemical reviews, 2004, 104(10): 4303-4418.
9. Xu K. Electrolytes and interphases in Li-ion batteries and beyond[J]. Chemical reviews, 2014, 114(23): 11503-11618.

10. Bruce P G, Scrosati B, Tarascon J M. Nanomaterials for rechargeable lithium batteries[J]. Angewandte Chemie International Edition, 2008, 47(16): 2930-2946.
11. Cabana J, Monconduit L, Larcher D, et al. Beyond intercalation-based Li-ion batteries: the state of the art and challenges of electrode materials reacting through conversion reactions[J]. Advanced materials, 2010, 22(35): E170-E192.
12. H. Li, G. Yang, X. Miao, A. Hong, Efficient microwave hydrothermal synthesis of nanocrystalline orthorhombic LiMnO2 cathodes for lithium batteries, Electrochemica Acta 55 (2010) 3397-3397.
13. Thiophene derivatives as novel functional additives for high-voltage $LiCoO_2$ operations in lithium-ion batteries, Electrochemica Acta 151 (2015) 429-436.
14. S. Muto, K. Tatsumi, Y. Kojima, H. Oka, H. Kondo, K. Horibuchi, Y. Y. Ukyo Effect of Mg-doping on the degradation of $LiNiO_2$ based cathode materials by combined spectroscopic methods, Journal of power sources 205 (2012) 449-455.
15. X. Yin, K. Huang, S. liu, H. Wang, H. Wang, Preparation and characterization of Na-doped $LiFePO_4$/C composites as cathode materials for lithium-ion batteries, journal of power sources 195 (2010) 4308-4312.
16. T. Doi, S. Yatomi, T. Kida, S. Okada, J. I. Yamaki, Liquid phase synthesis of uniformly nanosized $LiMnPO_4$ particles and their electrochemical properties for lithium-ion batteries, Crystal growth and design 9 (2009) 4990-4992.
17. Han T H, Lee W J, Lee D H, et al. Peptide/graphene hybrid assembly into core/shell nanowires[J]. Advanced Materials, 2010, 22(18): 2060-2064.
18. Arico A S, Bruce P, Scrosati B, et al. Nanostructured materials for advanced energy conversion and storage devices[M]//Materials for sustainable energy: a collection of peer-reviewed research and review articles from Nature Publishing Group. 2011: 148-159.
19. Hoffmann M R, Martin S T, Choi W, et al. Environmental applications of semiconductor photocatalysis[J]. Chemical reviews, 1995, 95(1): 69-96.
20. Grätzel M. Photoelectrochemical cells[J]. nature, 2001, 414(6861): 338-344.

21. Wang C, Yin L, Zhang L, et al. Ti/TiO_2 nanotube array/Ni composite electrodes for nonenzymatic amperometric glucose sensing[J]. The Journal of Physical Chemistry C, 2010, 114(10): 4408-4413.
22. Armstrong G, Armstrong A R, Bruce P G, et al. TiO_2 (B) nanowires as an improved anode material for lithium-ion batteries containing $LiFePO_4$ or $LiNi_{0.5}Mn_{1.5}O_4$ cathodes and a polymer electrolyte[J]. Advanced Materials, 2006, 18(19): 2597-2600.
23. Yang X, Teng D, Liu B, et al. Nanosized anatase titanium dioxide loaded porous carbon nanofiber webs as anode materials for lithium-ion batteries[J]. Electrochemistry communications, 2011, 13(10): 1098-1101.
24. Qiao H, Xiao L, Zhang L. Phosphatization: A promising approach to enhance the performance of mesoporous TiO_2 anode for lithium-ion batteries[J]. Electrochemistry communications, 2008, 10(4): 616-620.
25. Qiao H, Luo Q, Wei Q, et al. Electrochemical properties of rutile TiO_2 nanorods as anode material for lithium-ion batteries[J]. Ionics, 2012, 18(7): 667-672.
26. Panda S K, Yoon Y, Jung H S, et al. Nanoscale size effect of titania (anatase) nanotubes with uniform wall thickness as high-performance anode for lithium-ion secondary battery[J]. Journal of Power Sources, 2012, 204: 162-167.
27. Ren Y, Liu Z, Pourpoint F, et al. Nanoparticulate TiO_2 (B): an anode for lithium-ion batteries[J]. Angewandte Chemie International Edition, 2012, 51(9): 2164-2167.
28. Wang Y, Chen T, Mu Q. Electrochemical performance of W-doped anatase TiO_2 nanoparticles as an electrode material for lithium-ion batteries[J]. Journal of Materials Chemistry, 2011, 21(16): 6006-6013.
29. Ali Z, Cha S N, Sohn J I, et al. Design and evaluation of novel Zn doped mesoporous TiO_2 based anode material for advanced lithium-ion batteries[J]. Journal of Materials Chemistry, 2012, 22(34): 17625-17629.
30. Jung H G, Yoon C S, Prakash J, et al. Mesoporous anatase TiO_2 with high surface area and controllable pore size by F^--ion doping: applications for high-power Li-ion battery anode[J]. The Journal of Physical Chemistry C, 2009, 113(50): 21258-21263.
31. Xiao P F, Lai M O, Lu L. Electrochemical properties of nanocrystalline TiO_2 synthesized via mechanochemical reaction, J. Electrochimica acta, 2012, 76: 185-191.

32. Pal M, Garcia Serrano J, Santiago P, et al. Size-controlled synthesis of spherical TiO_2 nanoparticles: morphology, crystallization, and phase transition[J]. The Journal of Physical Chemistry C, 2007, 111(1): 96-102.
33. Bing Z, Yuan Y, Wang Y, et al. Electrochemical characterization of a three dimensionally ordered macroporous anatase TiO_2 electrode[J]. Electrochemical and solid-state letters, 2006, 9(3): A101-A104.
34. Fu L J, Zhang T, Cao Q, et al. Preparation and characterization of three-dimensionally ordered mesoporous titania microparticles as anode material for lithium-ion battery[J]. Electrochemistry Communications, 2007, 9(8): 2140-2144.
35. Z. lin, W. Yue, D. Huang, J. Hu, X. Zhang, Z. Y. Yuan, X. Yang, Pore lengh control of mesoporous Co3O4 and its influence on the capacity of porous electrodes for lithium-ion batteries, RSC Adv. 2012, 2, 1794-1797.
36. Z. lin, W. Yue, D. Huang, J. Hu, X. Zhang, Z. Y. Yuan, X. Yang, Pore lengh control of mesoporous Co3O4 and its influence on the capacity of porous electrodes for lithium-ion batteries, RSC Adv. 2012, 2, 1794-1797]
37. Klug H P, Alexander L E. X-ray diffraction procedures: for polycrystalline and amorphous materials[J]. X-Ray Diffraction Procedures: For Polycrystalline and Amorphous Materials, 2nd Edition, by Harold P. Klug, Leroy E. Alexander, pp. 992. ISBN 0-471-49369-4. Wiley-VCH, May 1974., 1974: 992.
38. Kruk M, Jaroniec M. Gas adsorption characterization of ordered organic-inorganic nanocomposite materials[J]. Chemistry of materials, 2001, 13(10): 3169-3183.
39. ang P, Zhao D, Margolese D I, et al. Generalized syntheses of large-pore mesoporous metal oxides with semicrystalline frameworks[J]. Nature, 1998, 396(6707): 152-155.
40. Saravanan K, Ananthanarayanan K, Balaya P. Mesoporous TiO_2 with high packing density for superior lithium storage[J]. Energy & Environmental Science, 2010, 3(7): 939-948.
41. Kavan L, Rathouský J, Grätzel M, et al. Surfactant-templated TiO_2 (anatase): Characteristic features of lithium insertion electrochemistry in organized nanostructures[J]. The Journal of Physical Chemistry B, 2000, 104(50): 12012-12020.
42. Kavan L, Kratochvilová K, Grätzel M. Study of nanocrystalline TiO_2 (anatase) electrode in the accumulation regime. Journal of Electroanalytical Chemistry, 1995, 394(1-2): 93-102.

43. Stashans A, Lunell S, Bergström R, et al. Theoretical study of lithium intercalation in rutile and anatase, J. Physical Review B, 1996, 53(1): 159.

44. Oh S W, Park S H, Sun Y K. Hydrothermal synthesis of nano-sized anatase TiO_2 powders for lithium secondary anode materials[J]. Journal of power sources, 2006, 161(2): 1314-1318.

45. Sudant G, Baudrin E, Larcher D, et al. Electrochemical lithium reactivity with nanotextured anatase-type TiO_2. Journal of Materials Chemistry, 2005, 15(12): 1263-1269.

46. Jiang C, Wei M, Qi Z, et al. Particle size dependence of the lithium storage capability and high-rate performance of nanocrystalline anatase TiO_2 electrode. Journal of Power Sources, 2007, 166(1): 239-243.

47. Kang J W, Kim D H, Mathew V, et al. Particle size effect of anatase TiO_2 nanocrystals for lithium-ion batteries. Journal of the Electrochemical Society, 2011, 158(2): A59-A62.

48. Lee K H, Song S W. One-step hydrothermal synthesis of mesoporous anatase TiO_2 microsphere and interfacial control for enhanced lithium storage performance. ACS applied materials & interfaces, 2011, 3(9): 3697-3703.

49. Mehraz S, Luo W, Swiatowska J, Bezzazi B, Taleb A, Hydrothermal Synthesis of TiO2 Aggregates and Their Application as Negative Electrodes for Lithium-Ion Batteries: The Conflicting Effects of Specific Surface and Pore Size. Materials, 2021, 14: 916

General conclusion and perspectives

During this thesis, the objectives were, on the one hand, to prepare TiO_2 nanomaterials with controlled properties and, on the other hand, to improve the performance of TiO_2 as an insert material for lithium-ion battery applications.

We have highlighted the possibility to prepare titanium dioxide nanoparticles of different morphologies, using hydrothermal synthesis in alkaline NaOH solution. The hydrothermal synthesis method, allowed us to control at the same time, the crystallinity, the size and the morphology of the prepared particles. Among the synthesis parameters that we varied, there are the temperature, the reaction time in the reactor (autoclave), and the nature of the TiO_2 precursor used for the synthesis. The nature of the latter, in the form of TiO_2 aggregates, is original compared to the literature and has helped to better understand the mechanisms of TiO_2 nanosheets, nanotubes and nanoribbons.

In a first step, we used the $TiOSO_4$ precursor, for the synthesis of nanopowders based on TiO_2 aggregates of anatase phase and controlled size. The different characterizations have shown that the aggregates are formed by TiO_2 nanoparticles, whose size varies from 4 to 10 nm. By using these TiO_2 aggregates as precursor, an alkaline solution of NaOH, and by varying the temperature and the reaction time, we have demonstrated a control of the morphology. Depending on the synthesis conditions, we obtained nanosheets, nanotubes, nanoribbons and nanourschins. For the different morphologies, the synthesis time was lower or equal to 6 h, which is a record compared to those reported in the literature for other precursors.

Moreover, the synthesis involves two intermediates: sodium titanates and titanic acids, and it takes place in three steps. First the synthesis in autoclave, then the powder obtained undergoes ion exchange and the sodium titanate is transformed into titanic acid, and finally a heat treatment. For reaction times of 6h and at the temperature of 100°C or 150°C, we observed the formation of nanourchin. The formation of this morphology, we explained it by a disordered assembly of TiO_2 nanosheets. At the temperature of 200°C and for a time of 6h, we observed the formation of nanoribbons of small thickness (<10nm) and a diameter of 50 to 100nm. For the temperature of 200°C and a reaction time of 6h we observed the formation of nanoribbons, while for the short times of 15min and 180min we observed TiO_2 nanosheets and nanotubes respectively. By high resolution electron microscopy characterization, we have highlighted the coiling of nanosheets which evolves in a later time to nanotubes. Moreover, we observed a coexistence of nanosheets of the size of TiO_2 nanoparticles, with nanosheets of slightly larger diameter. These different morphologies are probably the different stages of the same nanoribbon morphology formation. During the synthesis in alkaline medium of NaOH, there is insertion of Na^+ ions in the TiO_2 structure and its exfoliation in a second step, to form the nanosheets of larger size by coalescence. Our different observations are in the direction of a mechanism involving the processes of exfoliation and coalescence, and not the process of dissolution of the nanoparticles and formation of TiO_2 octahedra, which will assemble later to form the nanosheets. Our suggestion of an exfoliation/coalescence mechanism was supported by other experiments. Using precursors of different sizes of TiO_2 aggregates, we have shown that different sizes of nanoribbon are obtained in the same trend direction as the aggregates. Moreover, as the nanoribbons are obtained at longer times under the same conditions as the nanotubes, prove that they are a morphological evolution of the latter by coalescence.

Concerning the phases of the different TiO_2 morphologies, we have shown that nanosheets, nanotubes and nanourchins crystallize under the TiO_2(B) phase, while nanoribbons crystallize as a mixture of phases, which depends on the synthesis temperature and the size of TiO_2 nanoparticles in the precursor. For a synthesis temperature of 100°C, we observed a phase mixture with a predominance of the Brookite phase at the expense of the anatase phase. For a precursor synthesis temperature of 200°C, we observed nanoribbons with a TiO_2(B)/anatase phase mixture with a predominance of TiO_2(B).

TiO_2 powders of different morphologies have been used as anode materials for lithium-ion batteries, and we have evaluated their performance in terms of specific capacity and cyclability. Our results showed that the morphology has an influence on the capacity only during the first cycles. During the following cycles the capacity decreases and stabilizes in a second time. By scanning electron microscopy, we have shown that the different morphologies are transformed into aggregates, during the first cycles by a disintegration process. During the insertion/removal processes of lithium ions, a volume variation occurs, and it is at the origin of the observed disintegration phenomenon. The difference between the capacities of the different TiO_2 morphologies, during the first charge/discharge cycle, can be explained both by the specific surface of the aggregates and by the properties of their porosity in terms of pore size and connectivity. Furthermore, we have also shown that changes in the morphology of the powders during the preparation of the batteries are to be taken into account to explain the variations of the specific capacity. During the following cycles, as all the TiO_2 morphologies transform into aggregates of TiO_2 nanoparticles, we can assume that the pore connectivity is the same for all the powders, and that the specific capacity of the powders is mainly influenced by the specific surface area and by the pore size.

To confirm the role of pore connectivity, we prepared powders formed by a mixture of nanorods and TiO_2 aggregates by the hydrothermal method. By varying the synthesis temperature, we were able to vary the coverage rate of nanorods by aggregates. Moreover, by testing these powders as anode materials for lithium-ion batteries, we have shown that the specific capacity of the batteries during the first cycles, strongly depends on the coverage rate of the nanorods by the aggregates and thus on the connectivity of the pores. The electrochemical results of the discharge/charge cycles of the battery showed that both the highest capacity and the best cyclability were observed for the powder prepared at the synthesis temperature of 230°C. This was explained by the large specific surface of these powders, as well as by the connectivity of their pores. Indeed, the large specific surface of the powders allows to reduce the diffusion paths of the lithium ions, and to increase considerably the surface of the active material in contact with the electrolyte and thus with the lithium ions. This results in an improvement of the speed of the discharge/charge cycles, and the specific capacity of the battery. Moreover, the variation of the coverage rate of the nanorods by the aggregates, probably also allows to modify the connectivity of the pores within the anode, which probably allowed to optimize its accommodation to the volume variations during the cycling. Normally, this volume variation is at the origin of the formation of cracks, which causes the disconnection of pieces of the active material and thus the loss of cyclability and the decrease of the specific capacity.

We have also shown by scanning electron microscopy, that for the following cycles, the powders are formed only by aggregates with the absence of rods. Moreover, if we assume that the connectivity of the pores in the aggregates is the same, the specific capacity of the battery is controlled only by the specific surface and the pore properties in terms of size and connectivity.

From this thesis work, we can note several unanswered questions that can be the subject of perspectives. First of all, which pore connectivity structure can better accommodate the volume variations of the electrodes? Furthermore, how to find a balance between improving the specific capacity of the battery while keeping the electrode volume variation low. To achieve this goal, the design of different TiO_2 and SiO_2 configurations such as SiO_2@TiO_2 core-shell nanoparticles may be a promising way. SiO_2 has a very high specific capacity, but also a very large volume variation, during the charging and discharging processes, which accelerates the decrease of the capacity and the cyclability. The important volume variation of SiO_2 electrodes is a hindrance to the development of batteries with SiO_2 as anode material. The presence of a TiO_2 layer could decrease the magnitude of the volume variation and thus its impact on cyclability. Other configurations of SiO_2 and TiO_2 are to be considered. The recombination of the two oxides can increase the specific capacity of the battery, while reducing the volume variation of the electrodes, during the processes of charge and discharge.

Annexes

X-ray diffraction (XRD)

We used X-ray diffraction (XRD), to determine the crystal phases, observation of possible structural changes in the prepared powders during the synthesis process and during battery cycling, as well as calculation of the crystal size. When the powders are exposed to X-ray beams, each atom of the crystal scatters a wave that propagates in space due to the oscillation of the conduction electrons. The diffraction phenomenon results from the interference of the scattered waves. These interferences are either constructive when the atoms are arranged regularly with a characteristic distance, or destructive in the opposite case.

In order to identify the phases present in the prepared TiO_2 powders, the ICDD (International Center for Diffraction Data) database was used as reference.

The distance between the interreticular planes d_{hkl}, for a family of crystal plane (h,k,l) (h,k,l designate the Miller indices), can be calculated from the Bragg formula below (Eq.1):

$$2d_{hkl} \sin \theta = n\lambda \qquad (1)$$

Where λ is the wavelength of the x-ray beam, θ is the angle between the incident x-ray beam and the powder surface, and n is the reflection index.

Depending on the geometry of the crystallographic system, the characteristic structure parameters a, b, c, α, β and γ of a phase can be calculated, using the Bragg relation. For example, for a cubic system, a = b = c and $\alpha = \beta = \gamma = 90°$, the distance between the interreticular planes d_{hkl} and the characteristic parameters of the mesh is expressed by the following formula (Eq. 2):

$$d_{hkl} = a / \sqrt{(h^2 + k^2 + l^2)} \qquad (2)$$

Moreover, using the Scherrer equation and the half-value width of the diffraction peaks (FWMH), the average size of the T_{hkl} crystallites can be evaluated according to the following Debye-Scherrer equation (Eq. 3):

$$T_{hkl} = \frac{K\lambda}{\sqrt{(L^2 - l^2)}\cos\theta} \qquad (3)$$

With k is a geometric factor equal to 0.89, λ is the wavelength used, θ is the Bragg angle, L is the half-value width of the peak expressed in radian and l is the contribution of the device to the half-value width, which is equal to $4.66\ 10^{-3}$ rad under the used conditions.

The two sources of error in the calculation of the crystallite size are related to the evaluation of both the contribution of the device to the line broadening (l), and the width at half height of the lines (L). When the crystallite size becomes very small, the width of the diffraction lines becomes very important. The half-value widths of the lines are calculated from mathematical refinements. The profile of the X-ray diffraction lines can be modeled by Lorentzian functions or by the convolution product of Gaussian and Lorentzian functions (pseudo-Voigt approach).

The Inorganic Crystal Structure Database (ICSD) diffractograms used as reference for anatase and rutile TiO_2 are presented in Figure 1 and Figure 2.

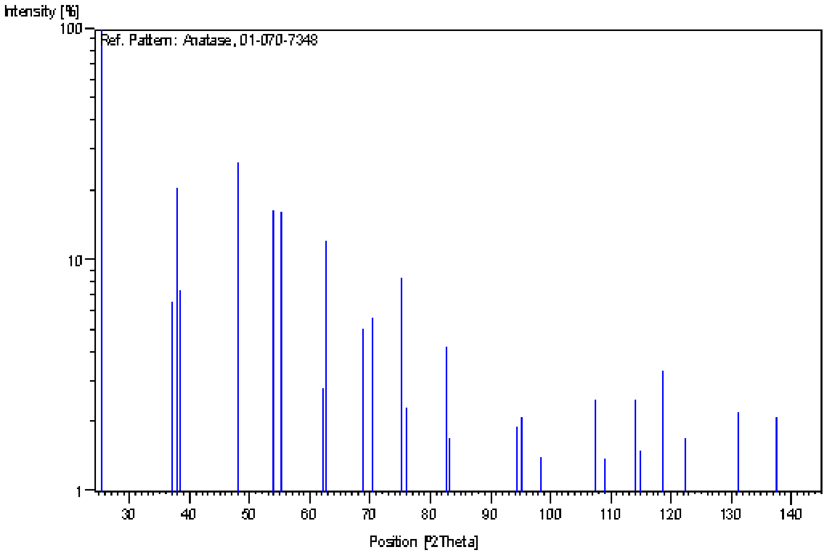

Figure 1: ICSD sheet n° 01-070-7348 for TiO_2 anatase.

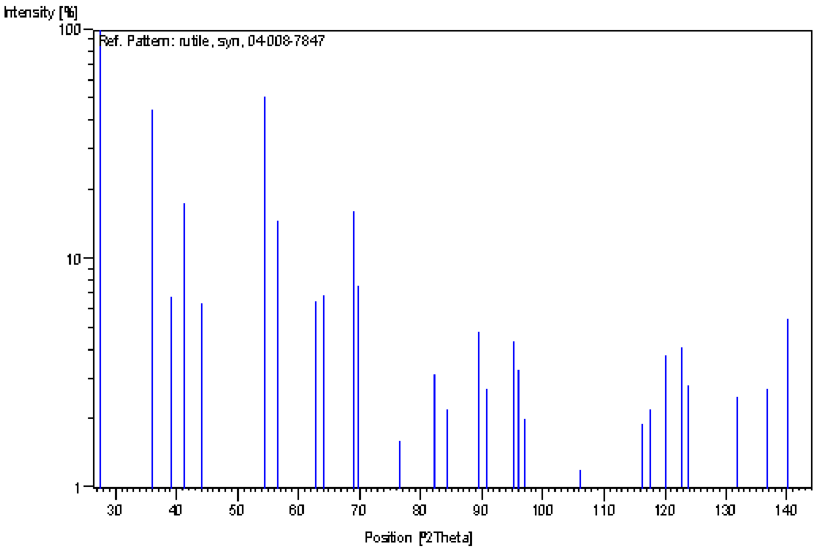

Figure 2: ICSD 04-008-78 for rutile TiO_2 .

In the case where the diffractograms show a mixture of phases, for example for a mixture of anatase and rutile, the fraction of the anatase phase can be estimated by the Spurr equation (Eq. 4):

$$f = 1/(1 + 1.26\ (I_R/I_A)) \qquad (4)$$

With f is the mass fraction of the rutile phase in the sample, IR is the intensity of the rutile peak (110) located at about 27.44°, and IA is the intensity of the anatase peak (101) located at about 25.36°.

The net area of the peaks of the diffractograms is proportional to the concentration of the phase, using an absorption term. The method of integral intensities allows to obtain the proportional concentrations of the different phases according to the law.

$$c_i = m_i I_i A$$

With c_i is the concentration of phase i, I_i is the integral intensity of a given peak of i, m_i is a calibration coefficient specific to the phase and the instrument used and A is the absorption term, identical for all phases. All crystalline phases must be identified so that the sum of the concentrations is equal to 100%.

The diffractograms presented in this report were made by a Siemens D5000 type diffractometer, in Brentano Bragg geometry, equipped with a copper anticathode ($\lambda K\alpha 1$ = 0.154

nm, $\lambda\ K\alpha 2 = 0.1544$ nm). The incidence angle 2θ varies from 20 to 80°, with a step size of 0.04 and a measurement time of 7s per step.

Scanning Electron Microscopy (SEM)

The morphology and size of TiO_2 powders have been characterized by scanning electron microscopy (SEM) based on the principle of electron-matter interaction. By focusing an electron beam on the surface of the material, two types of electrons are emitted: secondary electrons and backscattered electrons. The secondary electrons come from the outer electrons of the conduction band (Fig. 1), and are very weakly bound to the nucleus of the atom. The number of secondary electrons collected depends strongly on the surface, which must be oriented parallel to the incident beam. The detection of these secondary electrons ejected by the incident electron beam provides information on the topography of the sample. As for the backscattered electrons, they are the result of the quasi-elastic interaction between the electrons of the incident beam and the atomic nuclei of the material (Fig. 1), and they provide a qualitative analysis of the sample. Finally, to form an image, the beam must scan an area of the sample, so that the different impact points form a precise point in the image.

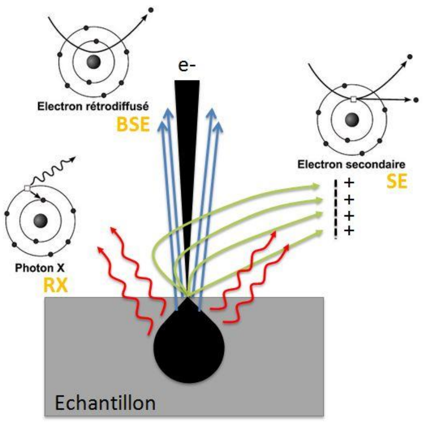

Figure 3: Diagram showing the radiation emitted by atoms under an electron beam.

The scanning electron microscopy images presented in this manuscript were made at Chimie Paris tech on a SEM-FEG Ultra 55 Zeiss microscope. This microscope is equipped with an EDX (Energy Dispersive X-ray Microanalysis) analyzer. Indeed, the X-ray photons emitted by the atoms are sorted at the detector level, it is thus possible to attribute each photon detected to a chemical element. Moreover, the counting of photons according to their energies allows a quantitative analysis. The EDX spectra obtained allow a qualitative and quantitative elemental analysis of the metal present in the TiO_2 powders.

Transmission Electron Microscopy (TEM) and electron diffraction

Transmission Electron Microscopy has been used to characterize the morphology, crystallinity and size of TiO_2 powders. The principle of TEM is based on the interaction of a flow of electrons accelerated by a potential difference of about 80 to 120 kV, with a sample, this interaction leads to the formation of an image. Two types of microscopes have been used for the realization of the images presented in this thesis: a conventional TEM and a high resolution one. The conventional microscope is a 100kV JEOL 1011, and the high resolution one is a JOEL 2100 operating with an acceleration voltage of 200 kV. The latter microscope allows to reach a point resolution of 0.18 nm and a fringe resolution of 0.14 nm. At this resolution, this TEM also provides information on the assembly of atoms and their periodicity in terms of atomic planes. By electron diffraction, we can also have information on the crystallinity of the samples. The different characterizations presented in this thesis were performed by Sandra Casale, from the Service Commun de Microscopie Electronique of Sorbonne University.

X-ray photoelectron spectrometry (XPS)

It is a physical method of chemical analysis, which consists in bombarding the surface of the sample by monochromatic X-rays. These rays cause the ionization of the atoms of the sample by photoelectric effect. The kinetic energy E_c of these photoelectrons is measured, which gives the spectrum of the intensity of the electrons according to the measured energy.

Each incident X photon has the same energy, E_x=h σ, since the beam is monochromatic (h being Planck's constant and σ the frequency of the incident light wave). During the interaction with the atom, part of this energy is used to break the bond, it is the binding energy (BE), the rest is transferred to the electron in the form of kinetic energy (Fig. 4).

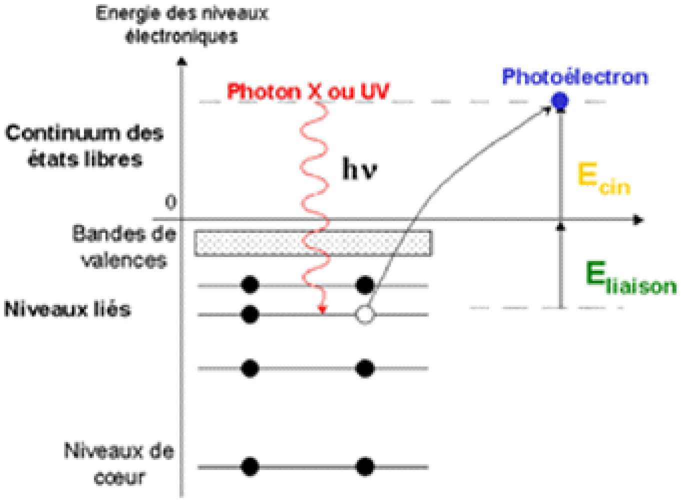

Figure 4 : Scheme of the energy diagram illustrating the excitation of an electron by an X photon.

E_L is characteristic of a given electronic layer, for a specific element. By fixing Ex and measuring Ec, it is possible to determine E_L and thus the nature of the excited atom. The kinetic energy spectrum thus presents peaks, and one can determine the binding energy corresponding to each peak by the following Einstein relation:

$$E_L = E_x - E_c \qquad (6)$$

The energy of the incident X-ray photon is of the order of magnitude of the ionization energy of the core electrons: their emission gives the XPS peaks that are essentially characteristic of the nature of the atom; while the chemical information (especially the degree of oxidation) is derived from the small displacements of the XPS peak corresponding to the variation of energy between valence layers, the latter (corresponding to the UV/visible/near-IR range in general) is weak compared to that of X-rays. There is globally little interference between the peaks of the different elements. Even when a peak can correspond to several elements, there is generally a way to remove the ambiguity by studying the whole elementary spectrum: presence/absence of a secondary peak, relative intensity of the peak's characteristic of the suspected elements, study of the Auger peaks... Semi-quantitative analyses can also be extracted from the normalized XPS spectra based on the integral of the peaks. The signal under each peak of element A is proportional to the number of atoms of type A.

Finally, the intensity of the signal as a function of the thickness, d, of the sample is damped by a factor exp(-d/λ), with λ, the mean free path of the electrons in the material: the further away from the surface, the less likely it is that the ejected electrons will be detected, i.e. the smaller their contribution to the total signal. Thus, 70% of the detected signal comes from the first λ nm, and beyond 3λ, the contribution is negligible. λ being of the order of 1 to 2 nm, the depth of analysis is therefore 3 to 6 nm, which is why the XPS technique is a surface analysis technique. We finally have access to the chemical composition of the surface of the analyzed material over a depth of less than about 10 nanometers, by comparison with known spectra.

The XPS analyses carried out in the framework of this thesis were performed by Pierre Dubot at the Institute of Materials Chemistry Paris - Est.

Gas adsorption (BET, BJH)

The specific surface of nanoparticles was determined by the BET (Brunauer Emmett-Teller) method, which makes it possible to evaluate the accessible surface of a powder per unit of mass. The specific surface depends strongly on the size of the particles, and it is the more important as the size of the particles is small. The principle of the method is based on the formation of a mono-molecular layer of an inert gas on the surface of the powder used to determine its specific surface (Brunauer, Emett and Teller or BET analysis). In addition, capillary condensation and in particular the study of the adsorption and desorption branches make it possible to evaluate the volume of the pores and their distribution in size (Barrett, Joyner and Halenda or BJH analysis). Prior to analysis, the samples are heat treated at elevated temperatures under vacuum or circulating gas to remove any contaminants. Volumetric adsorption analyses allow to evaluate the specific surface, the total volume of the pores and their distribution. A known mass of powder is placed in a cell which is degassed for one hour at 150° C. After degassing, a nitrogen/helium flow (30/70 ratio) is injected for the adsorption part, and the powder is cooled with liquid nitrogen at 77K. The adsorbed nitrogen surface allows the measurement of the available surface per unit of mass. The measurements were carried out on a Micromeritics analyzer model ASAP 2020.

Within the framework of this thesis, the adsorption measurements were carried out in collaboration with Juliette Blanchard, CNRS researcher in the Surface Reactivity Laboratory (UFR 926, Sorbonne University).

Electrochemical measurements

The galvanostatic cycling tests were performed with Swagelok half cells. These cells have the advantage of being reusable and easy to assemble and disassemble. These cells are composed of the following elements:

- A positive electrode, made of a mixture of active material (80%), TiO_2 in our case, with carbon (7%), graphite (7%) and PTFE binder (7%).
- A Whatman paper disc, made of GF/D grade borosilicate fiberglass, soaked in electrolyte.
- A lithium metal pellet acting as a negative electrode.

The current collectors are made of stainless steel for the graphite and lithium electrodes, while the Swagelok body is made of Teflon PFA. The reference electrolyte used is 1M LiPF6 dissolved in a 1:1:1 volume ratio mixture of ethyl carbonate (EC), di-ethyl carbonate (DEC) and dimethyl carbonate (DMC), (EC/DEC/DMC). The cell diagram is shown in Figure 5:

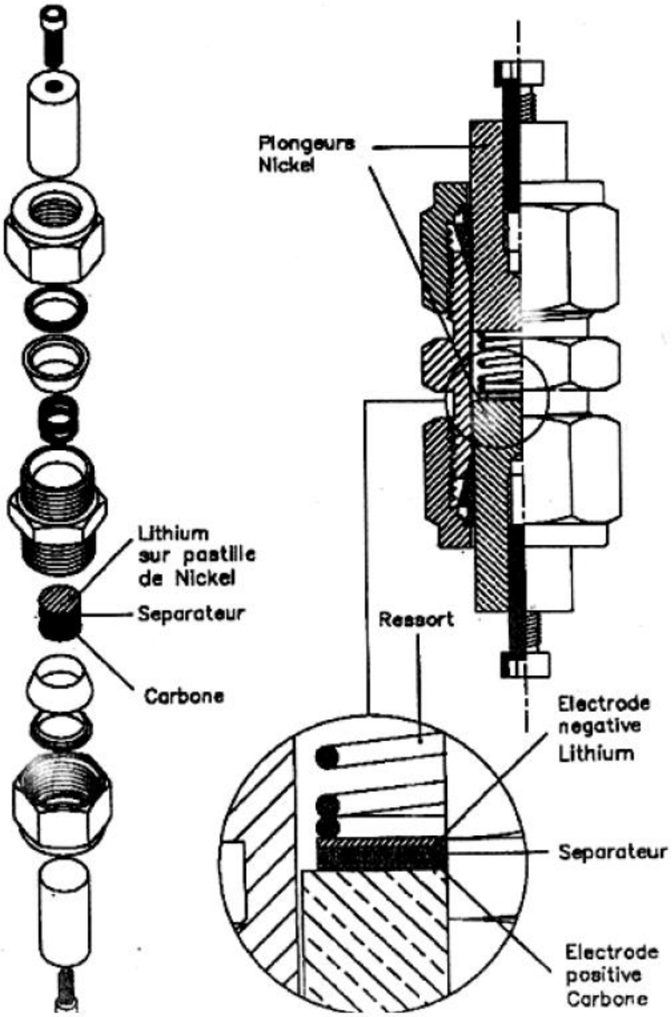

Figure 5 : Schematic of a Swagelok half-cell

Résumé de la thèse (en Français)

Dans le contexte actuel ou la protection de l'environnement a pris une importance majeure, et ou le réchauffement climatique est devenu une préoccupation mondiale, les énergies renouvelables sont identifiées par les experts des énergies comme des technologies matures pour assurer une alternative pérenne aux énergies fossiles (charbon, pétrole, gaz). Ces derniers, sont des sources principales de la pollution environnementale et du réchauffement climatique. Dans le cadre de sa politique énergétique pour ses pays membres, l'Union Européenne a fixé des objectifs ambitieux, en termes de développement des énergies renouvelables. Outre l'amélioration de l'efficacité énergétique, l'Union Européenne souhaite porter la part des énergies renouvelables à au moins 30 % du mix énergétique d'ici à 2030. A l'instar de Paris, certaines sont allées plus loin encore, se fixant un objectif de 50 %, puis de 100 % d'ici à 2050.

Les énergies renouvelables, telles que, le photovoltaïque, l'éolien, l'hydraulique, la biomasse ou la géothermie, offrent l'avantage d'être des énergies vertes non polluantes et durables, mais leur dépendance des conditions climatiques les rende intermittentes et non disponibles à la demande. Cet obstacle frein leur utilisation à grande échelle, ce qui a nécessité le développement de systèmes de stockage adaptés, pour assurer un approvisionnement continuel à tout instant et à tout moment de l'année. Les systèmes de stockage de l'énergie vont aussi contribuer à augmenter la part des énergies renouvelable dans le mix énergétique, et atteindre les objectifs ambitieux fixés par l'UE à ses pays membres. On estime que le marché des batteries pourrait représenter 250 milliards d'euros dès 2025.

Afin d'optimiser l'exploitation des énergies renouvelables et palier à leur problématique d'intermittence, différents systèmes de stockage ont été développés, pour conserver l'énergie et assurer sa restitution à la demande. Historiquement, les batteries au plomb ont été les premières à répondre au besoin du stockage de l'énergie. Elles ont l'avantage d'être économique et facilement recyclable, mais néanmoins présentent l'inconvénient d'être polluantes de l'environnement à plus long terme. En effet, la présence du plomb dans l'un de ses constituant, et qui est un métal lourd dangereux pour la santé humaine et l'environnement, risque d'être libérer dans l'environnement en fin de vie de la batterie. Aujourd’hui, les batteries à lithium-ion représentent la technologie de stockage la plus mature à court terme et la plus populaire, pour un usage domestique (véhicule électrique, les dispositifs portatifs, les vélos, les scooters, les trottinettes électriques, les robots industriels, l’outillage, le stockage de l’électricité sur les réseaux etc.), de télécommunication (téléphone portable) et spatial (engins spatiaux). Les batteries à lithium-ion présentent l’avantage de pouvoir restituer l’énergie rapidement et pour de longue période de manière fiable (plus de 10 ans). Par ailleurs, elles possèdent l’avantage d’avoir une densité élevée de stockage de l’énergie, et de fonctionnement dans des conditions extrêmes de variations de température importantes, de chocs, de vibrations et de longue durée. D’autres technologies innovantes de batterie moins polluantes et plus puissantes ont été développées, pour répondre au besoin grandissant d’un stockage durable de l’énergie. Parmi ces technologies il y a : les batteries à sodium-ion et les batteries à électrolyte solide.

Les batteries actuelles à lithium-ion sont constituées de deux électrodes, une anode et une cathode, plongées dans un électrolyte. Elles fonctionnent par des cycles de charge et décharge au cours des quels les ions lithium se déplacent d’une électrode à l’autre à travers un électrolyte. Pour les différents usages des batteries à lithium-ion, Il est primordial de fournir l’énergie avec les mêmes performances pendant plus d’une dizaine d’années. L’éventuel vieillissement de l’un des constituants de la batterie, peut nuire à son fonctionnement optimal et induire une diminution de ces performances. Les phénomènes de vieillissements touchent les différents constituants de la batterie, et se manifeste par un changement de leurs propriétés. La qualité des différents constituant de la batterie influencent considérablement ces performances en termes de durée de vie, de cyclabilité et de puissance. La croissance d’une couche de passivation à l’interface électrode-électrolyte (Solide Electrolyte interphase (SEI)), favorisent une meilleure réversibilité d’insertion des ions lithiums sans intercalation de solvant, toute en conservant un bon transfert de charges. Par ailleurs, la structure, l’architecture et la composition des matériaux d’électrode jouent aussi un rôle important dans l’optimisation des performances des batteries. Cependant, leurs évolutions au cours du cyclage de la batterie est encore mal compris et sujet d’actualité dans le domaine des batteries. Plusieurs résultats dans la littérature ont mis en évidence, l’importance de la porosité et la surface spécifique des poudres utilisées, comme matériaux d’électrodes, dans la détermination des performances des batteries.

Dans l’optique d’une compréhension des différents paramètres influençant les performances des batteries à lithium-ion, les travaux de recherche dans le cadre de cette thèse sont orientés vers l’étude des différents mécanismes à l’origine d’un contrôle de la morphologie de nanoparticules de dioxyde de titane, lors d’une synthèse hydrothermale. Par ailleurs, l’intérêt d’un contrôle de la morphologie des nanoparticules de dioxyde de titane, afin de les utiliser comme matériaux d’anode pour les batteries à ion-lithium a été exploré. L’importance de la porosité et la surface spécifique des poudres de dioxyde de titane préparées, dans la détermination des performances des batteries à ion lithium a été étudiée.

Le Chapitre I est une étude bibliographique de l’état de l’art, sur les nanoparticules de dioxyde de titane et les batteries à lithium-ion. La première partie a été consacrée principalement aux méthodes de synthèses de nanoparticules de dioxyde de titane, avec une attention particulière à la méthode hydrothermale. Nous avons présenté dans cette partie, les différents paramètres caractérisant les nanoparticules de TiO_2. Les applications des nanoparticules de TiO_2 ont été aussi abordées. La deuxième partie de ce chapitre a été consacrée aux batteries à lithium-ion et l’intérêt d’utiliser les nanostructures de TiO_2 comme matériaux d’anode. Une attention particulière a été apportée au positionnement des travaux réalisés par rapport à la littérature dans le domaine.

Par la suite, le manuscrit est structuré en articles exposant les résultats obtenus, et chaque article est précédé par un résumé, décrivant de manière succincte les résultats reportés dans cet article. Les différents résultats reportés, discutent du mécanisme à l’origine du contrôle de la morphologie, dans le cas de la synthèse hydrothermale des nanoparticules de TiO_2.

Nous avons mis en évidence la possibilité de préparer des nanoparticules de dioxyde de titane de différentes morphologies, en utilisant la synthèse hydrothermale en solution alcaline de NaOH. La méthode de synthèse hydrothermale permet de contrôler à la fois, la cristallinité, la taille des particules ou encore la morphologie. Parmi les paramètres de synthèse que nous avons fait varier, il y a la température, le temps de réaction dans le réacteur (autoclave), et la nature du précurseur de TiO_2 utilisé pour la synthèse. La nature de ce dernier sous forme d’agrégat de TiO_2, est originale par rapport à la littérature, et a permis d’aider à mieux comprendre les mécanismes de formation : des nanofeuillets, des nanotubes et des nanorubans de TiO_2.

Dans un premier temps, nous avons utilisé le précurseur de $TiOSO_4$, pour la synthétise de nanopoudres à base d'agrégats de TiO_2 de phase anatase et de taille contrôlée. Les différentes caractérisations ont montré que les agrégats sont formés de nanoparticules de TiO_2, dont la taille varie de 4 à 10 nm. En utilisant ces agrégats de TiO_2 comme précurseur, une solution alcaline de NaOH, et en faisant varier la température et le temps de réaction, nous avons mis en évidence un contrôle de la morphologie. Selon les conditions de synthèse, nous avons obtenu des nanofeuillets, des nanotubes, des nanorubans et des nanoursins. Pour les différentes morphologies, le temps de synthèse était inférieur ou égale à 6 h, ce qui est un record par rapport à ceux rapportés dans la littérature pour d'autres précurseurs.

Par ailleurs, la synthèse implique deux intermédiaires : les titanates de sodium et les acides titaniques, et elle se déroule en trois étapes. D'abord la synthèse en autoclave, par la suite la poudre obtenue subit des échanges d'ion et le titanate de sodium est transformé en acide titanique, et enfin un traitement thermique. Pour les temps de réaction de 6h et à la température de 100°C ou 150°C, nous avons observé la formation de nanoursin. La formation de cette morphologie, nous l'avons expliqué par un assemblage désordonné de nanofeuillets de TiO_2. A la température de 200°C et pour un temps de 6h, nous avons observé la formation de nanorubans de faible épaisseur (<10nm) et d'un diamètre de 50 à 100nm. Pour la température de 200°C et un temps de réaction de 6h nous avons observé la formation de nanorubans, tandis que, pour les temps court de 15min et 180min nous avons observé respectivement des nanofeuillets et des nanotubes de TiO_2. Par une analyse par microscopie électronique à haute résolution, nous avons mis en évidence l'enroulement des nanofeuillets, qui évolue dans un temps ultérieur vers des nanotubes. Par ailleurs, nous avons observé une coexistence de nanofeuillets de la taille des nanoparticules de TiO_2 avec des nanofeuillets de diamètre un peu plus grand. Ces différentes morphologies sont probablement les différentes étapes de formation d'une même morphologie de nanoruban. Probablement durant la synthèse en milieu alcalin de NaOH, il y a insertion des ions Na^+ dans la structure de TiO_2 et son exfoliation dans une seconde étape, pour former les nanofeuillets de taille plus grande par coalescence. Nos différentes observations vont dans le sens d'un mécanisme impliquant les processus d'exfoliation et de coalescence et non pas le processus de dissolution des nanoparticules et formation d'octaèdre de TiO_2, qui vont s'assembler par la suite pour former les nanofeuillets. Notre suggestion de mécanisme par exfoliation /coalescence a été supportée par d'autres expériences. En utilisant des précurseurs de différentes tailles d'agrégats de TiO_2, nous avons montré qu'on obtient des nanorubans de différentes tailles dans le même sens de tendance que les agrégats. Par ailleurs, comme les nanorubans sont obtenus à des temps plus long dans les mêmes conditions, que les nanotubes, prouvent qu'ils sont une évolution morphologique de ces dernies par coalescence.

Concernant les phases des différentes morphologies de TiO_2, nous avons montré que les nanofeuillets, les nanotubes et les nanoursins cristallisent sous la phase de TiO_2(B), alors que les nanorubans sous forme d'un mélange de phases, qui dépend de la température de synthèse et de la taille de nanoparticules de TiO_2 du précurseur. Pour une température de synthèse de 100°C, nous avons observé un mélange de phases avec une prédominance de la phase Brookite aux dépens de la phase anatase. Dans le cas d'une température de synthèse de 200°C, nous avons observé des nanorubans avec un mélange de phases TiO_2(B)/anatase avec une prédominance de TiO_2(B).

Les poudres de TiO_2 de différentes morphologies ont été utilisées comme matériaux d'anode, pour les batteries à lithium-ion, et nous avons évalué leurs performances en termes de capacité spécifique et de cyclabilité. Nos résultats ont mis en évidence, que la morphologie n'a d'influence sur la capacité, que lors des premiers cycles. Durant les cycles suivants la capacité diminue pour se stabiliser dans un second temps. Par microscopie électronique à balayage, nous avons montré que les différentes morphologies se transforment en agrégats, lors des premiers cycles par un processus de désintégration. Lors des processus d'insertion/désinsertion des ions de lithium, une variation de volume se produit, et elle est à l'origine du phénomène de désintégration. La différence entre les capacités des différentes morphologies de TiO_2, lors du premier cycle de décharge/charge, peut s'expliquer à la fois par la surface spécifique des poudres et par les propriétés de leur porosité en termes de la taille des pores et leurs connectivités. Pour mettre en lumière le rôle de la connectivité des pores, nous avons préparé des poudres formées par un mélange de nanobatônnets et d'agrégats de TiO_2. Selon les conditions expérimentales de synthèse, nous avons fait varier le taux de couverture des nanobatônnets par les agrégats, ce qui a pour effet de modifier la connectivité des pores dans la poudre. En testant ces poudres comme matériaux d'anode, pour les batteries à lithium-ion, nous avons montré que la capacité spécifique des batteries, dépend fortement du taux de couverture des batônnets par les agrégats et donc de la connectivité des pores.

Le dernier chapitre est consacré à la conclusion générale, qui fait la synthèse des résultats marquants de la thèse, et fait ressortir l'apport des travaux réalisés à l'identification des paramètres clés, pour la préparation de batteries à lithium-ion avec de meilleures performances. Par ailleurs, suite à la conclusion, des voies pour l'amélioration des performances des batteries à ion-lithium ont été évoquées, et pourront être l'objet de perspectives pour la suite de ces travaux de thèse. L'utilisation de différentes configurations de TiO_2 et SiO_2 comme par exemple des nanoparticules cœur-coquille de $TiO_2@SiO_2$ sont à prévoir, pour augmenter considérablement la capacité spécifique de la batterie à lithium-ion. Le SiO_2 possède une très grande capacité spécifique, mais aussi une très grande variation de volume, lors des processus de charge et décharge, ce qui accélère la baisse de la capacité et de la cyclabilité. D'autre configuration de SiO_2 et de TiO_2 sont a envisagé. La recombinaison des deux oxides peut augmenter la capacité spécifique de la batterie, toute en réduisant la variation de volume des électrodes lors des processus de charge et décharge. La variation de volume importante des électrodes de SiO_2, est un frein au développement de batteries avec SiO_2 comme matériaux d'anode. La présence d'une couche de TiO_2 pourrait diminuer l'ampleur de la variation de volume et donc son impact sur la capacité.

RÉSUMÉ

Les nanomatériaux de dioxyde de titane (TiO_2) sont de potentiels matériaux d'électrode, pour l'application batterie à ion lithium, et pourrons remplacer le graphite, qui est l'actuel matériau d'anode. Ces nanomatériaux ont l'avantage d'avoir une faible variation de volume, lors de l'insertion/désertion des ions lithium, et une capacité volumétrique élevée. Dans ces travaux de thèse, nous avons synthétisé des nanomatériaux de différentes morphologies en utilisant des nanoagrégats de TiO_2 comme précurseur, une solution alcaline de NaOH et la méthode de synthèse hydrothermale. En faisant varier la température et le temps de réaction, nous avons montré qu'il est possible de préparer différentes morphologies de TiO_2, tels que les nanofeuillets, les nanotubes, les nanoursins et les nanorubans. En faisant varier les conditions de synthèse, nous avons pu comprendre certains mécanismes de formation des différentes morphologies, par des processus d'exfoliation/coalescence et enroulement. Nous avons utilisé les poudres préparées, comme matériaux d'anode pour les batteries à lithium-ion, et nous nous sommes intéressés à l'influence de la morphologie des poudres sur la capacité et la cyclabilité des batteries à lithium-ion. Nos résultats ont mis en évidence la transformation de la morphologie des poudres, lors des premiers cycles de décharge/charge en agrégats de TiO_2, par un processus de désintégration. Après, les premiers cycles, nous avons montré que c'est plutôt la surface spécifique et la porosité des nanoagrégats de TiO_2, qui dominent les performances des batteries à lithium-ion.

Par ailleurs, nous avons préparé des nanobâtonnets de TiO_2, avec différents taux de couverture de nanoagrégats de TiO_2, en faisant varier principalement la température, et en utilisant la méthode de synthèse hydrothermale. En utilisant ces poudres comme matériaux d'anode pour les batteries à ion lithium, nous avons montré que les variations du taux de couverture des nanobâtonnets par les agrégats a une influence sur les performances des batteries, en terme de capacité et de cyclabilité. Ce résultat, nous l'avons expliqué entre outre par différentes connectivités des pores dans les poudres préparées.

MOTS CLÉS

Nanomatériaux de TiO_2, matériaux d'anode, morphologies, porosité, batteries à lithium-ion.

ABSTRACT

TiO_2 nanomaterials are a promising candidate as anode materials for Lithium-ion batteries application, and could soon replace graphite, which is actually the most used material as negative electrode. TiO_2 nanomaterials offer the advantage of low volume variation during the discharging/charging cycling processes and high volumetric capacity.

In the framework of this thesis work, different TiO_2 nanomaterial morphologies were prepared, using TiO_2 aggregates as precursors, alkaline solution of NaOH and the hydrothermal synthesis method. By changing the synthesis temperature and time, we demonstrate that it is possible to prepare different morphologies of TiO_2 nanomaterials, such as nanosheet, nanotube, nanourchin, and nanoribbon. We also managed to understand some aspects of the morphology's formation mechanism, involving mainly exfoliation/ coalescence and enrolling processes. We used the prepared powders as anode materials for lithium-ion batteries, and we demonstrate that the morphologies have a strong influence only during the first discharging/charging cycles. Our results show that different morphologies are transformed into aggregates through disintegration processes, as a consequence of volume variation during the cycles. After these first cycles, the performance of lithium batteries is strongly influenced by the aggregate properties, in terms of the specific surface and the porosity of prepared powders.

Furthermore, we prepared TiO_2 nanorods decorated by TiO_2 aggregates with different coverage rats, depending mainly on the synthesis temperature. By using these powders as anode materials for lithium-ion batteries, we demonstrated that the variation of the coverage rate parameter has a strong influence on the lithium-ion batteries performance. We explained this partly in terms of the powder connectivity changing with the rate coverage of the nanorods by the aggregates.

KEYWORDS

TiO_2 nanomaterials, Anode materials, morphologies, porosity, Li-ion batteries.